Simulation of Simultaneously Negative Medium Metamaterials

Xiao Wang

Thesis submitted to the faculty of the Virginia Polytechnic Institute and State University in partial fulfillment of the requirements for the degree of

Master of Science
in
Electrical Engineering

Advising Committee

Amir I. Zaghloul (Chair)
Lamine M. Mili
Luiz A. DaSilva

September 21, 2009
Falls Church, Virginia

Keywords: Simultaneously Negative, Medium, Simulation, Metamaterials, DNG Medium

Simulation of Simultaneously Negative Medium Metamaterials

Xiao Wang

ABSTRACT

Metamaterials are artificial materials and named by those who work in the microwave material area. According to existing documentation, the metamaterials have relative permittivity and/or relative permeability of values less than 1, including negative values. If the material has negative permittivity and permeability at the same time, the material is also referred to a simultaneously negative medium, or DNG medium. Such medium has several features that any natural medium is not equipped with: negative refraction, backward phase, and evanescent wave amplification [5]. Though the medium does not exist in nature, it seems that it can be artificially made through synthesizing metallic insertions inside the natural dielectrics [2]. Due to its unique feature of negative refraction and this feature is not equipped with any reported natural medium, the concept of making perfect lenses with metamaterials has attracted attentions in recent years. However a number of questions need to be answered: How can we quantize the refractive index of the metamaterial given that the permittivity and permeability are known or vice versa; can the metamaterial be made isotropic medium under effects of different incident angles? The answer to the first question will help us to define the dimension of the lenses more efficiently; and the answer to the latter question will help determine if such medium is capable of being used to make lenses.

Previous publications from others demonstrated the negative refraction phenomenon of metamaterials though this phenomenon is restricted to a very narrow band [4] [11]. The derivation of the negative refractive index through full-wave simulation and comparison with its value through calculating the simulated negative permittivity and permeability obtained from the simulated scattering matrix have not been reported. The work carried in this thesis fully explored the ways to address this and answer those questions mentioned in previous paragraph. To fully understand the negative refraction effect of metamaterial, the author built a mathematical geometric model to calculate refractive index for rectangular metamaterial slab. With this approach, the refractive

index can be obtained provided that incident and peak-receive angle are known. In order to achieve a metamaterial with isotropy property, the author also presented three different types of metamaterial slabs: parallel-arranged, vertical-arranged and cross-arranged slab of capacitive-loaded-loops (CLL) in front of standing probes or posts, which are also called CLL-P slabs. The three arrangements are differentiated by the way unit cell is oriented. With the geometric model, the author obtained refractive indexes for three metamaterial slabs at different incident angles through numerical simulation. The refractive indexes have negative values at all circumstance, which shows the negative refraction phenomena unique to the metamaterial. Unlike the other two CLL-P slabs, the cross-arranged CLL-P slab has near constant refractive index and constant received amplitude regardless of incident angles. This result can be attributed to the symmetrical topology of unit cell in x-y plane. To better explain refractive effects occurred for those three CLL-P slabs, the author also employed a way to calculate the effective permittivity and permeability using scattering matrix. Based on effective permittivity and permeability obtained, the analytical values of refractive indexes have been calculated at resonance point. To check the refractive indexes calculated from two different methods: using Snell's Law based geometric approach and using permittivity/permeability obtained from scattering matrix, two results are compared against each other and agree well. Knowing effective permittivity and permeability is very useful for calculating other parameters of the CLL-P slab such as wave impedance and mismatch loss etc. With all the simulation for parallel-arranged, vertical-arranged, and cross-arranged CLL-P slabs, from simulation results, it is found that the cross-arranged slab has the property of isotropy at different incident angles since the coupling between incident magnetic field and CLL loop will maintain constant. As a validation process, the CLL-P simulation result in parallel waveguide is compared with prior simulation (HFSS) and measurements of refractive focusing of the same structure, and both simulation results agree with measurements.

The full-wave simulation tools FEKO that employs the Method of Moments (MoM) is used in the two ways of estimating the negative refractive index of the medium.

Author's Acknowledgements

I want to give sincere appreciation to my advisor Professor Amir I. Zaghloul for the support and guidance he provided in the study of this topic, as well as help in the preparation of this thesis. I also take this opportunity to give thanks to my colleague Junwei Dong, for the help he provided on my research.

Table of Contents

List of Figures

Chapter 1 Introduction

1.1 Introduction

In 1968, V. G. Veselago put forward the concept of a medium having simultaneously negative permittivity ε and permeability μ [1]. In his article, he believed that such medium was allowed by Maxwell equations, and would have an interesting and unusual electrodynamics property: negative refraction ($\boldsymbol{n} < 0$). The medium with such property is also called NIM (negative-index medium, which is contrary to most media existing in nature with positive refractive index (PIM $\boldsymbol{n} > 0$). In fact, NIM is a broader concept than the medium with simultaneously negative permittivity ε and permeability μ, or double negative medium, which is referred to DNG medium for simplicity. DNG medium must be NIM, but not vice versa.

In a conventional medium, traveling planar wave can be described by electric field intensity vector **E**, magnetic field intensity vector **H**, and wave vector **k**, which follow a right-handed triplet, so conventional medium is also called right-handed medium (RHM). However, in DNG medium, **E**, **H**, and **k** form a left-handed triplet, which is shown in Figure 1.1.

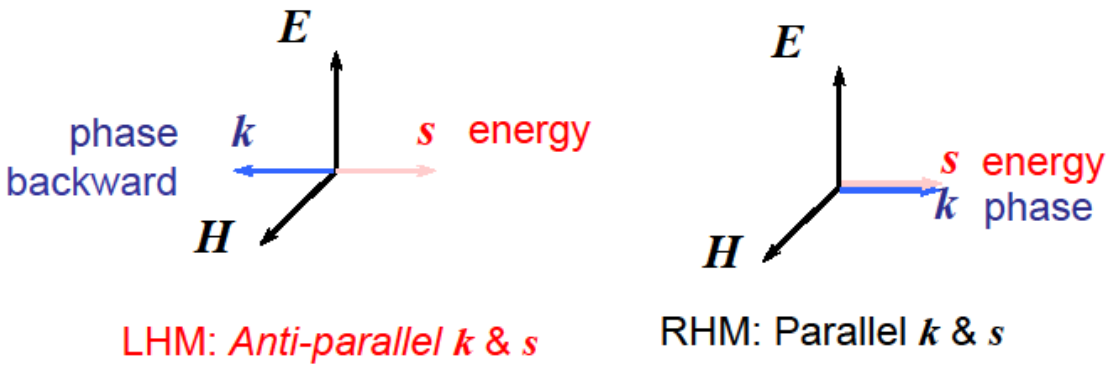

Figure 1.1 Orientation of field quantities E, H, Poynting vector s, and wave vector k in left-handed medium (LHM) and right-handed medium (RHM).

Though, **E**, **H**, and **k** follow left-hand rule in NIM, the Poynting vector **s**, which describes the energy flow direction maintains right hand relationship with **E** and **H**. In NIM, the wave vector **k** is anti-parallel to the Poynting vector **s**. For this reason, sometimes NIM is also called backward-wave medium.

1.2 Finding NIM medium

There is no known material with simultaneously negative permittivity ε and permeability μ existing in nature. So though the concept was put forward more than 40 years ago, there was no progress on this subject until J.B. Pendry et al. [2] and D. R. Smith et al. [3] [4] published papers to claim the creation of artificial material with negative ε and μ. Before this happened, people had known that the effective permittivity of plasmas could be characterized as a function of frequency. This becomes negative when frequency is closely below a plasma frequency ω_p. In this case, the propagation constant in the plasma is imaginary, and electromagnetic waves incident on the plasma suffer reactive attenuation and are reflected. So the plasma frequency is very similar to the modal cutoff frequencies of electromagnetic waveguides, where waveguide can be regarded as an inductively loaded free space when frequency is below cutoff frequency. The metals are plasmas; the real part of the permittivity is negative when it is close to plasma frequency. But the plasma frequency of metals is usually very high, and beyond the microwave range; besides the negative permeability is not achievable around plasma frequency where negative permittivity is achieved. So it is not practical to use the metal close to plasma frequency to form a medium with both negative permittivity and permeability. In [2], Pendry et al. introduced a periodic array of non-magnetic conducting units, which also can be called split ring resonators (SRR). They found that the split ring array shows effective permeability μ_{eff} as a function of frequencies close to structure resonance frequency: it has large positive effective μ_{eff} near the low frequency side of the

resonance and, most strikingly, the array has negative μ_{eff} near the high frequency side of the resonance.

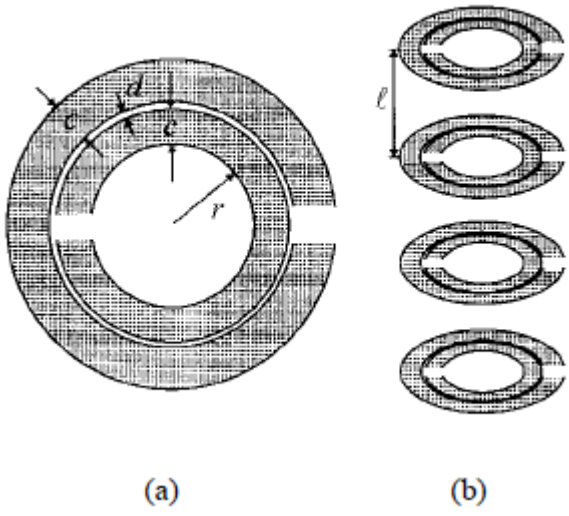

Figure 1.2 (a) Plan view of a split ring showing definitions of distances. (b) Sequence of split rings shown in their stacking sequence. Each split ring comprises two thin sheets of metal [2].

The finding of negative μ_{eff} is extremely important. Beside the reason that the medium with negative permeability is difficult to find, it is also relatively easy to combine this medium with negative permittivity ε_{eff} to form a left-handed medium described by Veselago.

This finding not only has the meaning to reach an area where researcher and scientist never touched, but also it could bring people broad potential applications of this medium. Perfect lens is a good example. In [5], J. B. Pendry mentioned to use negative refractive medium to make a perfect lens for the first time.

The concept of lens comes from optical lens whose curved surface focus light by the virtue of refraction index contrast, which can be illustrated in Figure 1.3. From figure, we

know that the performance of lens is totally decided by the medium or dielectric which comprises the lens. However, no matter how better we can make the lens, we still come to one limitation: the traditional optical lens can not focus the light into an area which is less than a square of wavelength due to its characteristics of positive refraction index [5].

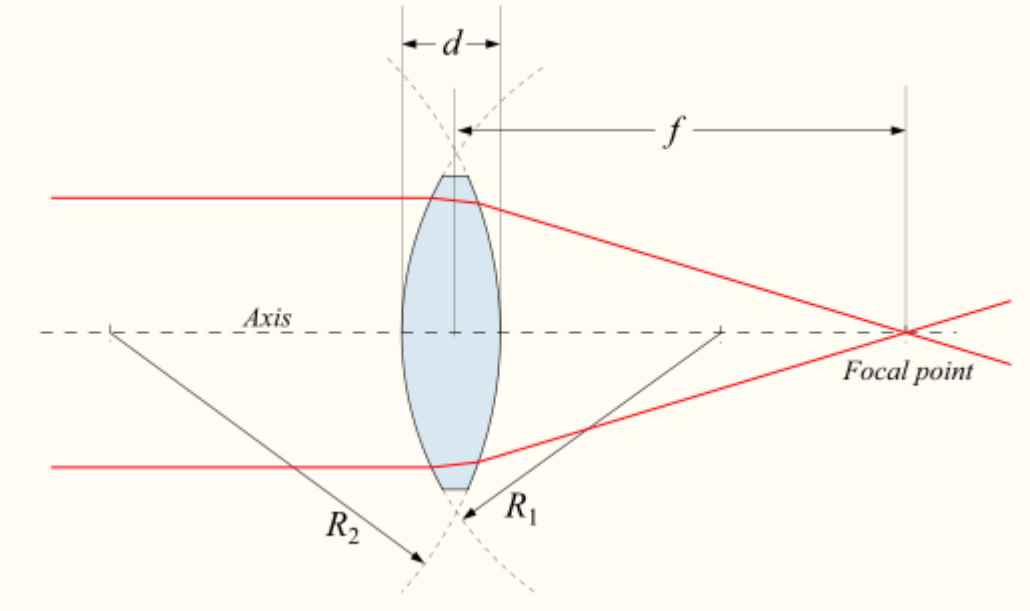

Figure 1.3 Parallel lights passing through converging lens.

So the question comes as how about we change lens medium or dielectrics to a totally different medium like negative refractive medium. Instead of using conventional lens like converging lens, Pendry [5] proposed a lens with parallel-sided slab composed by negative refractive medium. As illustrated in Figure 1.4, with the help of negative refractive medium, the lights, which can be considered as a form of electromagnetic waves, diverging from point source in PIM medium will be bent when passing the interface between PIM and NIM medium and converge at first focal point. The lights will diverge again when leaving first focal point, and be bent again when passing the second NIM-PIM interface, and finally be converged at second focal point in PIM. In most cases, people find it difficult to understand how lights or waves can be focused when passing through PIM-NIM interface. In fact, in order to have waves to be focused and re-imaged as source, we need to have two conditions met: Phase compensation and amplitude compensation.

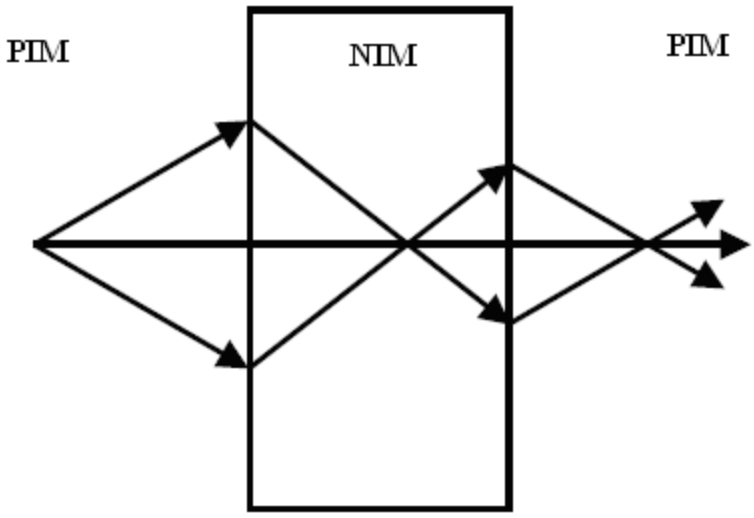

Figure 1.4 Lights diverging from point source passing through perfect lens with DNG medium and converging in focal point inside the lens and diverging and focus again outside the lens [5].

It is relatively easier to understand phase compensation from previous description. When the wave is propagating inside NIM medium, the phase is traveling backward. With the increasing of traveling distance inside NIM medium, the phase will reach the same value as the source point located in other side of the interface. How about amplitude compensation? In [5], Pendry mentioned that it is another form of wave besides propagating wave, evanescent wave, which contributes to amplitude compensation. The evanescent wave has the characteristics that its amplitude will increase with the traveling distance though there is no energy transporting for evanescent wave. So in this case, we find that propagating wave can cancel phase delay, and evanescent wave compensate amplitude decay, which are caused by distance travelled. Thus make re-focus possible in perfect lens.

Following theoretical work and analytical model built by J. B. Pendry, people have been trying to use experimental ways to prove the existence of negative refraction phenomena. The first measurements which can be found in literature were carried out by R. A. Shelby, D. R. Smith, S. Schultz [6]. The NIM medium used by Shelby et al. is a

two dimensional periodic structure made of unit cells and each unit cell is composed by copper strip and split ring resonator on interlocking strips of standard circuit board material shown in Figure 1.5. A prism of fabricated NIM medium was posed between incident wave and a detector. A narrow beam-width wave with polarization parallel to the wires was incident perpendicular to the prism face. The detector is a waveguide which can be displaced at different angle to receive scattering waves at the other side of the prism of the NIM medium.

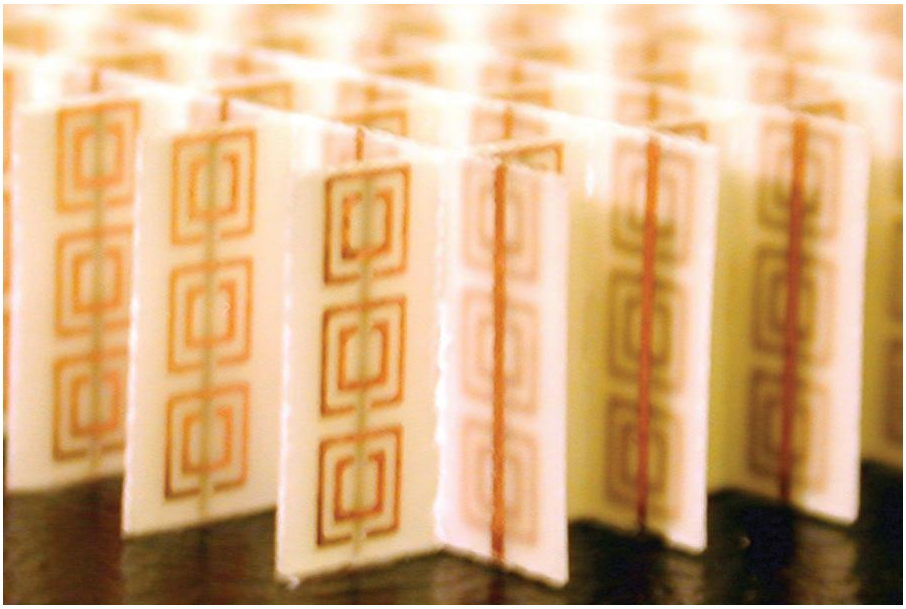

Figure 1.5 Photograph of NIM medium used by Shelby et al. for measurements [4].

From peak value of the received signal, Shelby et al. noticed that the refracted peak power point from NIM medium, shown in Figure 1.6, is on the left side compared with the refracted peak power point from Teflon, which is usually referred to as a PIM or right-handed medium (RHM).

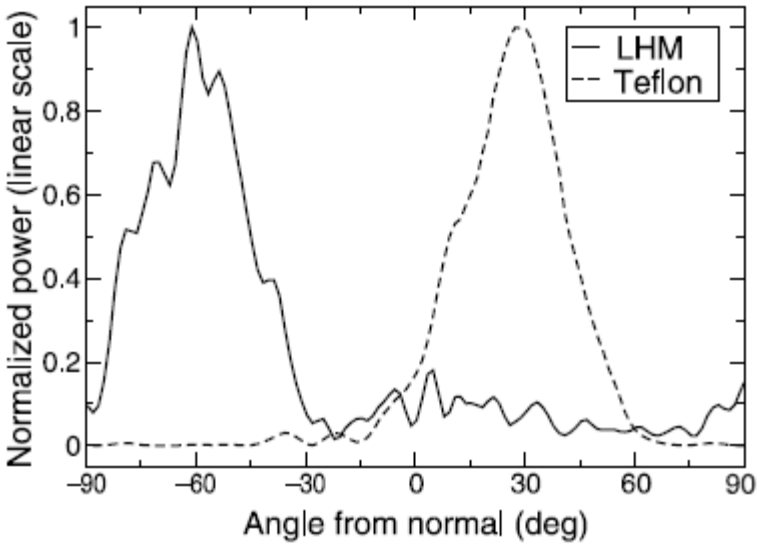

Figure 1.6 Measured received power at 10.5 GHz at different angles for both Teflon (dashed curve) and LHM medium (solid curve) – from Shelby et al [4].

The explanation of this lies in that a negative refraction happened between the second NIM-PIM interfaces. Based on the location of measured peak point, Shelby et al. applied Snell's law, and calculated refraction index. The calculated refraction index shows a function of frequencies, and falls below zero in certain frequency band. Also the result matched well with analytical value. The meaning of Shelby's experiment lies in that the negative refraction phenomenon, which was an assumption for NIM through theoretical deduction and simulation previously, is confirmed to exist through measurement.

Following the work from Shelby et al., several similar experiments have been done by different researchers to show negative refraction effect [6]-[11]. In a most recent one [11], J. S. Derov did experiment in a different way. He used a prism shaped 1-D NIM medium with an incident narrow beam-width wave at varying angles. In his experiment, two types of unit cell, SRR (split ring resonator) and Greek Key, were used to build different prisms of NIM medium or metamaterials with different apex angles. Through experiment, Derov et al. found that the calculated refractive indexes are negative and almost constant for different incident angles for both NIM media, though it was thought

1-D NIM medium was anisotropic and discontinuous due to the nature of the resonator and post.

As we can observe that so many years after the concept of NIM medium was given by V. G. Veselago, J. B. Pendry turned the concept into a possibility that a NIM medium, metamaterial can be realized in an artificial way. This is further proved by D. R. Smith, R. A. Shelby, J. S. Derov etc. through experiments in recent years. The reason that researchers spent so much resources to prove the existence of metamaterial lies in its potential applications in the microwave area. Those applications include perfect lens, or super lens described before, beam scanning antenna, and magnetic walls etc. All these applications are using the unique properties, such as negative refraction, backward wave, that metamaterial can achieve superior performance which can not be obtained by using normal PIM medium.

1.3 Critique

Though researchers achieve significant progress on implementing and proving the existence of metamaterial, there are a few publications [12-14] that are questioning if real metamaterial can be achieved, as well as negative refraction phenomenon. In [12], P. M. Valanju et al. claimed that it was the group propagation and refraction, instead of phase propagation and refraction, that people should look at when considering what happens in PIM-NIM interface; and group refractive index is always positive though phase refractive index is negative due to dispersion in NIM medium (shown in Figure 1.7). The claim from Valanju is contradictory to previous Veselago, Pendry, and so many other people's belief: both phase and group velocity show negative refraction when wave enters NIM medium from PIM-NIM interface; the directions of the phase and group velocity in metamaterial are anti-parallel.

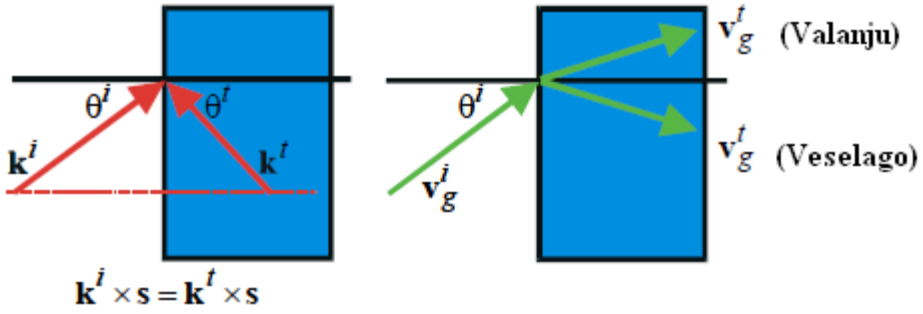

Figure 1.7 On the left, refraction for phase front when incident wave entering from PIM to NIM; on the right, refraction for group velocity in the PIM-NIM interface [12].

In [14], Ben Munk provided a series of theoretical investigations, as well as various numerical simulations to contradict previous work done by other researchers to indicate that there is no negative refraction existing in nature, at same time he gave a few alternative explanations to the experimental results obtained by other people. For example, he was questioning Boeing's "Phantom Works" [6], which is an experiment very similar to what Shelby did [4] to prove the existence of negative refraction. After observing the measurement results in [6], Ben Munk indicated that the pattern of refracted wave was very similar to surface wave radiation, which usually exists over about 10% of bandwidth. So the negative refraction phenomena claimed by other people might be caused by a surface wave, or just be one of side lobes from refracted wave. Based on this, Ben Munk concluded that the artificial periodic structure of material could not produce negative refraction.

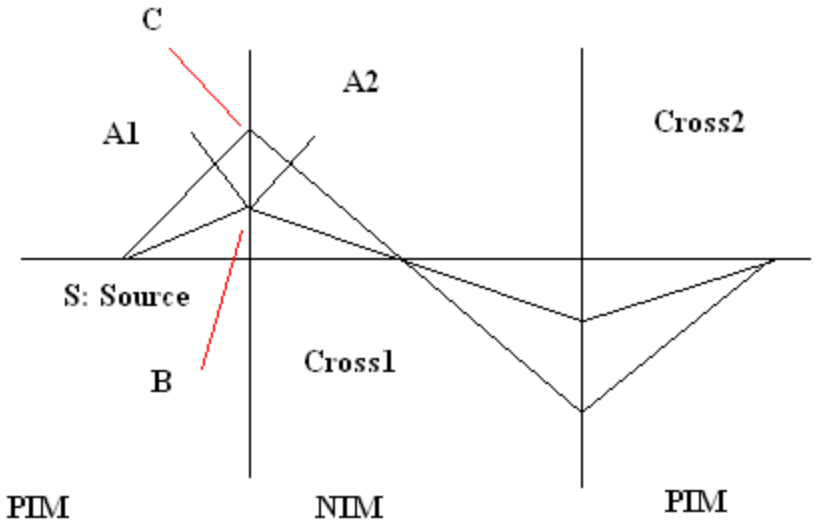

Figure 1.8. Illustration of ray traveling for super lens, it might involve negative time for two different rays arrive at focal point at same time.

Another example given by Munk, which was also used by Valanju [12], claimed that super lens is impossible. His explanation is given as follow. As shown in Figure 1.8, the two rays diverging from source S-A1 and S-B in PIM medium need to converge at focal point in NIM medium at same time in order to make super lens work. However it will take negative time for ray S-A1 to travel distance CA2, since it already takes additional time to arrive at C compared with ray S-B. Is it possible for electromagnetic wave to travel non-zero distance with negative time duration? Per Ben Munk, it is very difficult to figure out the physical meaning of negative time. So it is not realistic to implement super lens based on NIM medium.

1.4 Scope of Work

At 1999, when Rodger Walser coined the term “metamaterial” for NIM medium which is conceived by Veselago, he used Greek word “meta” to indicate the medium does not exist in nature. It is a macroscopic, man-made, three dimensional, and periodic

cellular architecture that is designed to produce an optimized combination of two or more responses to a specific excitation. So does metamaterial really exist? As we can see from different references, different conclusions can be obtained regarding this medium, either through mathematic deduction or experimental measurement. Due to the nature of this problem and the potential applications of this medium, it is worthy for us to take time and effort to study. The initiative of this thesis work is also driven by whether we can improve traditional lens design by using metamaterials, or make the lens smaller. Chapter 2 will cover the most important characteristics of metamaterials: negative refraction. Before doing that, we will thoroughly investigate the claim about existence of negative permittivity ε and permeability μ in the medium separately, as well as if they can co-exist at same time in some artificial structures. Based on this, the mechanism of wave propagation in metamaterials will be introduced. Several characteristics, like negative refraction, amplitude amplification, which metamaterial has, will be described. Some mathematic deduction will be covered based on the contribution of Pendry, and a series of potential applications of metamaterial based on those features such as perfect lens etc will be introduced. Following theory, Chapter 2 will also give a brief introduction to two types of metamaterial composition approaches: transmission line model and split ring resonators. The split ring resonator technique is our focus; and it can achieve negative ε and μ at certain frequency band. In Chapter 3, starting from the initiative of making smaller and perfect lens, a capacitive-loaded-loop and post (CLL-P) periodic structure which can be considered as one type of metamaterial is built based on split ring resonator technique, and a parallel waveguide test bed is built to study the performance of CLL-P slab. Numerical simulation results by using FEKO (http://www.feko.info), a commercial EM software, for CLL-P slab inside of parallel waveguide under different feeding methods (coaxial feed, waveguide feed, and planar wave feed method). The analysis of the simulation results will also be covered.

In Chapter 4, a study of variously arranged CLL-P slab and corresponding characteristics is carried under planar wave with different incident angles. The refraction geometric model is built to calculate the refractive index. Also we cover how to obtain effective permittivity and permeability through scattering matrix, which will further help

us to understand the principle of metamaterial. As mentioned, making a perfect lens constitutes our goal. The characteristic of homogeneity of CLL-P slab is essential to whether we can make a perfect lens. This includes whether we can achieve a constant negative refractive index, effective permittivity ε and permeability μ under different incident angles.

Chapter 5 reviews all the simulation work carried in this thesis, and presents a conclusion. The conclusion will help to answer some questions we have in Chapter 1: Is negative index refraction existing for artificial periodic structure? Is NIM medium isotropic or anisotropic? What are the effective permittivity ε and permeability μ for metamaterial at its working frequency band? And finally is perfect lens possibly implemented? Base on above discussion, conclusions are drawn.

Chapter 2 Synthesis and Characteristics of LHM

2.1 Permittivity and Permeability

When electromagnetic wave passes through dielectrics or medium, it interacts with dielectrics and medium at atomic and molecular level. This kind of interaction can be described by permittivity and permeability at a macroscopic level. Different dielectrics have different interaction with applied field, thus have different electromagnetic characteristics: permittivity ε and permeability μ. The definitions of both are listed as follows: Permittivity is a physical quantity that describes how an electric field affects, and is affected by, a dielectric medium, and is determined by the ability of a material to polarize in response to the field, and thereby reduce the total electric field inside the material. Thus, permittivity relates to a material's ability to transmit (or "permit") an electric field. Permeability is the degree of magnetization of a material that responds linearly to an applied magnetic field, or permeability relates to a material's ability to transmit (or "permit") a magnetic field.

From above description, it seems that we have to access and change its structure or lattice at atomic or molecular level in order to change permittivity and permeability of dielectrics. This is a difficult task for those who want to synthesize medium with simultaneously negative permittivity and permeability, since we do not have this medium in nature. But for a moment of thought, this might be true. Let us take an example, when electromagnetic wave passes through the medium where there are obstacles, which has much smaller dimension than incident wave length, the resulted scattering wave can be much different compared with wave passing through a medium where there is no any obstacle inside. This example provides researchers an alternative approach when trying to find simultaneously negative permittivity and permeability medium. If we touch the medium at a relatively larger or practical scale, which is still a fraction of wave length size, the permittivity and permeability of the medium can be changed. For this reason, we call this kind of medium "artificial medium". The artificial medium or dielectric, which is originally introduced by Winston E. Kock [16], is not a new concept now. When doing metallic lens design, Kock noticed that his stacked metal plates, which consist of metal

lenses, in free space showed a positive refractive index less than unity when incident wave length is substantially longer than the spacing of plates. Soon he made analogy between his arranged metal plates and artificial dielectric media, and did extensive experiment to study the relationship between wave properties and arranged metal plates, and found that the diffraction would happen when wavelength is comparable to spacing of plates. He acknowledged that his metal plates acted like the crystalline lattice of solid medium, and permittivity and permeability could be changed away from individual material in certain situation. Kock was the first one to realize that the dielectric or medium can be artificially made to meet our needs at a practical level.

2.2 Achieve Negative Permittivity and Permeability

It is possible to synthesize artificial medium with permittivity and permeability which meet certain needs from previous section, which should also include simultaneously negative permittivity and permeability medium (DNG). However, this problem was treated separately at the beginning, and it is negative permittivity that researchers were looking into firstly.

Permittivity of the plasma is a function of frequency. We call permittivity at specific frequency effective permittivity at that frequency. When frequency is dropping below a plasma frequency ω_p, the effective permittivity becomes negative, which causing the propagation constant k in the plasma imaginary from this representation: $k = \omega\sqrt{\mu\varepsilon} = \omega\sqrt{\varepsilon} = i\omega\beta$ ($\mu = 1$). In this case, the plasma acts like waveguide working under cutoff frequency, and the incident waves suffer reactive attenuation and will be reflected. In fact, the metals are known as Plasmon, which is a collective oscillation of electron density, and the real part of permittivity of metals is negative right below plasma frequency. In order to synthesize negative permittivity medium, we rely on above property of medium. However, the plasma frequency ω_p of a metal is usually in ultraviolet region of the spectrum. Besides, when the frequencies approach lower end, the effective permittivity, dominant by its imaginary part, will cause absorptive resonance, thus increased dissipation. So it is essential to reduce the plasma frequency of metal in

order to achieve a negative permittivity with low absorption. We will show it is possible from the rest of this section.

Noticing that the density of electrons confined with certain period lattice decides the plasma frequency of the lattice, J. B. Pendry [17] proposed a periodic structure that consists of thin conducting wires. Due to the confinement of thin metal wire in relatively bigger lattice as background, the density of electrons in the lattice is reduced extremely; at same time thin metal lines have their mass enhanced because of self-inductance incurred by wire array. Those two factors contribute together to bring effective plasma frequency of lattice down to 6 orders of magnitude, which is falling into gigahertz range. So array of thin metal wire can be used to achieve negative permittivity at microwave frequencies range.

Compared with achieving negative permittivity, achieving negative permeability is a much difficult task for the researchers. In order to synthesize isotropic negative permeability medium, people turned into the effort to find the magnetic analogue of a good electric conductor which is used to build negative permittivity medium. The good electric conductor that consists of negative permittivity has electric fields and currents along the wire axis, same thing should happen for a good magnetic conductor, where magnetic fields and currents flows along the corresponding wire axis. Unfortunately, this is almost impossible. The reason lies in that the magnetic materials that exist in nature, such as ferrites, are usually heavy and have an undesirable mechanical property, and barely can be used for synthesis purpose. J. B. Pendry proposed a structure, which is named as split ring (shown in Figure 2-1), in [2] to have a negative effective permeability in microwave (gigahertz) range.

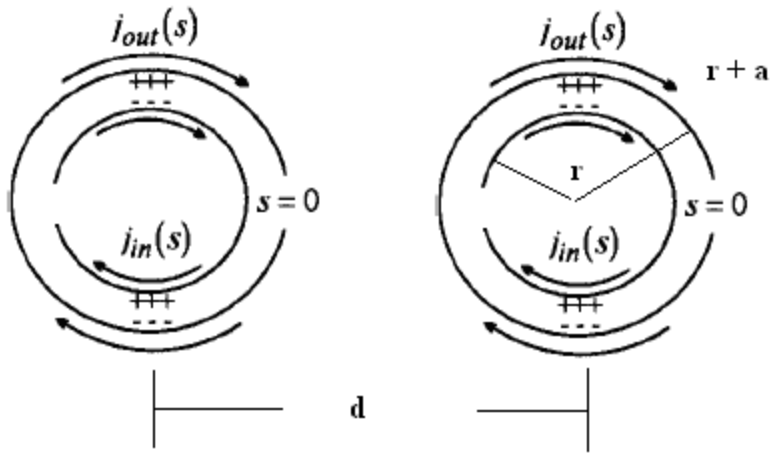

Figure 2.1 Fields and currents illustration on cut-plane of split ring.

As we can see from Figure 2.1, there is considerable capacitance between inner and outer rings, which support strong electric fields. Electric fields further interact with magnetic fields oriented with normal to cut-plane of the rings. As a result, there are currents excited on both inner and outer ring, though the currents are prevented from flowing around due to gaps, induced by magnetic fields. The synthesized capacitance, together with the natural inductance of split ring cylindrical structure, makes split rings resonant and has an effective relative permeability as follows[2]:

$$\mu_{eff} = 1 - \frac{\pi r^2 / a^2}{1 - \frac{2\sigma i}{\omega r \mu_0} - \frac{3dc_0^2}{\pi^2 \omega^2 r^3}} \tag{2-1}$$

Where r is the radius of split ring, a is the spacing distance between rings, and d is distance between inner and outer rings from Figure 2.1.

It is apparent that the split ring resonator (SRR) will achieve resonance and large effective permeability at resonance frequency $\omega_0 = \sqrt{\frac{3dc_0^2}{\pi r^3}}$, which is also given in [2]. Also the effective permeability will show negative values when second term of (2.1) is

greater than unity, which corresponds to the frequency range between resonance frequency and magnetic plasma frequency $\omega = \omega_0 / \sqrt{(1 - \frac{\pi a^2}{r^2})}$.

Figure 2.2 shows effective permeability versus frequency simulation result for split ring at following configuration (configuration 1):

r = 0.0002 meter,

a = 0.0005 meter,

d = 0.00001 meter,

σ = 0.5.

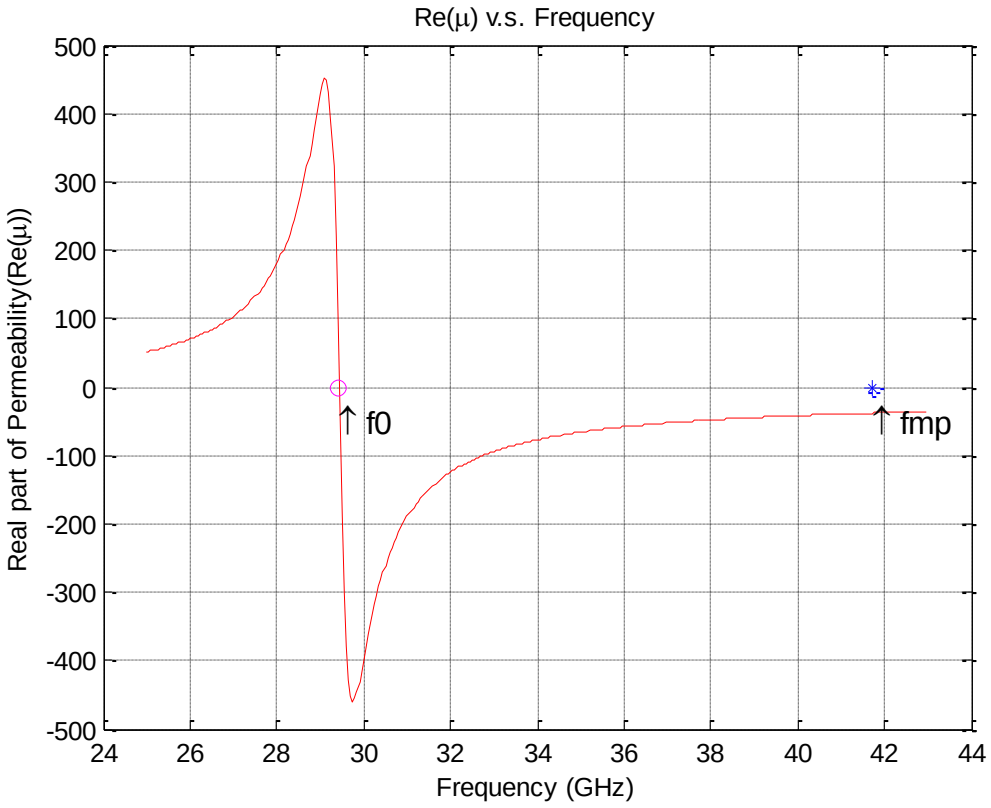

Figure 2.2 Effective permeability versus frequency for split ring under configuration 1, where red circle represents resonance frequency and blue star represents magnetic plasma frequency.

From figure, we can see that the split ring achieve resonance at 28.75 GHz, and effective permeability has positive value when frequency is below resonance frequency f_0

. On the right side of resonance frequency, effective permeability shows negative value, even beyond magnetic plasma frequency. The band between resonance and plasma frequency is called negative permeability working region.

In fact, the split ring structure is very flexible to achieve desired negative permeability working region. By changing the distance between inner and outer ring, the resonance frequency will change correspondingly, the negative permeability working region also moves as a result. Figure 2.3 gives an example of this. In this figure, all the parameters are same as configuration 1 except the distance between inner ring and outer ring changes to 0.00015 meter, which is called configuration 2. As expected, the negative μ_{eff} area moves to higher band as resonance frequency increases.

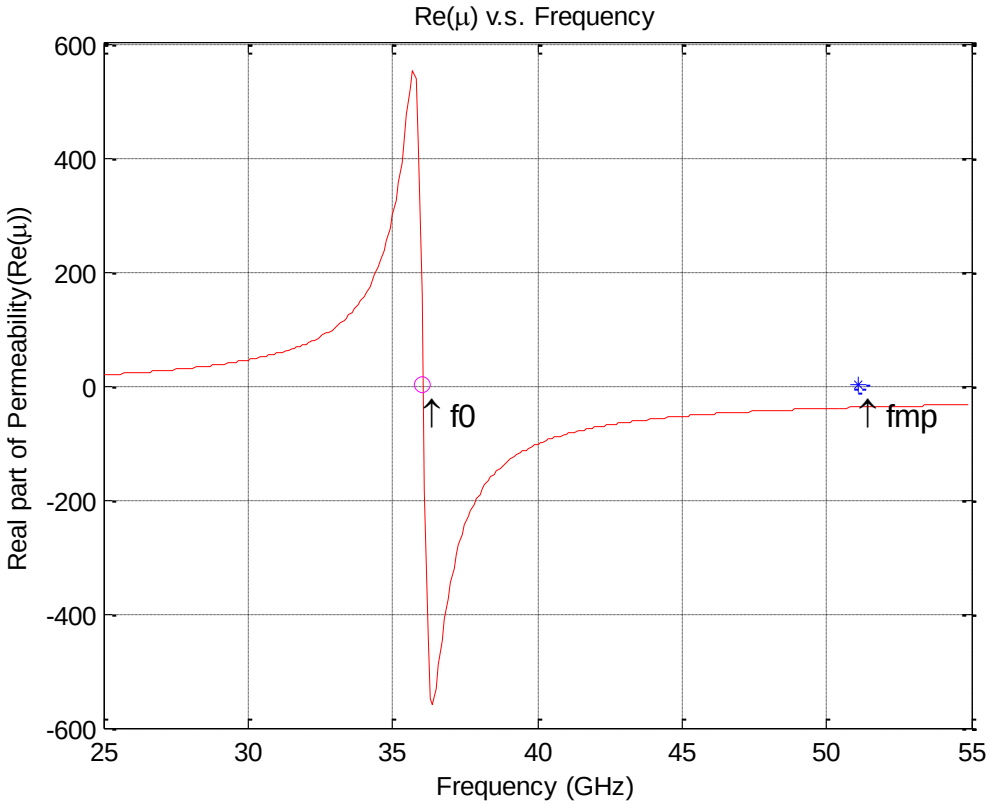

Figure 2.3 Effective permeability versus frequency for split ring under configuration 2, where red circle represents resonance frequency and blue star represents magnetic plasma frequency.

2.3 Synthesis of DNG Medium

As described in section 2.2, thin wire lattice, which consists of dipole shaped thin wire or post, can be used to create negative permittivity medium; and SRR lattice composed by split rings can be used to build negative permeability medium. In lattices, the thin post and split ring form the unit cell, and work like atoms or molecules in the normal medium that exist in nature. The difference is that the unit cells are millions of times larger than atoms and molecules, and have several orders of magnitude smaller plasma frequencies as normal medium plasma frequencies. Thus it is relatively easier to adjust their working frequency range to fit the needs through adjustment of dimension of unit cells as well as the spacing between unit cells within the lattice. By synthesizing the unit cell through combination of a thin post and split ring; one can artificially obtain simultaneously negative permittivity and permeability medium, or DNG. This medium will work at a given microwave frequency range by adjusting the internal dimension of unit cell, as well as the spacing between the unit cells. A typical unit cell composed of thin wire or post and ring is shown in Figure 2.4. The ring is in the form of a capacitive-loaded-loop. The unit cell is called capacitive-loaded-loop plus post (CLL-P).

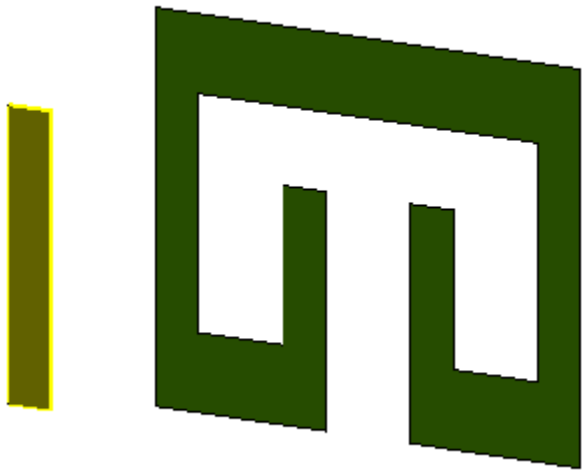

Figure 2.4 The CLL-P unit cell of artificial DNG medium composed by thin wire or post and split-ring-like capacitive-loaded-loop.

The thin wire or post as well as the split-ring-like CLL are etched in printed medium or dielectric. The synthesized medium consists of several interlaced printed media, which are further composed by repeated unit cells. The earliest synthesized DNG medium reported in publication was by Shelby et al. [6], which is also shown in Figure 1.5. Since thin wire or post and split ring works well close to its resonance frequency, the approach to use them to build DNG medium is also called resonator model for metamaterial. We can see that all the earlier work to find metamaterial was based on resonator approach.

2.4 Transmission Line Model of Metamaterial

Besides resonator model, there is another model, transmission line model [18], for metamaterial that is accepted by researchers. Though transmission line model is not the focus of this thesis, it helps to study and interpret the electromagnetic wave propagation behavior in the metamaterial to some degree. So a detailed look into this model is worthy.

As described in previous sections, the whole procedure of finding metamaterial is about how researchers find and use the analogy between natural medium and artificial metamaterial. In resonator model, the unit cell composed by a thin wire or post and a split ring, which also can be regarded as electromagnetic scatters, is the analogy of atom or molecule in the natural medium. The difference is that the unit cell is millions of magnitudes larger than atom or molecule in the natural medium and this difference greatly helps to reduce plasma frequency and make it possible to build metamaterial in the microwave range.

Transmission line model treats metamaterial as an isotropic and homogeneous medium, which is not always the case in resonator model. Thus, the metamaterial can be divided into many identical unit cells which can be modeled by a distributed network of reactance. Applying Maxwell's equation on each cell, those unit cells have identical effective permittivity and permeability as functions of frequencies. From macro scope point of view, the medium composed by many unit cells have same effective permittivity and permeability as unit cell. Here we give an example of unit cell of transmission line

model, and consider a granular volume of space in medium with dimensions of Δx, Δy, and Δz ($\Delta x = \Delta y = \Delta z = d$) in ***x***, ***y***, ***z*** axis directions. Those dimensions are diminutive when compared with wave length of incident wave, which means resulted fields inside the cell are same or static. By applying Maxwell's equation, the effective parameters of unit cell in transmission line model can be expressed by

$$\mu(\omega) = \frac{Z(\omega)/d}{j\omega} \tag{2-2}$$

and

$$\varepsilon(\omega) = \frac{Y(\omega)/d}{j\omega} \tag{2-3}$$

For any isotropic right handed medium, we should have $\mu(\omega) = \mu_0$, and $\varepsilon(\omega) = \varepsilon_0\varepsilon_r$. Replace left side of (2-2) and (2-3) with μ_0 and $\varepsilon_0\varepsilon_r$ respectively, we will have $Z = Z(\omega) = j\omega\mu_0 d$ and $Y = Y(\omega) = j\omega\varepsilon_0\varepsilon_r d$. A careful observation will make us do such conclusion: the unit cell has a series inductance $L = \mu_0 d$ and a shunt capacitance $C = \varepsilon_0\varepsilon_r d$. To get distributed quantities in unit length, we need to divide them by *d*, which are $L' = L/d = \mu_0$ and $C' = C/d = \varepsilon_0\varepsilon_r$. To summarize, the unit cell of any isotropic conventional medium with permittivity μ_0 and relative permeability ε_r can be represented a circuit with a series inductance with distributed inductance of μ_0, and shunt capacitance $\varepsilon_0\varepsilon_r$.

We can obtain propagation constant $\beta = \pm\sqrt{-ZY}$ for transmission line unit cell from following circuit wave function,

$$\frac{\partial^2 V_y}{\partial^2 x^2} + \frac{\partial^2 V_y}{\partial^2 z^2} + \beta^2 V_y = 0 \tag{2-4}$$

When *d* approach to 0, the distributed quantities are applied into β, we have

$$\beta = \pm\sqrt{-ZY} = \omega\sqrt{L'C'} = \omega\sqrt{\mu_0\varepsilon_0\varepsilon_r} \tag{2-5}$$

In (2-5), we take positive root for propagation constant β due to it is a conventional right handed medium. Phase velocity v_φ of the medium is related to its permittivity and permeability, which is given by $v_\varphi = \sqrt{\mu\varepsilon} = \sqrt{\mu_0\varepsilon_0\varepsilon_r}$. Thus we can write v_φ as

$$v_\varphi = \frac{\omega}{\beta} = \frac{1}{\sqrt{L'C'}} = \frac{1}{\sqrt{\mu_0\varepsilon_0\varepsilon_r}} = (\frac{\partial\beta}{\partial\omega})^{-1} = v_g \tag{2-6}$$

As we can see from (2-6), due to positive branch we choose for β, both group and phase velocity have positive value. This coincides with what we know for right handed medium. The refractive index for unit cell which represents corresponding medium, also can be defined as the ratio between free space light speed to phase velocity in the medium is also positive per (2-7)

$$n = \frac{c}{v_\varphi} = \frac{\sqrt{L'C'}}{\sqrt{\mu_0\varepsilon_0}} = \sqrt{\varepsilon_r} \tag{2-7}$$

Next we will show how we can apply transmission line model into simultaneous negative permittivity and permeability medium. The reason we spend so much effort to discuss transmission line model is that, as described before, the model is very helpful regarding to understanding and interpreting wave propagation and behavior inside the left handed medium. In transmission model which represent isotropic medium, the effective permittivity is connected with series inductance and permeability is connected with shunt capacitance as shown in (2-3) and (2-4). To make negative permittivity and permeability, we need to have negative series impedance for (2-2) and (2-3), and a negative admittance. Since we have reverse symmetry between right handed medium and left handed medium, it is not difficult for people to think replace series inductor by series capacitor and shunt capacitance with shunt inductor in the unit cell of the model. Then (2-2) and (2-3) become following format

$$\mu(\omega) = \frac{1/\,j\omega Cd}{j\omega} = -\frac{1}{\omega^2 Cd} \tag{2-8}$$

$$\varepsilon(\omega) = \frac{1/\ j\omega Ld}{j\omega} = -\frac{1}{\omega^2 Ld} \tag{2-9}$$

Similarly, we have distributed series capacitance *C' = Cd* and shunt inductance *L' = Ld*. Compared with right handed medium, the effective parameters of left handed medium shown in above two equations are negative, and explicit functions of frequencies. Correspondingly, the unit cell can be represented by a network composed by inductance and capacitance shown in Figure 2.5.

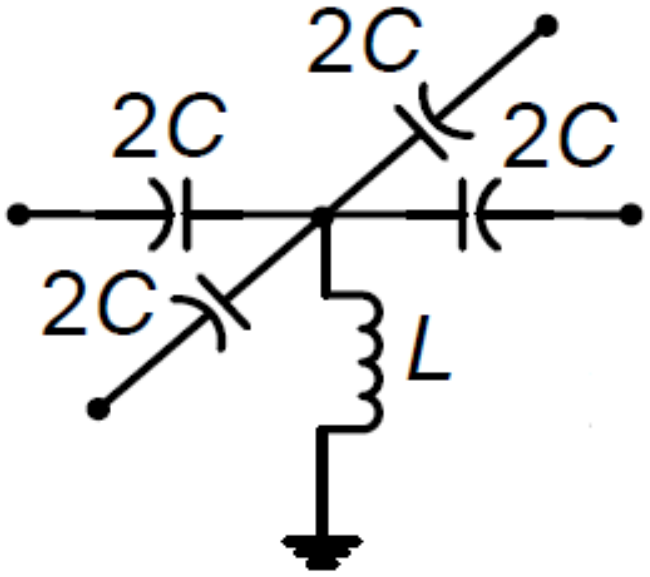

Figure 2.5 2D transmission line unit cell model for simultaneously negative permittivity and permeability [18].

Let us look at wave some characteristics in left handed medium through above model. Taking negative branch of (2-5), we have propagation constant as following format, and has inverse relationship with frequencies

$$\beta = -\sqrt{-ZY} = -\frac{1}{\omega\sqrt{L'C'}} \tag{2-10}$$

The phase velocity is the ration between angular frequencies and propagation constant

$$v_\varphi = \frac{\omega}{\beta} = -\omega^2\sqrt{L'C'} \tag{2-11}$$

And group velocity is the slope of angular frequencies versus propagation constant, and it has

$$v_g = \frac{\partial\omega}{\partial\beta} = \omega^2\sqrt{L'C'} \tag{2-12}$$

Above two equations clearly indicate that group velocity has opposite direction as phase velocity has, and group velocity has positive value. This observation matches with our expectation for left handed material (LHM). Though electromagnetic wave inside LHM is called backward wave, it only means that the phase will propagate backward; the group velocity direction (Poynting Vector), which is also considered as energy flowing direction is away from the source. The phase and group velocity direction are same in isotropic RHM, which means we do not see dispersion phenomenon. In LHM medium, the phase velocity direction is anti-parallel with group velocity direction; both of them are function of frequencies, which tells us LHM medium is dispersive. The negative phase velocity in LHM medium further suggested us the refractive index, which is denoted as the ration between free space light speed and phase velocity is negative.

$$n = \frac{c}{v_\varphi} = \frac{-\sqrt{\mu(\omega)\varepsilon(\omega)}}{\sqrt{\mu_0\varepsilon_0}} = -\frac{1}{\omega^2\sqrt{L'C'\mu_0\varepsilon_0}} \tag{2-13}$$

From above description, we know that transmission line model clearly explained that phase velocity, group velocity and refraction characteristics in both conventional RHM

and novel LHM medium. If we have to find the relationship between transmission line and resonator model, one can say that transmission line model includes the working area of resonator model. The resonator model working region corresponds to the transmission line model when unit cell is composed by series capacitance and shunt inductance.

2.5 EM Characteristics of Simultaneous Medium

2.5.1 Negative Refractive Index

Physical meaning of medium's refractive index is a measure of how much of the velocity of light (or wave) will be reduced when light (or wave) enters this medium from free space. Every medium existed in nature has positive refractive index. This implies that the refractive angle θ_2 shown in Figure 2.6, no matter how large or small it is, is on the opposite side of normal face as incident angle θ_1 stands.

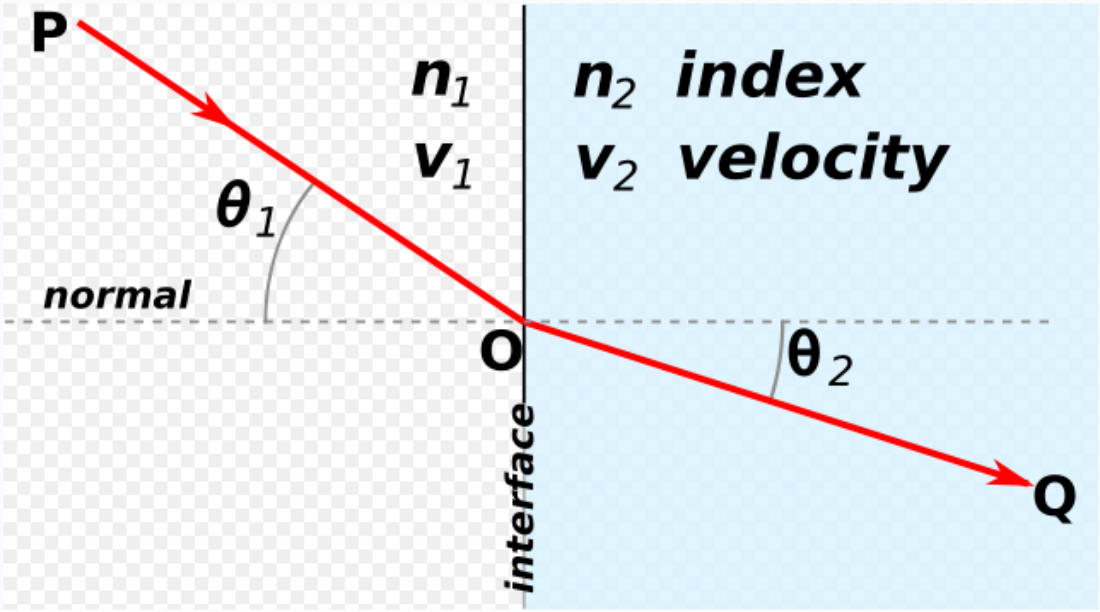

Figure 2.6 Conventional medium shows positive refractive index when wave enters from free space.

The incident angle θ_1 and refractive angle θ_2 have following relationship per Snell's Law:

$$n_2 / n_1 = \sin(\theta_1) / \sin(\theta_2) \Rightarrow n_2 = \sin(\theta_1) / \sin(\theta_2) \quad (2\text{-}13)$$

where n_1 is equal to 1 if medium 1 is free space. It clearly shows that refractive index of medium 2 is positive.

If we further dive into definition of refractive index, which is represented by (2-14), we know that refractive index is determined by relative permittivity and permeability of medium 2. Due to the positive sign taken by permittivity and permeability in conventional medium, *n* takes positive root for conventional medium. For artificial DNG medium, is there any possibility that *n* will take negative root or refractive angle will stay at same side of normal face as incident angle stands?

$$n^2 = \varepsilon_r \mu_r \tag{2-14}$$

In fact, negative refractive index is to be considered as one of the features which DNG medium has. As DNG medium is totally different one as conventional media, the wave propagation characteristics are also different with the conventional medium. The feature of negative refractive index proved by many previous experiments [4], [6] and [11] etc.

2.5.2 Left Hand Rule

Conventional medium follows right hand rule, which means the electric field intensity vector ***E***, magnetic field intensity ***H*** and Poynting vector ***k*** inside medium form right handed triplet. What will happen if both permittivity and permeability change the signs? Let us look at Maxwell-Faraday equation and Ampere's Law shown as (2-15) and (2-16) in time domain

$$\nabla \times \vec{E} = -\frac{\partial \vec{B}}{\partial t} \tag{2-15}$$

$$\nabla \times \vec{H} = \vec{J} + \frac{\partial \vec{D}}{\partial t} \tag{2-16}$$

Together with following material constitutive relations

$$\vec{B} = \mu\vec{H} \tag{2-17}$$

$$\vec{D} = \varepsilon\vec{E} \tag{2-18}$$

Let us consider a plane wave that has ***y*** polarization and is propagating along +***z*** direction. It has the form of $e^{i(kz-\omega t)}$, and the (2-15) and (2-16) reduce into

$$[\vec{k}\vec{E}] = \omega\mu\vec{H} \tag{2-19}$$

$$[\vec{k}\vec{H}] = -\omega\mu\vec{E} \tag{2-20}$$

If μ and ε are taking positive value, we can get $\vec{S} = \vec{E} \times \vec{H}$. One notices immediately, that this is a right hand triplet. If both μ and ε take negative value, we will have $\vec{S} = -\vec{E} \times \vec{H}$. The Poynting vector direction is opposite with the one has positive μ and ε, and the electric field intensity ***E***, magnetic field intensity and Poynting vector form left hand triplet.

As mentioned in section 2.4, Poynting vector direction, though follows left hand rule in DNG medium, is traveling away from the source. The phase velocity in DNG medium is opposite to Poynting vector or group velocity direction.

2.5.3 Backward Waves

Backward wave means that the phase traveling direction is toward source instead of away from source after electromagnetic wave enters the metamaterial. As discussed before, the energy flowing direction is always away from source no matter what kind of medium the wave is traveling in, the only difference is which side of normal face the energy will be flowing to. Negative phase advance is an unique feature which metamaterials have, and it is also one of contributors for the initiative of building perfect lenses or super lenses. In order to better understand how negative phase advance works; let us look at the example mentioned by Pendry [5].

If we consider electric field of an infinitesimal dipole antenna, we can use Fourier series to represent it

$$\vec{E}_{r,t} = \sum_{\sigma,k_x,k_y} E_\sigma(k_x, k_y) \times \exp(ik_z z + ik_x x + ik_y y - i\omega t) \tag{2-21}$$

Further we limit our interest in wave characteristics on z-axis, suppose the waves will be traveling from positive refractive index medium into metamaterial along z-axis. So we can re-write k_z as

$$k_z = \sqrt{\frac{\omega^2}{c^2} - k_x^2 - k_y^2} \tag{2-22}$$

In order to have wave propagate in the medium, ω^2/c^2 has to be greater than $k_x^2 + k_y^2$. Through mathematical deduction, we can get transmission coefficient for the wave entering the medium which has ε = -1, and μ = -1 as (2-23)

$$T = \exp(-i\sqrt{\frac{\omega^2}{c^2} - k_x^2 - k_y^2}\, d) = \exp(-ik_z d) \tag{2-23}$$

where *d* is the distance the wave travel inside the metamaterial.

Equation (2-23) tells us that the negative phase will be achieved after wave enters into the DNG medium, and this phase advance will get larger with the increase of *d*. This is a feature that the metamaterial has. Still considering this example, the infinitesimal dipole antenna which can be regarded as a point source, is in front of metamaterial slab. The waves diverge from the point source, and enter metamaterial along z-axis. The waves close to normal incident angle will have smaller traveling distance, which means smaller phase delay they will have before entering DNG medium, compared with the ones with larger incident angles. After entering DNG medium, all the waves tend to converge into one point inside the metamaterial according to Snell's Law. The case can be illustrated in

Figure 1.4. Inside metamaterial, the waves with larger incident angles will have longer travelling distance compared with the waves with smaller incident angles, thus the waves with larger incident angles will have bigger phase advance per (2-23) than the ones with smaller incident angles. Assuming refractive index of metamaterial is -1, which can be resulted from both ε and μ equal to -1, we will have all the waves converging inside the metamaterial to have same phases as source after traveling same distance as they have before entering metamaterial. In this way, an image is formed inside the material slab.

This is an interesting result, because this overcomes the concept of traditional lenses, which cannot work under resolution of one wave length with phase advance of metamaterial.

However phase compensation is not enough to build image at the other side of interface. Amplitude factor has been overlooked. The different rays with different incident angles will have different amplitude attenuations before they enter metamaterial. If we cannot have the amplitudes for different rays compensated accordingly inside DNG medium, we can not say an image in truly formed.

2.5.4 Evanescent Wave Amplifications

In section 2.5.3, we gave the constraint $\omega^2/c^2 > k_x^2 + k_y^2$ when we discussed the wave vector k_z. What will happen if ω^2/c^2 is less than $k_x^2 + k_y^2$? If it happens, the wave vector can be written as

$$k_z = i\sqrt{-\frac{\omega^2}{c^2} + k_x^2 + k_y^2} \tag{2-24}$$

If we replace k_z in (2-21) with (2-24), we know that the waves will have exponential decay along z-axis. In order to differentiate the propagating wave under real wave vector, here we call wave under imaginary wave vector evanescent wave.

Some part of waves will be transmitted into the DNG slab and some will be reflected at the interface between free space and the DNG slab. The transmitted and reflected waves can be written as:

$$E_t = t \exp(ik_z' z + ik_x x - i\omega t) \tag{2-25}$$

and

$$E_r = t \exp(-ik_z z + ik_x x - i\omega t) \tag{2-26}$$

where $k_z' = i\sqrt{k_x^2 + k_y^2 - \varepsilon\mu\omega^2 / c^2}$

By matching the fields at the interface, we will have

$$t = \frac{2\mu k_z}{\mu k_z + k_z'}, \qquad r = \frac{\mu k_z - k_z'}{\mu k_z + k_z'} \tag{2-27}$$

Through mathematic deduction, we find the reflection coefficient is zero and the transmission coefficient can be represented by $exp(-ik_zd)$ at the interface provided that both permittivity and permeability are equal to -1. If we replace (2-24) into the transmission coefficient, we can see the transmission coefficient will increase exponentially with the increase of distance which wave traveled inside the metamaterial slab. So the metamaterial does amplify the evanescent wave. In fact this result does not violate energy law since a evanescent wave does not transport the energy.

Let us go back to the example discussed in section 2.5.3, the waves now will have the amplitude compensated after they entered metamaterial: waves with greater incident angle will be compensated more since they traveled longer distance than the ones with smaller incident angle. Together with the phase compensation, the image will be formed inside DNG slab.

In recent years, the perfect lens has been attracting more attention with the progress on metamaterial research. With the negative refractive index metamaterial has the conventional thought that no lens can resolve finitely than wave length of the light or wave has been shook deeply. The phase compensation and evanescent wave amplitude amplification discovered through the metamaterial have raised the researchers' hopes that building a perfect lens through metamaterials is possible.

Despite the progresses on research, there are still some critiques [12] about the metamaterial from a number of researchers. Generally, those critiques can be divided in two categories: 1) There is no metamaterial and there is no negative refraction in so called "metamaterial", all the experiments to prove the existence of metamaterial use wrong interpretations; 2) There is a negative refraction in metamaterials, but it only happens for the phase velocity over very narrow frequency band, the energy flowing direction is still following the positive refraction.

In order to better address these critiques, simulations and experiments are to be conducted. The rest of the thesis is an attempt to prove the existence of negative refractive index.

Chapter 3 CLL-P Slab in Parallel Waveguide

3.1 Introduction

From previous discussion, we know that some metamaterials are composed of thin wire like probes and loop like strips in resonator model. The probe usually contributes to negative permittivity, and loop strip contributes to negative permeability. The proper combination of probes and loop strips will make simultaneously negative permittivity and permeability medium at certain frequency band. The behavior of incident wave in metamaterial, as well as the characteristics of this medium under incident wave is our interest.

Computer aided numerical analysis is crucial for us to better understand the properties of metamaterial. The reason that such analysis has to be carried on special software lies in following two factors: First, due to the complex boundary conditions in the materials, the existing asymptotic models (such as the single cell model) are not rigorous enough to capture the mutual couplings, especially around the resonant frequencies; second, the advancement of existing commercial software in recent years has offered fairly accurate and flexible toolkits that allow a complicated design to be customized and simulated efficiently. Two popular numerical methods adopted in the computational electromagnetic software are the method of moments (MoM) and the finite difference time-domain (FDTD) approach. The MoM is a frequency-domain current based solver, and the FDTD is a time-domain field based solver. The commercial software used in this study, FEKO, is a numerical tool using MoM.

In this chapter, we will introduce a capacitive-loaded-loop (CLL), which will be used to build metamaterial slab with posts. FEKO is used to do some numerical study about characteristics of metamaterial inside parallel plate waveguide with incident waves excited by three different ways, which include: coax cable excitation, waveguide excitation and planar wave excitation.

3.2 Coax Cable Excitation

In a resonator model, the unit cell of a metamaterial is usually built with inductively loaded probe or post and capacitive-loaded-loop (CLL). Post and CLL loop will contribute negative permittivity and permeability at certain frequency band respectively. The example cited most frequently is the split ring proposed by J. B. Pendry. In a split ring unit cell, a dipole is usually located in front of split ring resonator. When a incident wave reaches the dipole and split ring, it will generate electric field, and electric field will further create a circulating current inside the ring. Consequently the magnetic field will be generated due to the gaps existed in the split ring.

The resultant currents can different patterns depending on the polarization of incident electrical field and wave incident angle. When the incident wave with normal incidence angle has vertical electrical polarization, the electric field will create a strong and well balanced push-push current inside the split ring shown as Figure 3.1a. When the incident electrical field has a horizontal polarization, the electrical field will also create a weak circulating current in addition to the push-push current that is illustrated in Figure 3.1b. In fact, this circulating current exists for any incident angle as long as the electrical field direction is not perpendicular to the plane of the split ring.

Resulted from different current patterns, the magnetic field will also show a variance, as well as the effective permittivity and permeability.

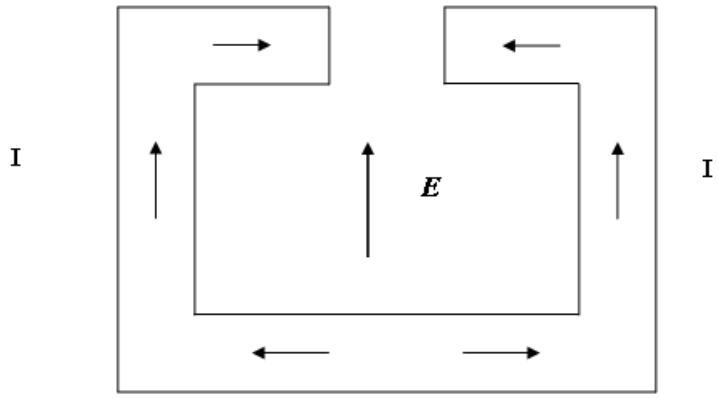

(a)

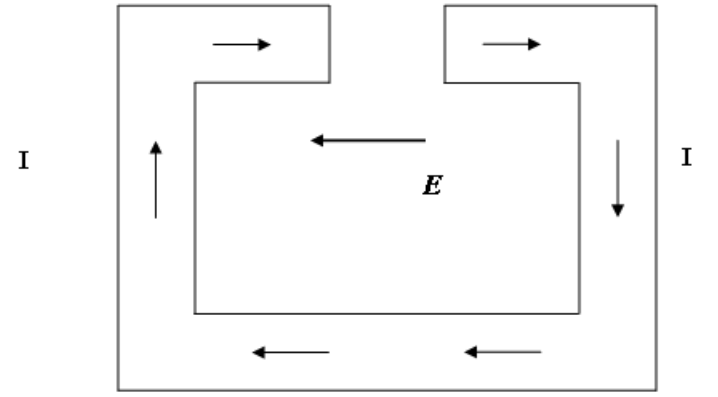

(b)

Figure 3.1 (a) Strong push-push current has been created for vertical polarization E-field. (b) Circulating current created for horizontal polarized E-field.

Split ring is not the only capacitive loaded loop that can be used as a magnetic resonator. Other resonators like Greek key, and AMC block, they all perform in a similar way as split ring when a post is posed in front of them. In our study, a CLL loop [19] is adopted, shown as Figure 2.3, and the dimension of the loop is designed in the way to have a resonance frequency at 45 GHz for the purpose of study. Total width of the loop is about 40 mils, and its height of the loop is about 20 mils. The gap in the loop, which prevents the current from flowing around the loop, is 8 mils, and the width of the loop is 4 mils.

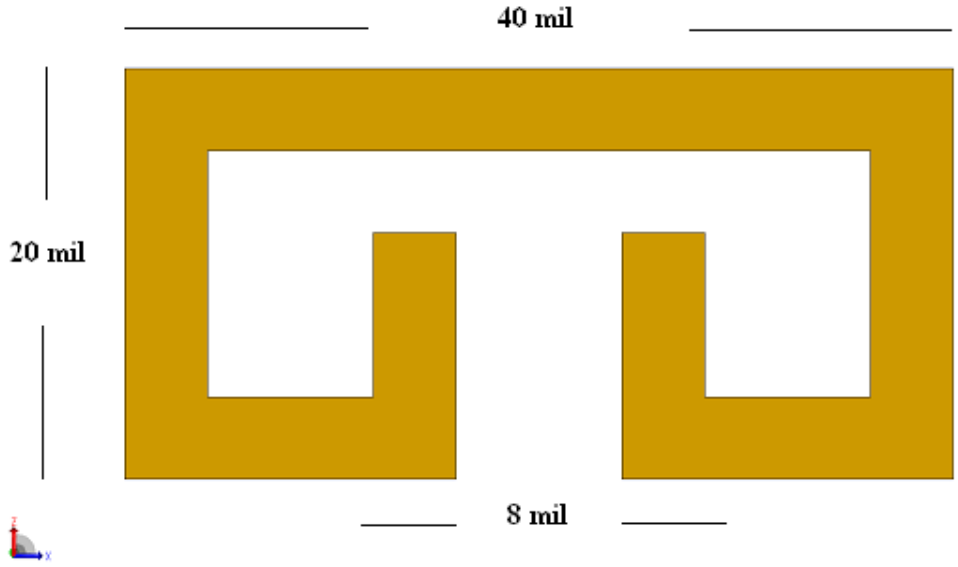

Figure 3.2 Dimension of capacitive loaded loop in simulation.

In order to form a periodic structure, two rows of 6 CLL loops are arranged in a same plane, and attached into a dielectrics slab (shown in Figure 3.3). The height of dielectrics slab is 61 mils, and the horizontal and vertical spacing between loops is 14 mils. To have posts in front of the CLL slab, a dielectrics slab with two rows of 6 posts or posts is closely aligned with the CLL slab. The height and width of the probe or post are 15 and 4 mils respectively. Thus one layer of CLL periodic structure is constructed.

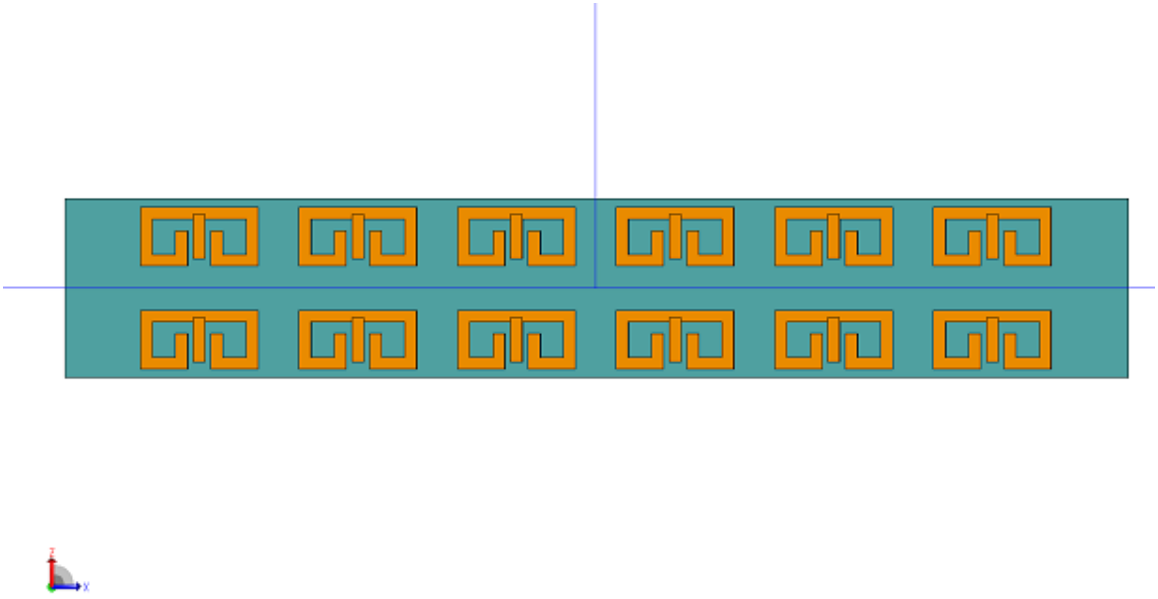

Figure 3.3 End view of CLL loop slab with dipoles in the front.

As we discussed earlier, due to the negative effective permittivity and permeability it provides, the metamaterial has different electromagnetic characteristics such as low resonant return loss, narrow bandwidth and focused effect when incident wave passes through it. With the metamaterial slab constructed above, we are able to examine and study those characteristics. To better confine the incident and scattering wave, we will have a test bed built in a parallel waveguide that is filled with dielectrics of relative permittivity ε_r = 2.2. A sketch view of the parallel-plate waveguide test bed is shown in Figure 3.4, where the length and height of the test bed are 666 and 362 mils respectively. The layers of metanaterial slabs are located in the middle of the test bed. Close to both ends, four coax cable fed probes are inserted, including one transmission probe and three receive probes.

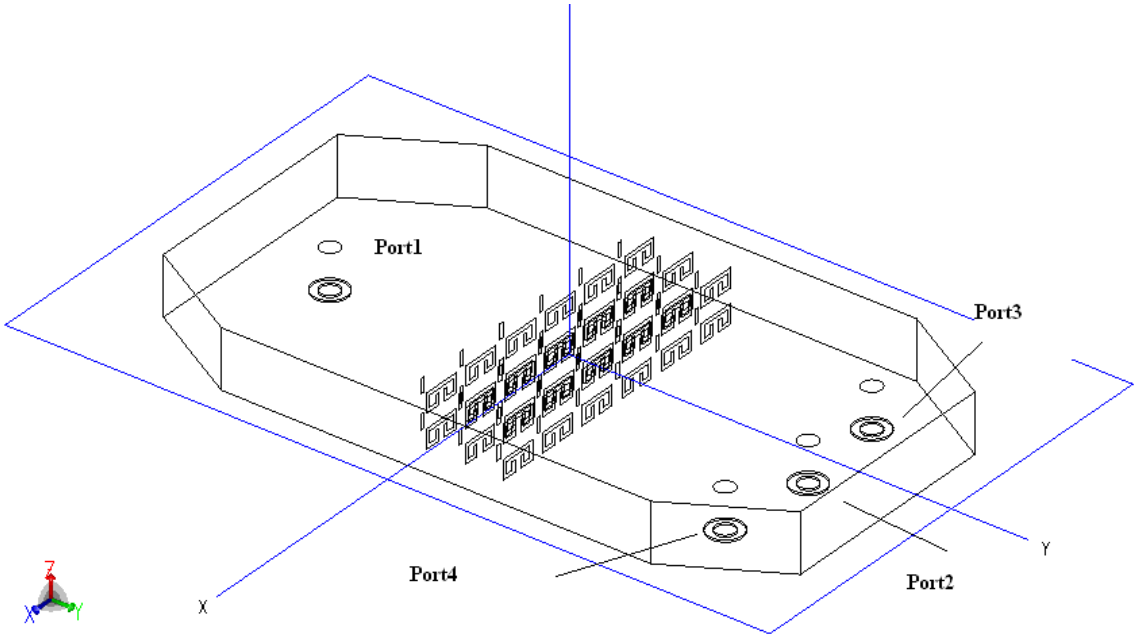

Figure 3.4 Sketch of parallel waveguide test bed with metamaterial slabs inside.

At one side of the test bed, transmission port (which is denoted as port 1), is 200 mils away from the first interface with metamaterial slab. This will insure that the metamaterial slab is in the far field of probe 1. At the other side, receive port 2, 3 and 4 are 200, 139.9, and 139.9 mils away from the second face of slabs. This makes all

receiving posts of equal distance from the transmitting port, or on a circular arc centered at the transmitting port 1. The metamaterial slabs and all receive ports are in the far field of one another. This is to make sure that the evanescent fields emanating from probe 1 and metamaterial slab can be attenuated sufficiently before reaching the slabs and receive ports.

The S parameters were calculated over the frequency band 45 to 47 GHz using the software simulation tool FEKO. As a comparison with simple dielectric medium, different scenarios were run to obtain S parameters by replacing metamaterial slab with dielectric slab. The corresponding simulated S parameters for scenarios with and without metamaterial slab are shown in Figure 3.5 (a) and (b). From figures it is observed that S11 amplitude has a minimum of -33 dB at 46 GHz frequency when metamaterial is inside the parallel-plate waveguide. When metamaterial slab is replaced with normal dielectrics slab, there is no resonance across the whole frequency band. The results indicate that the CLL-P slabs achieve resonance at this frequency, and less reflection happens between two metamaterial slab interfaces. From Figure 3.5 (a), it also can be found that the resonance has very narrow band width, which is 0.6 GHz (from 45.6 – 46.2 GHz) for a 3 dB band width.

To validate the FEKO simulation, results have been compared with the HFSS simulation and measurement data [15], shown in Figure 3.6 for the same structure with metamaterials. In this figure, measured S11, S21 and S31 are plotted in red, blue and green color respectively with fewer discrete points, while the simulated results (HFSS) are marked with same color but more samples. By comparing Figure 3.5 (a) and Figure 3.6, one can find both simulation results using FEKO and HFSS are matching with the measurements well, as well as they match with each other.

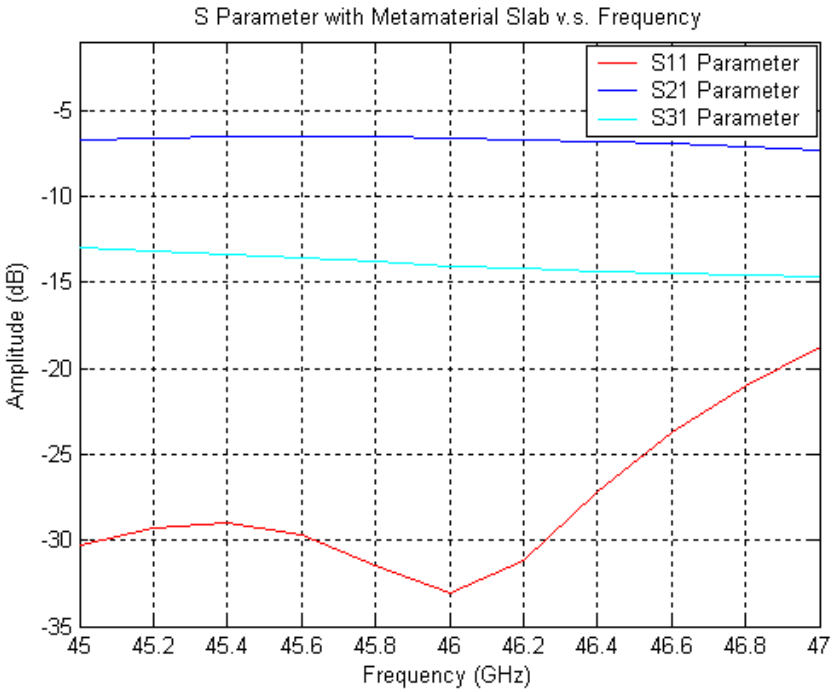

(a)

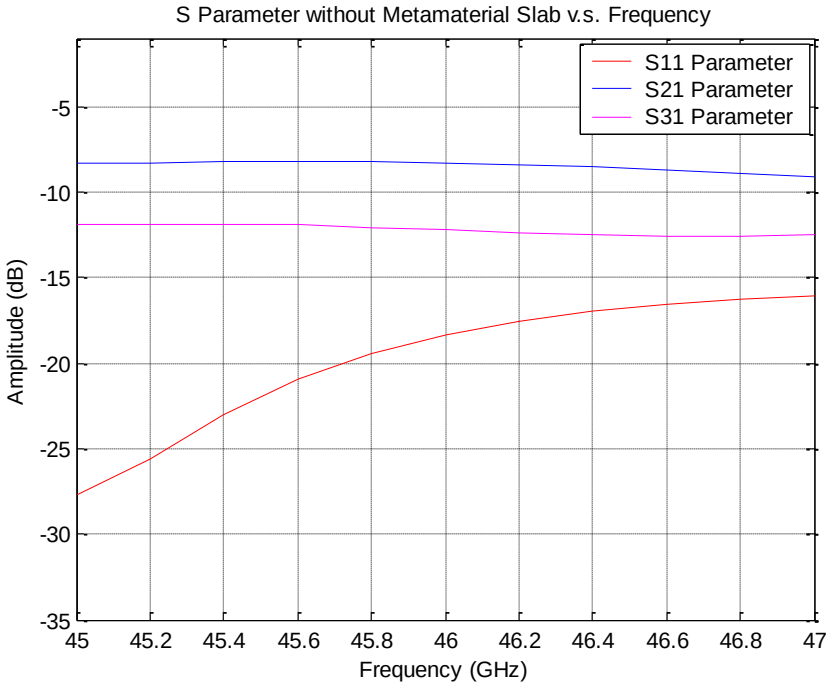

(b)

Figure 3.5 (a) S parameters for coaxial line feed probes with metamaterial slab presence (b) S parameters for coaxial line feed probes without metamaterial slab presence.

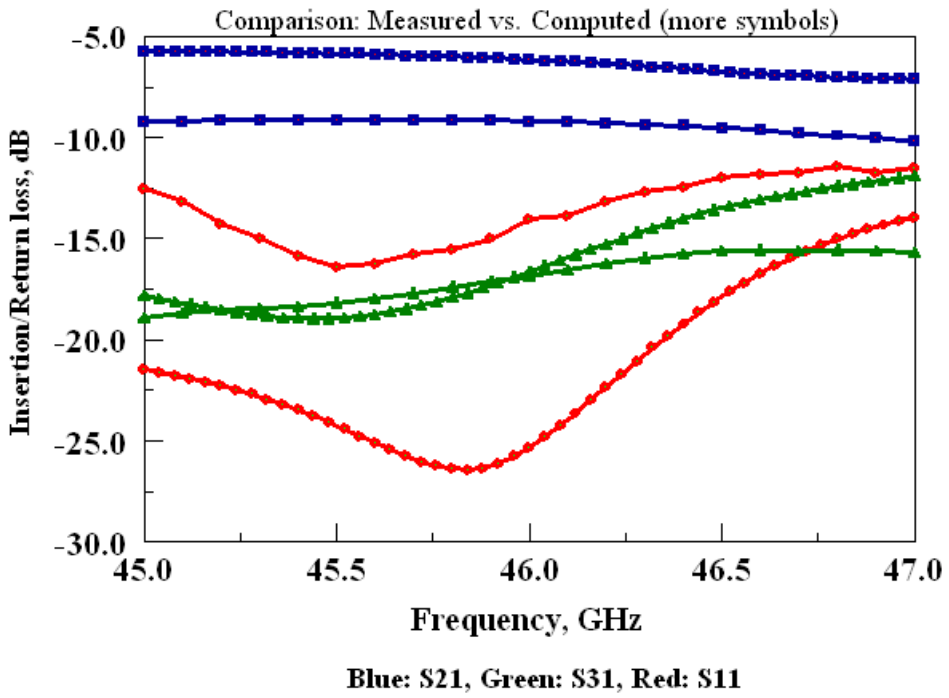

Figure 3.6 Prior simulation and measurement results obtained by A. Zaghloul et al. [15]

3.3 Rectangular Waveguide Excitation

The resonance itself does not help enough to explain how incident wave will perform under the influence of metamaterial from the negative refraction point of view. Besides, the incident wave created by coaxial cable feed is more like field excited by dipole, which does not have narrow beam width. When we consider the refraction or focusing effects, which the metamaterial brings to us, we want the incident wave to be in the form of narrow beam.

In order to create narrow beam width incident wave, waveguide is one option for its relatively easy design. In this section, rectangular waveguide will be used as an aperture antenna to create narrow-beam-width incident wave. There are two types of waveguides: TE mode and TM mode waveguide. For simplicity of the design, we only consider TE_{10} mode waveguide. Since the waveguide will be feeding a parallel-plate structure, its

dimensions need to be as small as possible in order to achieve far field effect inside the test bed. The dimension of the rectangular waveguide is usually represented by its width *a* and height *b*. The cut off frequency of TE_{10} mode waveguide with width a and height b can be represented as

$$f_{c10} = \frac{1}{2a\sqrt{\mu\varepsilon}} \tag{3-1}$$

The expected waveguide working frequency will be at 45 GHz, so the waveguide cut off frequency needs to be less than this value. From (3-1), we will have that the width *a* has to be greater than 2.25 mm. Since waveguide is filled with the dielectric material which has a relative permeability ε_r = 2.2, the match between waveguide and dielectric medium is also important. We take *a* = 3.3 mm and *b* = 1.1 mm, in this case the cut off frequency of waveguide will be 30.62 GHz per (3-1), and the wave impedance of waveguide at 46 GHz will have

$$Z = \frac{\eta}{\sqrt{1-(f_c/f)^2}} = \frac{\eta}{\sqrt{1-(30.62/46)^2}} \approx 4\eta/3 \tag{3-2}$$

The reflection coefficient between waveguide and dielectric medium can be written as

$$\Gamma = \frac{Z_1 - Z_2}{Z_1 + Z_2} = \frac{4/3 - 1}{4/3 + 1} = \frac{1}{7} \tag{3-3}$$

The reflection coefficient at 46 GHz is about -8.5 dB, which can be considered as a decent match between waveguide and surrounding medium. In the previous section, we mentioned the test bed for coaxial cable feed. Here we replace the coaxial cable feed with rectangular waveguide feed, and use simulation to obtain S parameters for metamaterial slab. The calculated S parameters are shown in Figure 3.7. As expected, S11 magnitude has a dip of -14.3 dB around 47 GHz, which suggests that CLL-P slab achieves resonance

at this frequency. Compared with result obtained from coaxial cable feed, we noticed that there is a resonance frequency shift; which can be attributed to difference of the wave impedance caused by different feeding methods in FEKO.

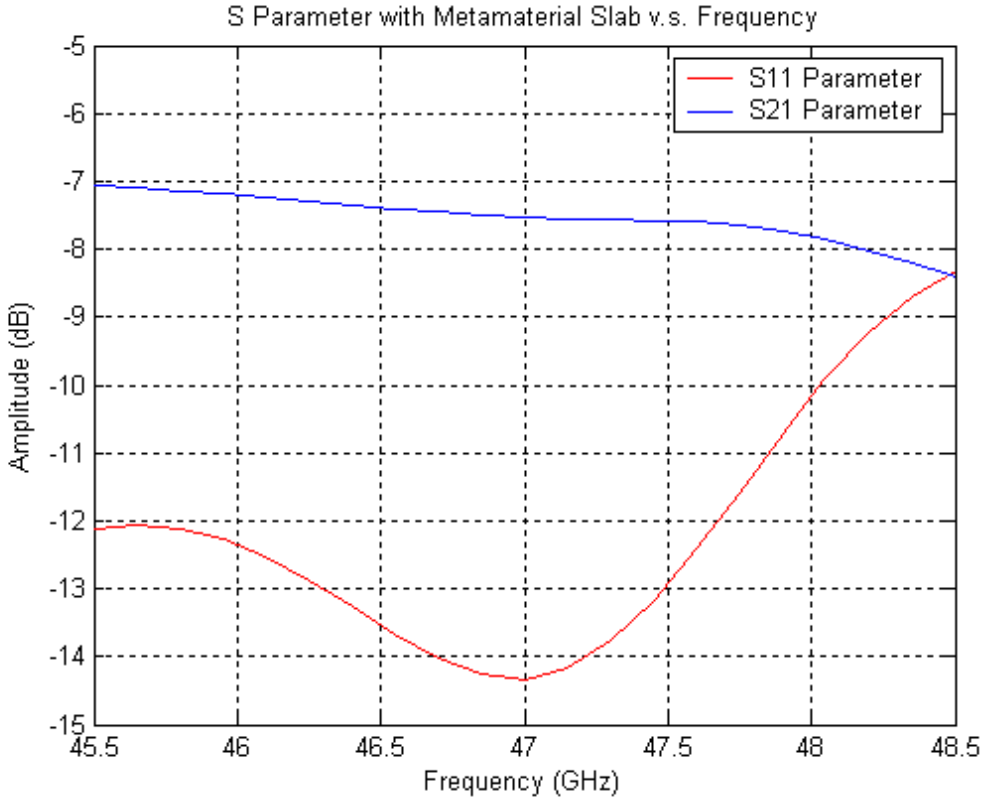

Figure 3.7 Simulated S parameters for metamaterial slab with waveguide excitation.

The system losses including conductor and dielectrics losses can be calculated from S parameters through following formula:

$$Loss\ (dB) = 20 * \log 10 (\sqrt{|S_{11}|^2 + |S_{21}|^2}) \qquad (3\text{-}4)$$

And the system loss is shown in Figure 3.8.

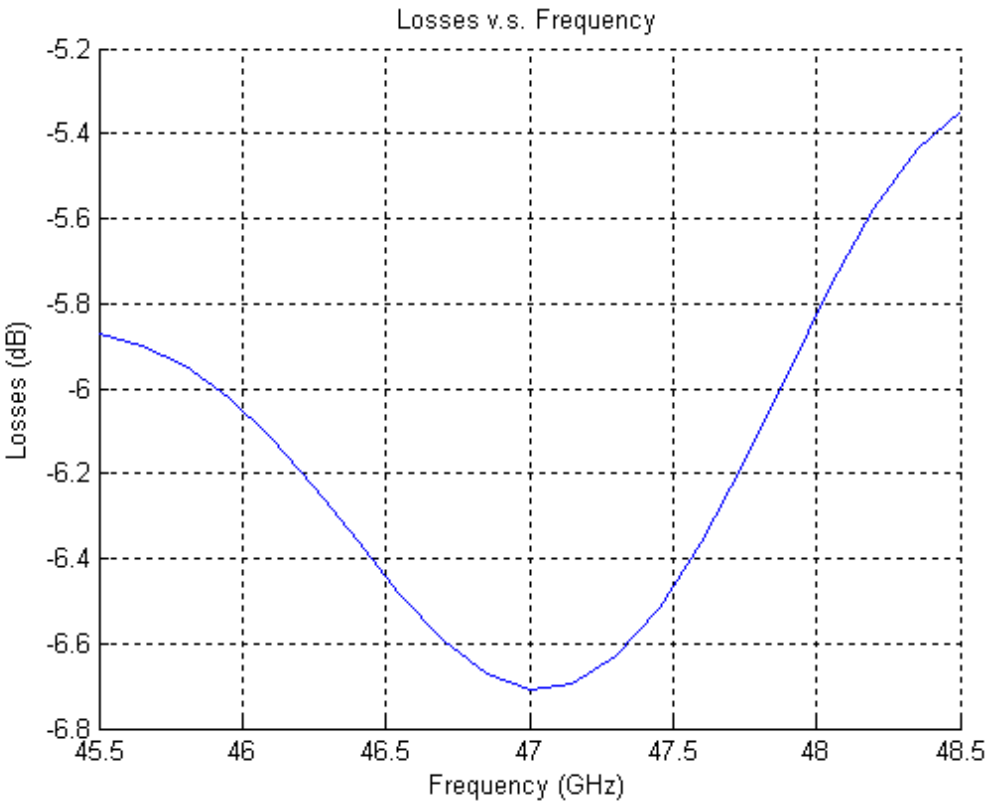

Figure 3.8 System losses for metamaterial slab with waveguide excitation.

From Figure 3.8, we can see that the system losses will have the minimum value around resonance frequency. This is what is expected; the metamaterial will have small losses at working region (around resonance frequency). For comparison, Figure 3.9 also illustrates the return losses and system losses for the test bed without metamaterial . As we can see that the resonance frequency has been shifted to left side by 0.75 GHz when there is no metamaterial slab in the test bed, and the resonance band is relatively broader than the case with the metamaterial.

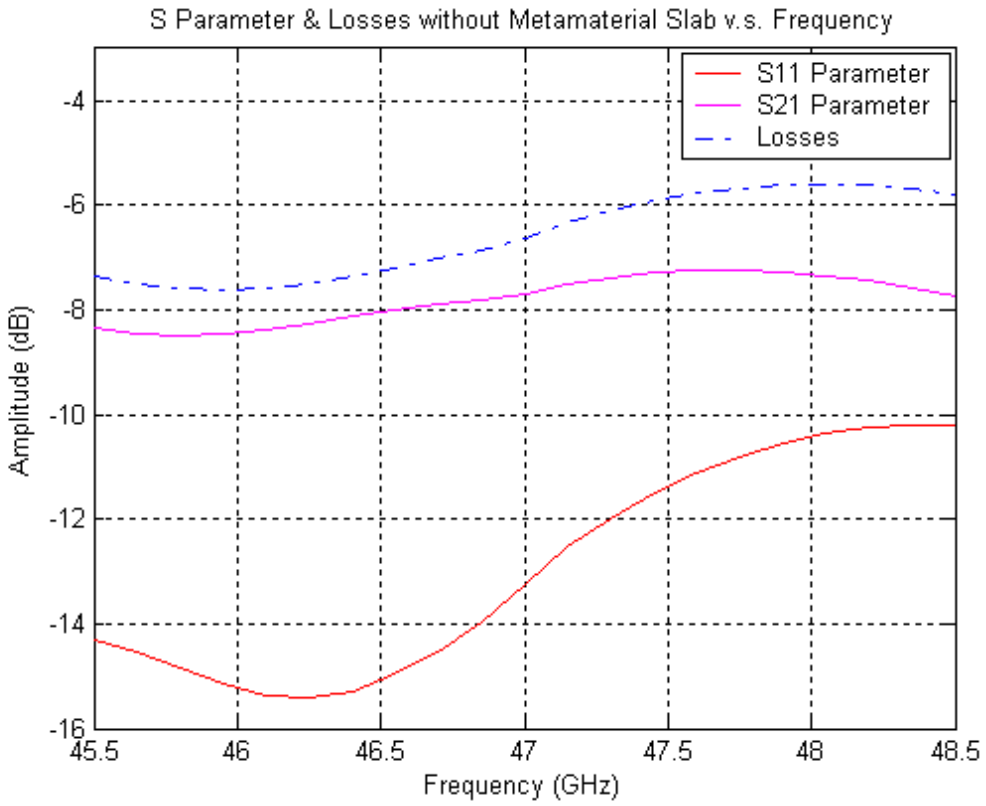

Figure 3.9 Return Losses and System losses for dielectrics slab with waveguide excitation.

To have a better understanding on how the metamaterial affects incident wave, we also can look at the field intensity distribution inside the waveguide. In [5], Pendry mentioned the possibility to make perfect lenses by using the metamaterial, which is, the incident waves diverge from a point source can be re-focused inside the metamaterial slab if the distance from point source to the first interface of metamaterial slab and the width of metamaterial slab are well chosen. Figure 3.10 is electric field intensity distribution at $z = 0$ plane of the test bed. On the left side of the test bed, it is the waveguide which provides TE_{01} mode excitation. The distance between waveguide center plane and the first interface of metamaterial slab is 250 mils.

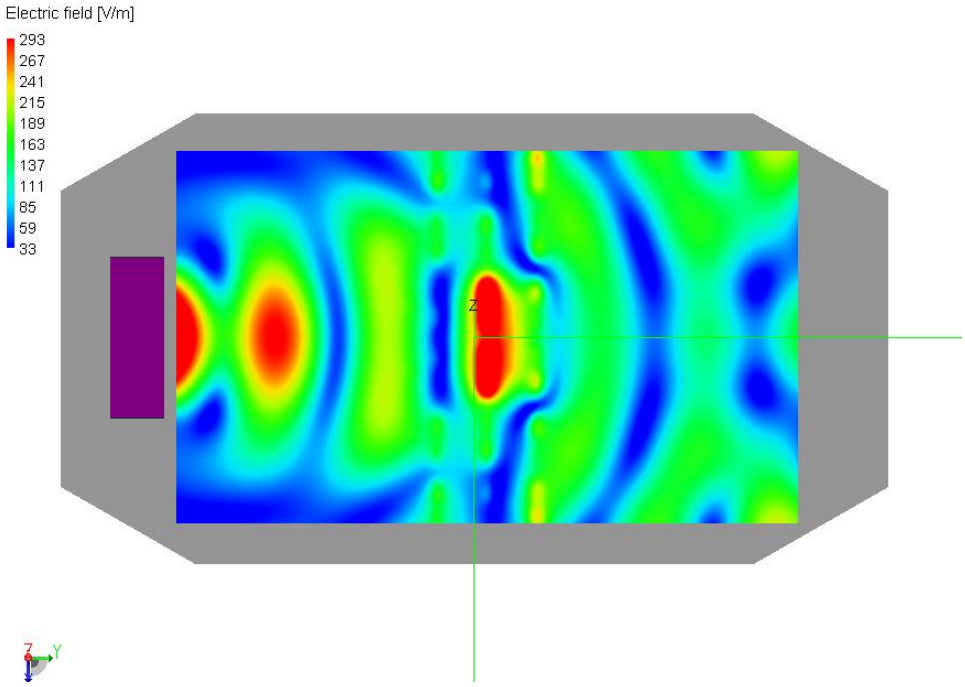

Figure 3.10 Electric field intensity at *z* direction (*z* = 0) with metamaterial showing focusing effect.

This distance can be considered as far field since it is much greater than $2D^2/\lambda$, thus the waveguide excitation can be regarded as a point source, which is further confirmed by Figure 3.10. Before the incident wave reaches slab, the wave is diverging from waveguide, and the wave front is sphere like shape. Once the wave hits the metamaterial slab (y = -50 mil), the ray start to converge, and focuses at y = 0 mil. After the foci, they begin to diverge again. As a comparison, Figure 3.11 shows $\boldsymbol{E_z}$ intensity at z = 0 when the metamaterial slabs are replaced by dielectric medium, it is not surprising that there is no focus effect happening at y = 0. There is a spot at right side of the parallel-plate waveguide with relatively high intensity value, it cannot be considered as a focus point due to the effect of diffraction and reflection existed close to the edge of the test bed.

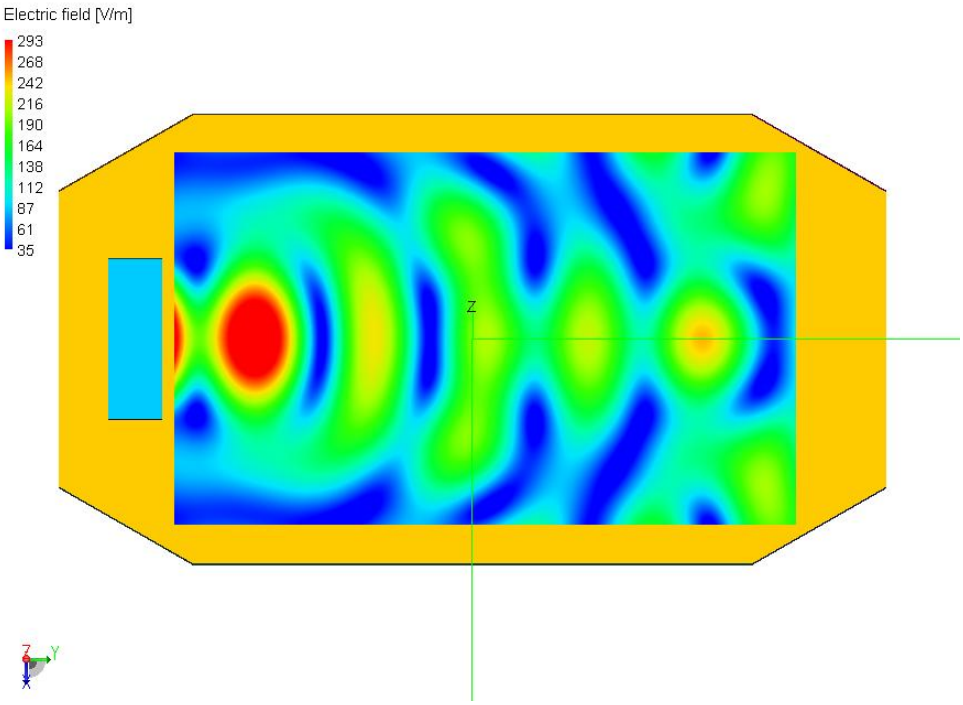

Figure 3.11 E_z field intensity distribution at z = 0 without metamaterial.

For the perfectly matched metamaterial with ε = -2.2 and μ = -1, the incident wave should form the second focus point at the right side of the test bed. The distance from the second focus point to the second interface of the metamaterial slab should be the same as the distance between waveguide source and the first interface of the metamaterial. However, it is difficult to demonstrate this in Figure 3.10. There are two possible reasons that contribute to this: 1) there is the reflection happening at the boundary of the parallel-plate waveguide; due to mismatch between free space and dielectrics inside the waveguide, the wave will bounce back once it hit the dielectrics boundary; 2) the metamaterial slab does not match with the dielectrics inside parallel-plate waveguide perfectly, and the exact image of the point of source can not be built due to losses caused by mismatch losses.

3.4 Planar Wave Excitation

From electric field intensity distribution at z = 0 plane, it clearly indicates that there is focus effect caused by metamaterial slabs. However we need to be very careful when we

approach this problem with consideration of the near field effect. There are a number of researchers who are questioning the methodology of negative refraction index experiments and measurements. The argument is that the location of the metamaterial is within the near field range of excitation. Since the electromagnetic waves are very active and not stable in near field, it is very difficult to prove that the focus effect shown in Figure 3.10 really caused by negative refraction or just unstable nature of near field. In order to conquer this, we need to have an excitation of source that is independent of the dimension of excitation; the excited fields are stable, and can be considered as far field in the area of interest. This is more like the far field of dipole antenna, whose wave fronts are infinite parallel planes of constant amplitude normal to the phase velocity vector. This reminds us of the planar wave, which has all the characteristics mentioned above. Planar wave excitation is one of excitations implemented in FEKO, where the planar wave is excited from infinite far field.

The parallel-plate waveguide discussed in previous sections are still used here as test bed, and the only difference is that the waveguide excitation is replaced by the planar wave excitation. Figure 3.12 shows the electric field intensity distribution along $z = 0$ plane for the normal incident planar wave with vertical polarization. As a comparison, Figure 3.13 illustrates the case when CLL-P slab are replaced by dielectric slab. At the first look of two figures, we may conclude that both patterns are similar, and there are no much differences between them.

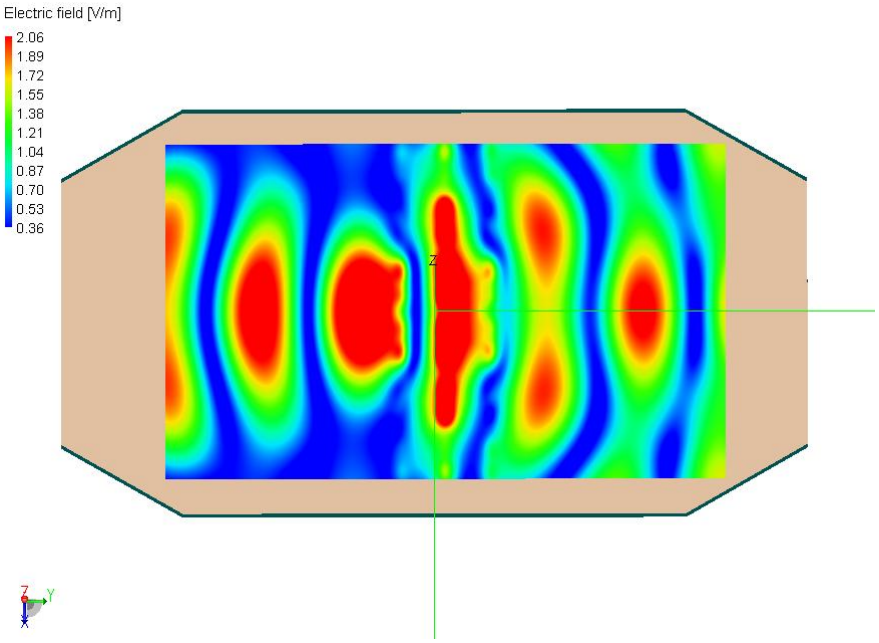

Figure 3.12 E_z field intensity distribution at $z = 0$ plane with normal incident planar wave on metamaterial slab.

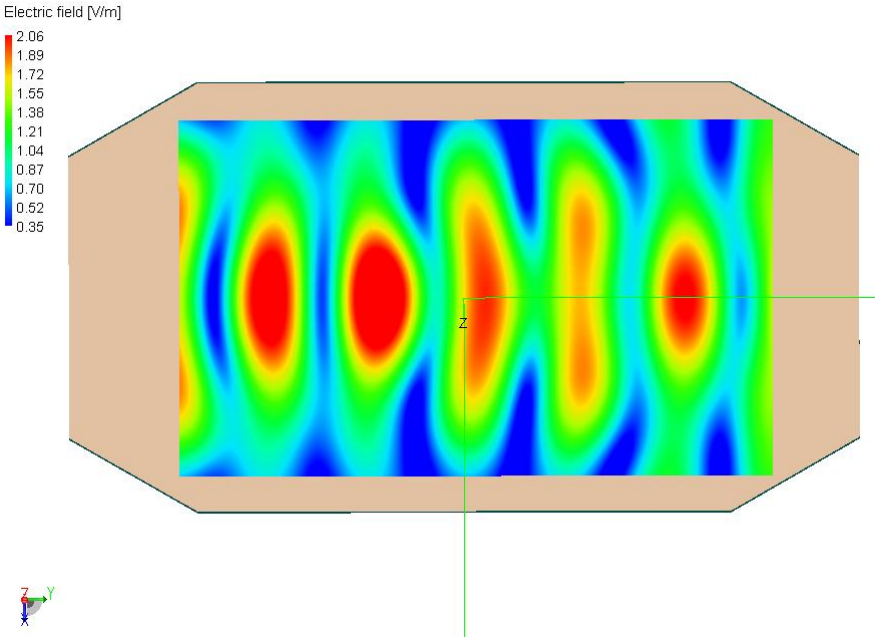

Figure 3.13 E_z field intensity distribution at $z = 0$ plane with normal incident planar wave on dielectrics.

However after a careful observation, we will find field intensity is much stronger at $y = 0$, as well as for the area $y > 0$ when CLL-P slabs are inside the parallel-plate

waveguide. This could be attributed to the focus effect caused by CLL-P slabs. The focus effect that the metamaterial has is the result of negative refraction. In the test bed that has CLL-P slabs, the refracted wave is on the opposite side in a direction normal to the interface, compared with the test bed that has no CLL-P slabs inside.

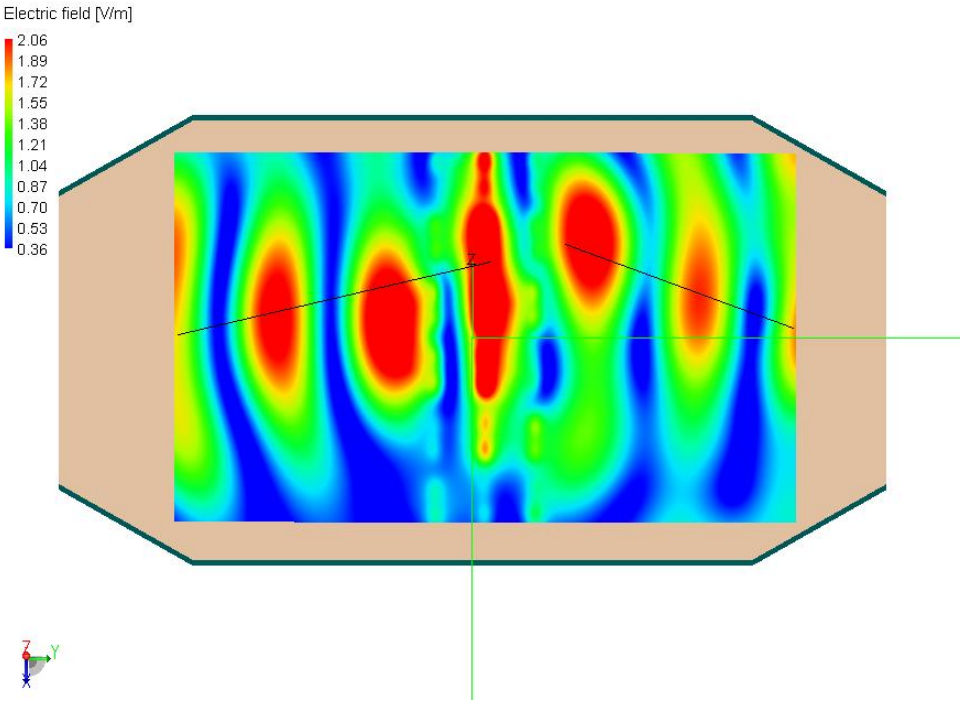

Figure 3.14 E_z field intensity distribution at z = 0 plane with 10 degree oblique angle incident planar wave on CLL-P slab.

Similar observations are made when the incident wave is at oblique angle. Figure 3.14 clearly indicates what happens when waves with oblique incident angle pass though the metamaterial slab. The black line in Figure 3.14 is marked to represent the propagation direction of the incident and scattering wave. Before the wave reaches the CLL-P slab interface, it travels along the direction with 10 degrees off the y axis, when it gets to CLL-P slab, the refraction happens. It is hard to quantify how much refraction we have here since the scattering waves are also affected by reflection and diffraction of the test bed boundary. This can be compared it with Figure 3.15, which is the E_z field intensity distribution at z = 0 plane without CLL-P slab. In this figure, we can observe that the scattering wave direction is also bent toward the bottom at right side, indicating a likely negative refraction. However this is caused by the reflection at the edge of the test

bed due to its limited size. One thing can be confirmed is that wave direction is bent more with CLL-P slab than without the CLL-P slab. This could suggest that negative refraction happens when incident wave enters and exits out of the CLL-P slab.

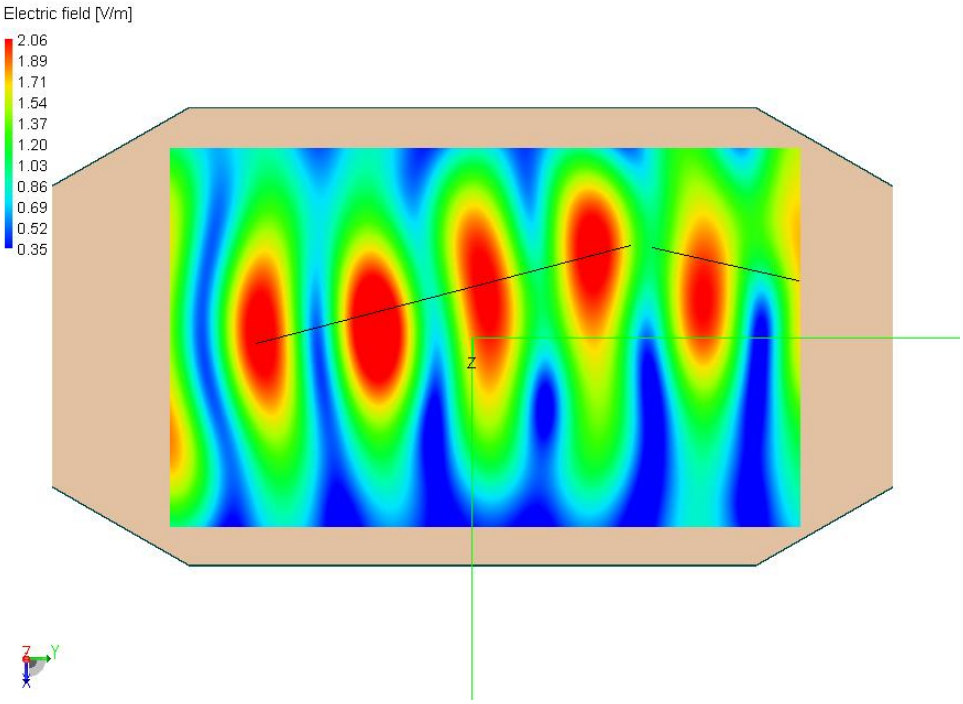

Figure 3.15 E_z field intensity distribution at z = 0 plane with 10 degree oblique angle incident planar wave on dielectrics.

Chapter 4 Characteristics of CLL-P Slab

4.1 Introduction

In previous chapters, we discussed simulation results of CLL-P slab in the parallel-plate waveguide. Through the comparison of two different scenarios: simulations with CLL-P slab and without CLL-P slab, we know that the negative refraction happens when the incident waves enter CLL-P slab. This is observed by simulation at normal and 10 degrees to normal incident angle. As a direct result of negative refraction, the waves will be focused at one point after travelling certain distance inside the CLL-P slab, and diverge again and form the second focus point after waves leave CLL-P slab. This agrees with the description about metamaterial made by J. B Pendry [5]. It shows that CLL-P loop-plus-post periodic structure is one type of metamaterial, which has the characteristics of negative refraction feature.

However the simulation result is not enough for us to answer the following questions on the metamaterial: What is the refractive index value if the negative refraction effect exists in the CLL-P slab? What are the effective permittivity and permeability of the CLL-P slab? Is the CLL-P slab an isotropic medium in terms of refraction characteristics? What are the losses of CLL-P slab? The answers to these questions can help us not only understand the features of metamaterial but also develop potential applications of metamaterial. In this chapter, an effort will be made to answer these questions. First we will develop some methodology to simulate the refractive index, and compare the refractive indexes for different arranged (including parallel, vertically and cross-arranged) CLL-P slabs at different incident angles, so that isotropic identity can be decided for those structures. We will also make elaborations on how to obtain effective permittivity and permeability of the metamaterial, because those two characteristic parameters should be simultaneously negative in order to have negative refraction based on V. G. Veselago's work in [1]. Lately, we will discuss the mismatch losses the simulation model has, and some simulation results at Ku-band.

4.2 Calculation of Refractive Index

In Chapter 3, all simulation results are obtained from the parallel-plate waveguide test bed that is filled with dielectrics. The disadvantages of this test bed result from two factors: the reflections and diffractions occurred at waveguide boundary affect the accuracy of simulation result due to the limited size of test bed; more software memory is consumed due to filled dielectrics inside parallel wave guide with the increase of waveguide dimension. In order to overcome this and simplify the process, all the simulations in this chapter are carried in vacuum, which means background is free space.

The refractive index of metamaterial has been discussed in several papers. Among them, Derov[11] mentioned the way to calculate it for wedge shaped metamaterial slab. Wedge shaped metamaterial slab is a popular model used by many refraction experiments and measurements, and Figure 4.1 shows the top view of prism like slab used in [11]. In his experiment, Derov used narrow beam width (14 degree of 3 dB beam width) horn antenna as transmitting and receiving antenna, and let incident wave enter prism normally, and measured maxima point at the other side of prism. Due to existence of apex angle, the incident wave will be refracted away from normal, and fall into either side of the normal plane of the prism exit faces depending on the characteristics of the prism.

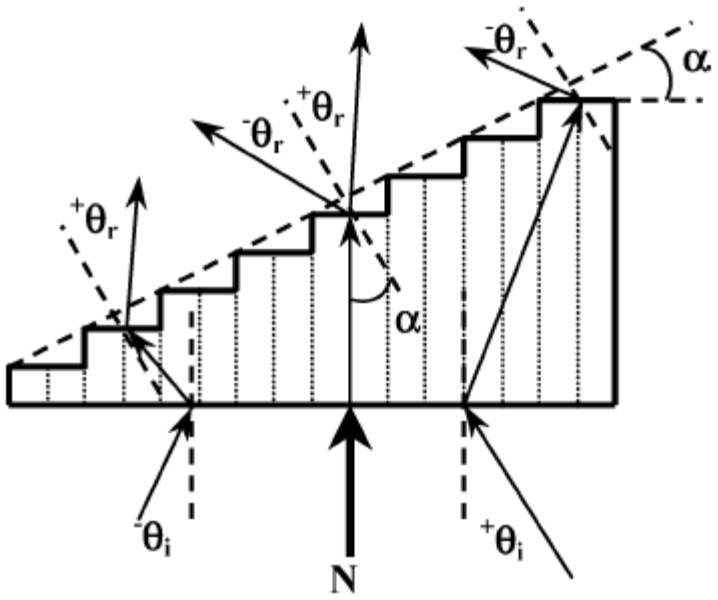

Figure 4.1. Top view of wedge shaped metamaterial slab used by J. S. Derov [11].

Based on Snell's Law, Derov used the measurements and calculated refractive indexes for different type of CLL-P slabs. In Derov's work, he made two assumptions: the refractions happened on both entrance and exit faces follow Snell's Law; and the refractive indexes are the same on both faces. Through the calculation, Derov found that the refractive index are almost same for different incident angles. Thus he concluded that the refraction behavior of metamaterial is almost isotropic. However, we notice that there is difference on how the CLL loops are arranged between entrance and exit face, we may not be able to make such assumption that the refractive indexes are equal when waves enter entrance face and leave exit face. In this thesis, instead of building the wedge shaped prism of metamaterial, we will use rectangular metamaterial slab. Based on the rectangular metamaterial slab, we can develop a way to calculate refractive index. Considering the case shown in Figure 4.2, a planar wave or narrow beam wave started from source travels a certain distance and enters metamaterial slab with an oblique angle θ_i. Due to negative refraction on the entrance face, the incident wave will be travelling towards a direction with angle θ_r to normal face. Once travelling wave hits the exit face

with same angle θ_r, it will have the second refraction. Due to entrance and exit planes being parallel, the wave that left the exit face will be parallel with the incident wave started from source. This means that the exit wave will have an angle of θ_i as illustrated in Figure 4.2.

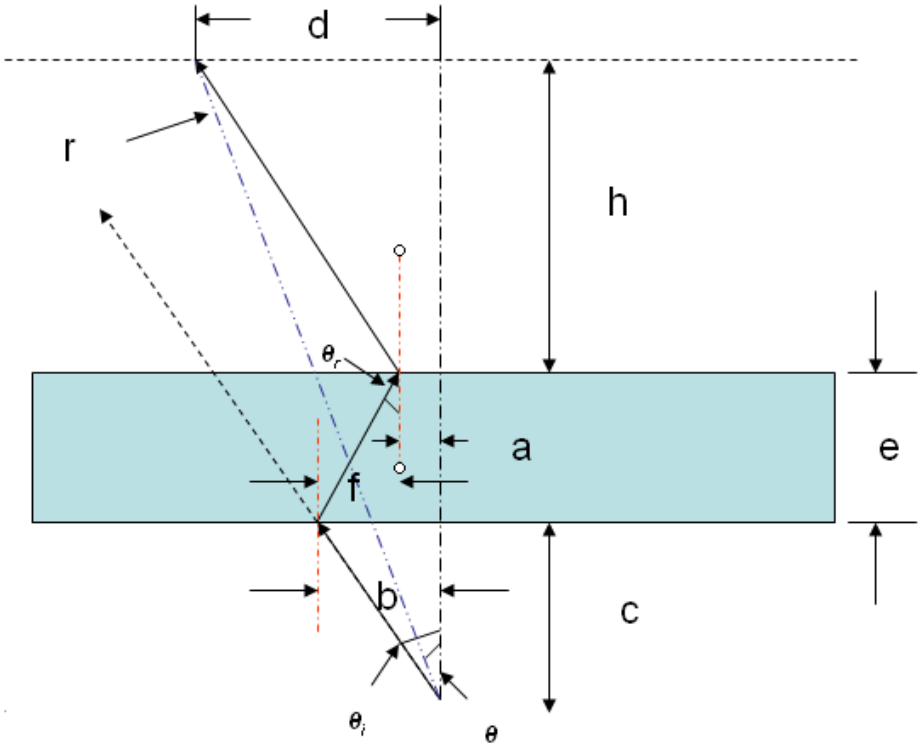

Figure 4.2 Negative refraction happened on a rectangular metamaterial slab.

At the receiving side, we assume that we can get the strongest electric field intensity or peak power at a certain direction, which has an angle θ with the source. In the simulation and experiment, other parameters except the refraction angle θ_r are known. Through certain geometric relationships, θ_r can be deducted from other known parameters. We take the example shown in Figure 4.2, and have following assumptions: the thickness of metamaterial slab is *d*, the distance from source to slab is *c*, and the distance between source and probe location, where the strongest electric field intensity is received, is *r*. The horizontal distance of incident wave traveling inside metamaterial slab, denoted as *f*, can be expressed by following formula through geometry.

$$f = c * \tan(\theta_i) - (r * \sin(\theta) - (r * \cos(\theta) - c - e) * \tan(\theta_i)) \quad (4\text{-}1)$$

If we use layout shown in Figure 4.2 in x-y plane of Cartesian coordinate system, and let the source correspond to origin point. The distance *f* should be negative since negative refraction happened. Once the distance *f* is calculated, we can decide the refraction angle by

$$\theta_r = \arctan(f / e) \quad (4\text{-}2)$$

Since *f* has negative value, the refractive angle θr will also have negative value, which means that the refractive and incident wave will be at the same side of incident normal face. Equation (2-13) gives the way to calculate refractive index in medium 2 (metamaterial) given that incident angle θ_i, refractive angle θ_r, and refractive index in medium 1 are known. And the refractive index of metamaterial slab can be represented by (4-3) given that medium 1 is free space.

$$n_2 = n_1 * \sin(\theta_i) / \sin(\theta_r) = \sin(\theta_i) / \sin(\theta_r) \quad (4\text{-}3)$$

It is not difficult to know that n_2 will also have negative value due to negative value taken by θ_r.

In refractive index experiment, a couple of factors can affect the result accuracy: beam-width of incident wave and the locations of excitation source and receiving probe. In order to avoid near field effect, the CLL-P slab needs to be posed in far field of the source. And the receiving probe is located along a circle which has the source at its center. To achieve narrow beam-width, horn or waveguide excitations are usually considered to be acceptable. In this simulation, we use waveguide as our excitation, the CLL-P slab is 210 mils away from waveguide excitation plane. This distance is much greater than $2*D^2/\lambda$, and the receive probes are 1000 mils away from waveguide center point. Figure 4.3 shows the E_z electrical field intensity at 1000 mils when waveguide is at 30 degree from normal.

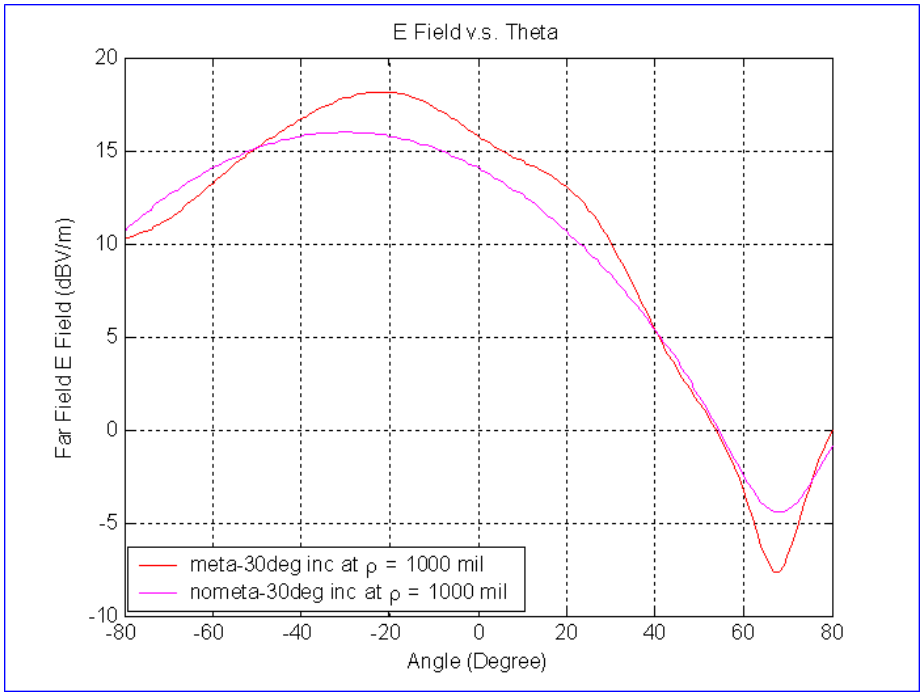

Figure 4.3 *Ez* field intensity at ρ = 1000 mil when waveguide is 30 degree from normal face.

In the figure, the red color represents the field intensity when parallel CLL-P slab is presented, and the pink color represents the field intensity when CLL-P slab is replaced by surrounding medium or free space. The field has a peak at 22 degree to normal, compared to the case without CLL-P slab, where the field maximum is at 30 degrees. The shift is due to the negative refraction. Using formula (4-3), the calculated refractive index is -0.79, this value aligns with typical refraction index of metamaterial that ranges from -1.4 to -0.6. Another observation from Figure 4.3 is that the peak field strength with CLL-P slab is greater than the peak value without CLL-P slab; this can be attributed to the focus effect which the metamaterial has. By changing waveguide incident angles, the relationship between refractive index and incident angles can be obtained and posted in Figure 4.4

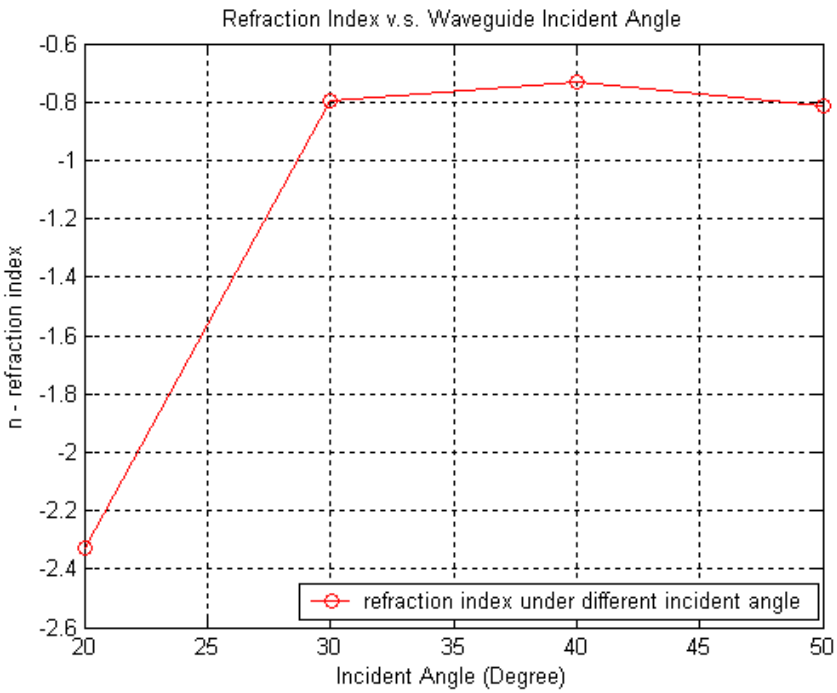

Figure 4.4 Calculated refractive index versus different waveguide incident angle (Waveguide TE_{10} mode).

From Figure 4.4, we notice that the refractive index varies slightly around -0.8 in the range of 30 ~ 50 degree for the incidence angles. Due to the limitation of test bed dimension, we do not include the result above 50 degree, where edge diffraction will affect the accuracy of results. The refractive index at 20 degree is shifted away from others.he The difference of refractive index at close-to-normal incidence angles indicate that the waveguide excitation might not be the best choice for such problem: the main beam of excited wave is not narrow enough, and results could be skewed by the relatively broader beam width. We also show field distribution for $z = 0$ plane with CLL-P slab at 30 degree incidence angle in Figure 3.5. We can see that incident wave is shifted toward the bottom due to negative refraction.

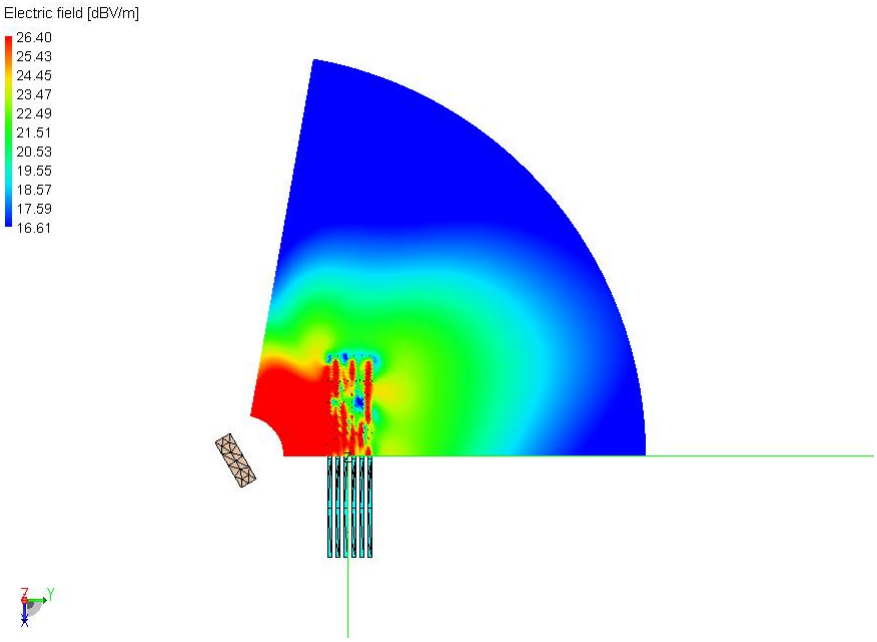

Figure 4.5 *Ez* field intensity distribution at *z* = 0 plane with CLL-P slab at 30 degree incidence angle.

This negative refraction effects are more obvious in the Figure 4.6(a) and Figure 4.6(b), which are the field distribution at 40 and 50 degree incidence angle. In Figure 4.6(b), we also can observe that the diffraction happens and causes the main beam tilt due to an incidence angle close to edge of the CLL-P slab.

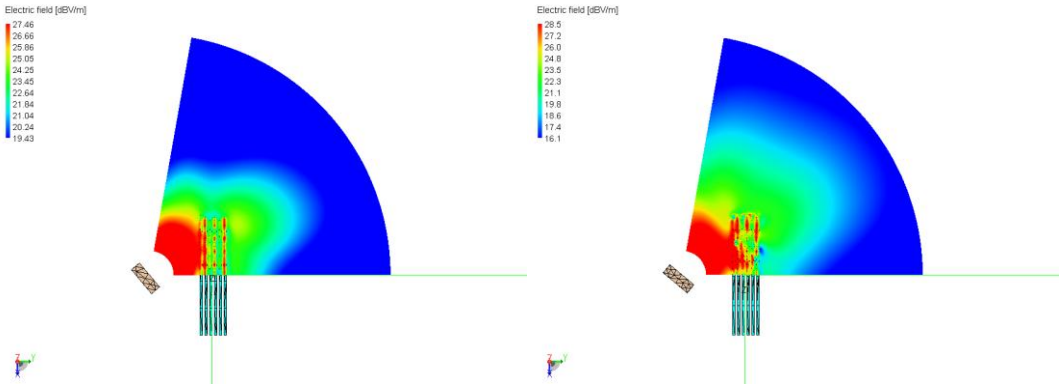

Figure 4.6 (a) E_z field intensity distribution at *z* = 0 plane with CLL-P slab at 40 degree incident angle. (b) E_z field intensity distribution at *z* = 0 plane with CLL-P slab at 50 degree incidence angle.

4.3 Calculation of Permittivity and Permeability

The cause of the negative refraction lies in the simultaneously negative permittivity and permeability that the metamaterial has. In other word, if we see negative refraction effect, it suggests that the medium has the negative permittivity and permeability. However the study of those two characteristics is not emphasized in metamaterial research. The effective permittivity and permeability are highly frequency dependent, and the knowledge of those two parameters is helpful for impedance match and reduction of medium loss. Usually permittivity and permeability are not easy to obtain directly, and need to be calculated through other parameters. Those parameters include wave impedance and refractive index, and we can use $\varepsilon = n / z$ and $\mu = n * z$ to calculate permittivity and permeability. The wave impedance and refractive index can be obtained through transmission and reflection coefficients, which further can be converted from S parameters. S parameters are often easily obtained either in numerical simulations or measurements. Also the S parameters are highly frequency dependent, which further determines the frequency dependent nature of the permittivity and permeability.

Let us look at the rectangular CLL-P slab we discussed before. To simplify the problem, we treat the slab as 1D problem. We assume that the slab has a width of *d*, and corresponding wave impedance and refractive index are *z* and *n* respectively. The transmission coefficient has following relationship with n and *d*:

$$t = \frac{1}{[\cos(nkd) - \frac{i}{2}(z + \frac{1}{z})\sin(nkd)]e^{ikd}} \tag{4-4}$$

where $k = \omega/c$ is the wave number of the incident wave.

The reflection coefficient can be represented through transmission coefficient by

$$\frac{t}{\exp(ikd)} = -\frac{1}{2}i(z - \frac{1}{z})\sin(nkd) \tag{4-5}$$

Two variables *n* and *z* exist in equation (4-4) and (4-5), and can be solved through combining those two equations. The refractive index can be written as

$$\cos(nkd) = \frac{1}{2t'}[1-(r^2 - t'^2)] = \mathrm{Re}(\frac{1}{t'^2}) - \frac{1}{2|t'|^2}(A_1 r + A_2 t') \tag{4-6}$$

where $t' = t\exp(ikd)$, $A_1 = r * t' + t' * r$ and $A_2 = 1 - |r|^2 - |t'|^2$. Both A_1 and A_2 are real values and will be zero in lossless medium. Similarly the impedance *z* can be represented by following formula

$$z = \pm\sqrt{\frac{(1+r)^2 - t'^2}{(1-r)^2 - t'^2}} \tag{4-7}$$

Through the expression of (4-7), we know that the impedance is a complex number and has two branches. Whichever branch is taken from the expression should match the characteristics of material, we know that CLL-P slab is a passive medium that should have a positive impedance, so the requirement of Re(*z*) > 0 should be met. If we further simplify (4-6), the imaginary part and real part of refractive index can have following formats.

$$\mathrm{Im}(n) = \pm\,\mathrm{Im}(\frac{\cos^{-1}(\frac{1}{2t'}[1-(r^2 - t'^2)])}{kd}) \tag{4-8}$$

and

$$\mathrm{Re}(n) = \pm\,\mathrm{Re}(\frac{\cos^{-1}(\frac{1}{2t'}[1-(r^2 - t'^2)])}{kd}) + \frac{2\pi m}{kd} \tag{4-9}$$

where *m* is a integer, and the requirement of Im(n) > 0 should be met when we consider which branch we need to take. As discussed before, the transmission and reflection

coefficients are relatively easier to obtain given that S parameters are available, which can be written as following:

$$t = s_{11} - \frac{s_{12} * s_{21}}{(1 + s_{22})} \tag{4-10}$$

and:

$$r = 1 - t \tag{4-11}$$

Now we have built a way to calculate the effective permittivity and permeability through scattering parameters, which are quite easier to obtain through either numerical simulations or measurements.

The planar wave is usually considered as better excitation for metamaterial since target material is definitely in far field of excitation and unstable near field effect can be eliminated. In our simulation, a new type of cross-arranged CLL-P slab, which is shown in Figure 4.7, has been built. And the drawing of a unit cell is listed in Figure 4.8.

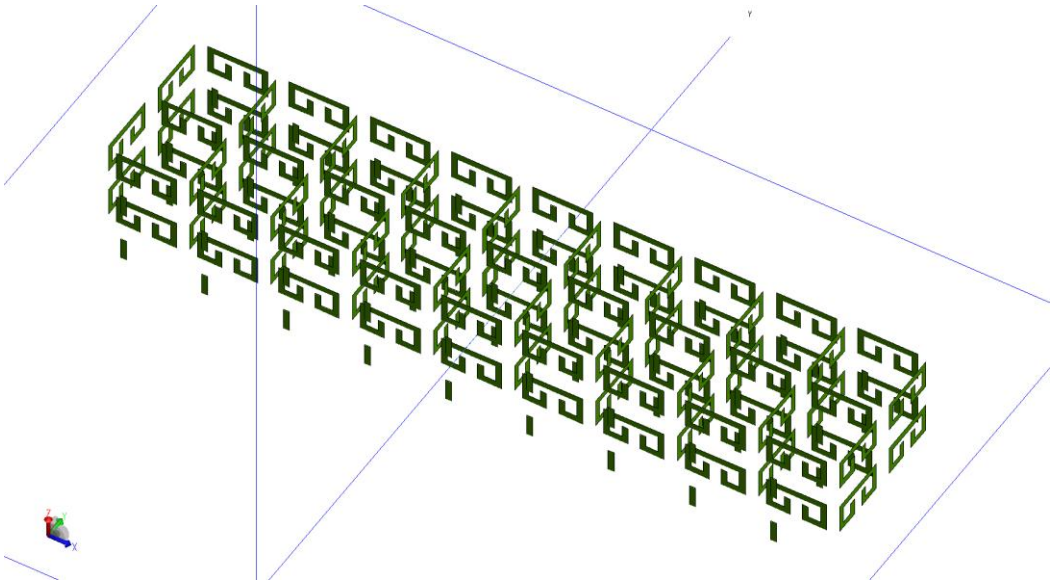

Figure 4.7 Sketch of cross-arranged CLL-P slab.

The dimension of CLL loop is the same as what we used in Chapter 3 (Figure 3.2). Four CLL loops arranged in both vertical and horizontal directions; a printed dipole lies in the middle of four cells, and equally distant to each CLL loop. The distance between front and back cell is 50 mils, and the distance between left and right cell is 54 mils. The advantage of this design is that it makes CLL-P slab more like an isotropic media. When incident wave with vertical polarization reaches the dipole, the dipole with same direction as polarization will create strong push-push current on all four CLL loops that surround it. Thus a magnetic field which extends to all direction will be created from four CLL loops.

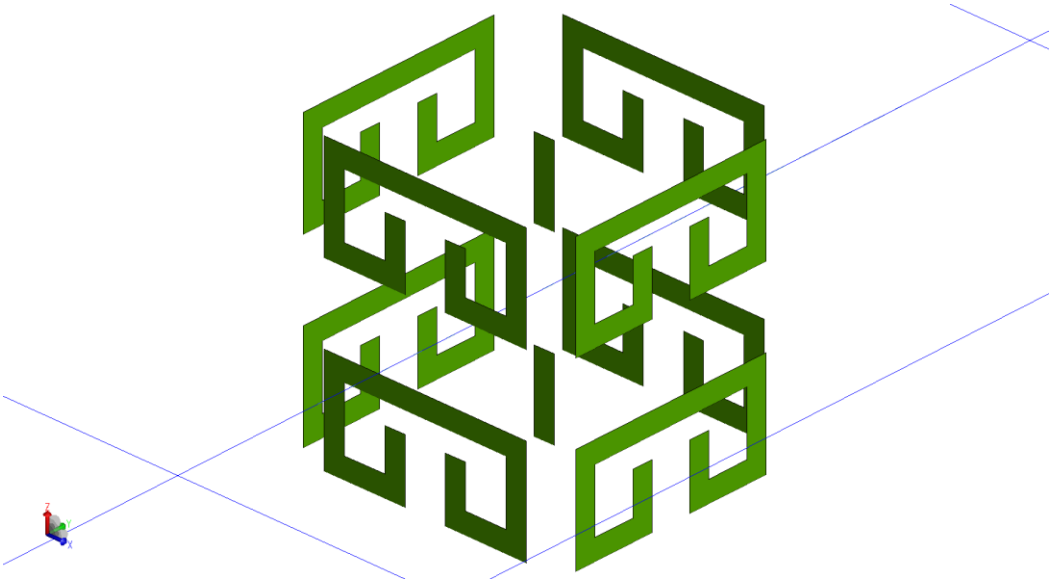

Figure 4.8 Unit cell of cross-arranged CLL-P slab.

Due to layout change of CLL loops, the resonance frequency of CLL-P slab will change accordingly. Figure 4.9 shows S11 amplitude in dB, it clearly shows that the return loss achieve minimum value (-8.8 dB) at 53.4 GHz, and indicates that CLL-P slab achieves resonance at that frequency. Using FEKO numerical analysis, complex S parameters can be obtained. With the approach specified by (4-8) to (4-11), and d = 125 mil; we can calculate the effective permittivity and permeability of the cross-arranged CLL-P slab around resonance point, which are shown in Figure 4.10 to 4.13. From the

effective parameters shown in those figures, we can see that real part of relative permittivity and permeability achieves negative values around resonance frequency.

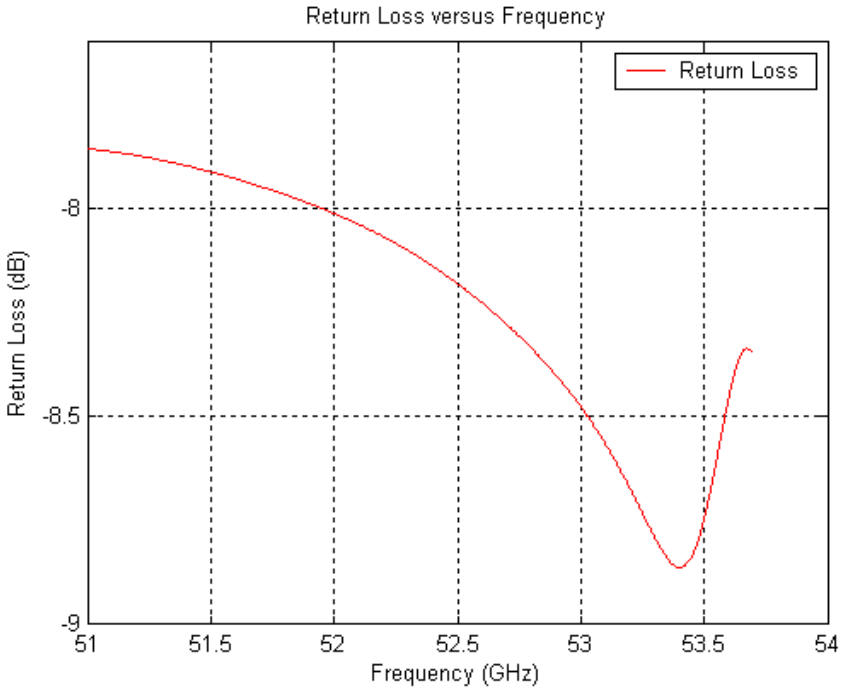

Figure 4.9 Return losses for cross-arranged CLL-P slab at different frequency point.

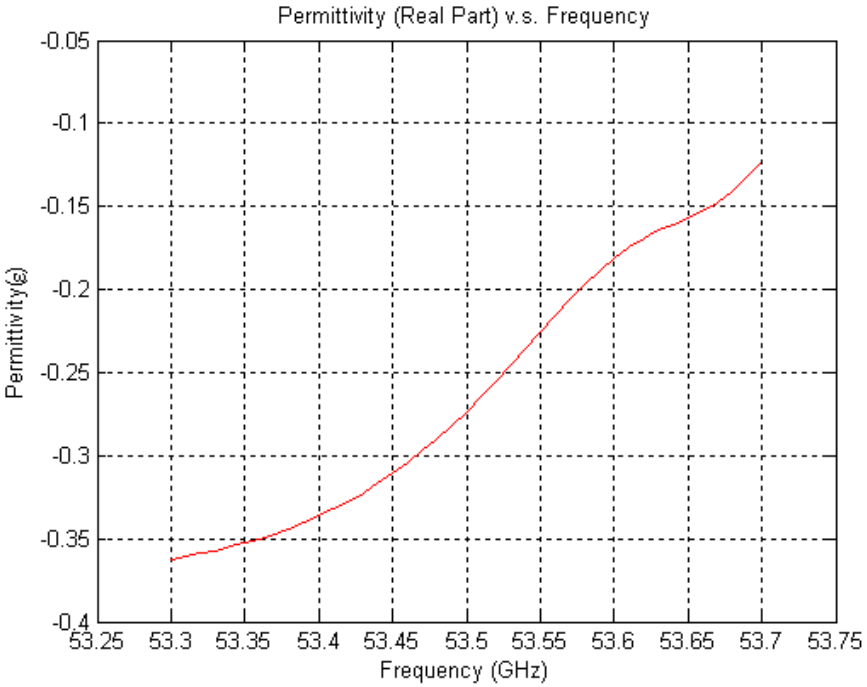

Figure 4.10 Real part of effective permittivity for cross-arranged CLL-P slab.

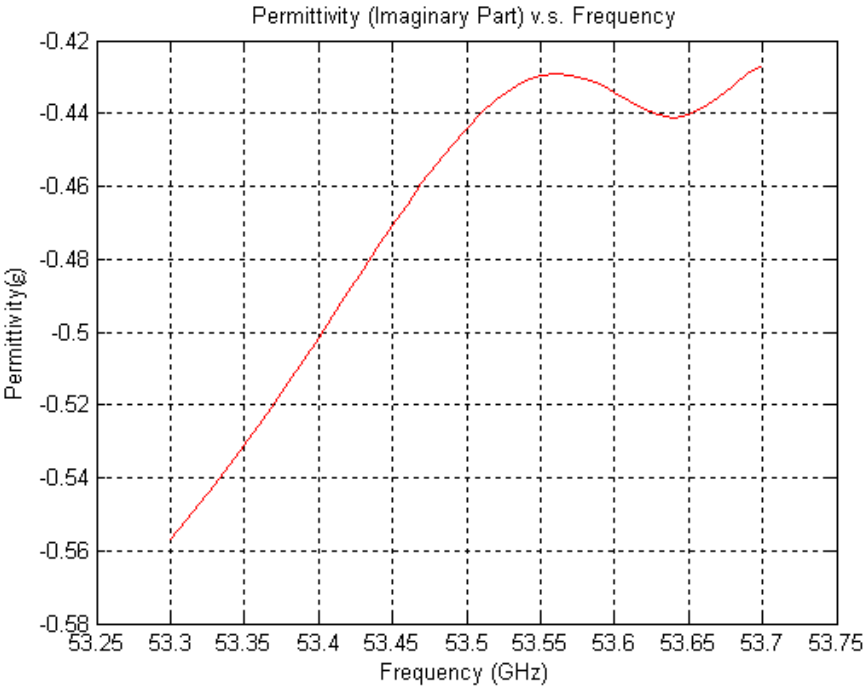

Figure 4.11 Imaginary part of effective permittivity of cross-arranged CLL-P slab.

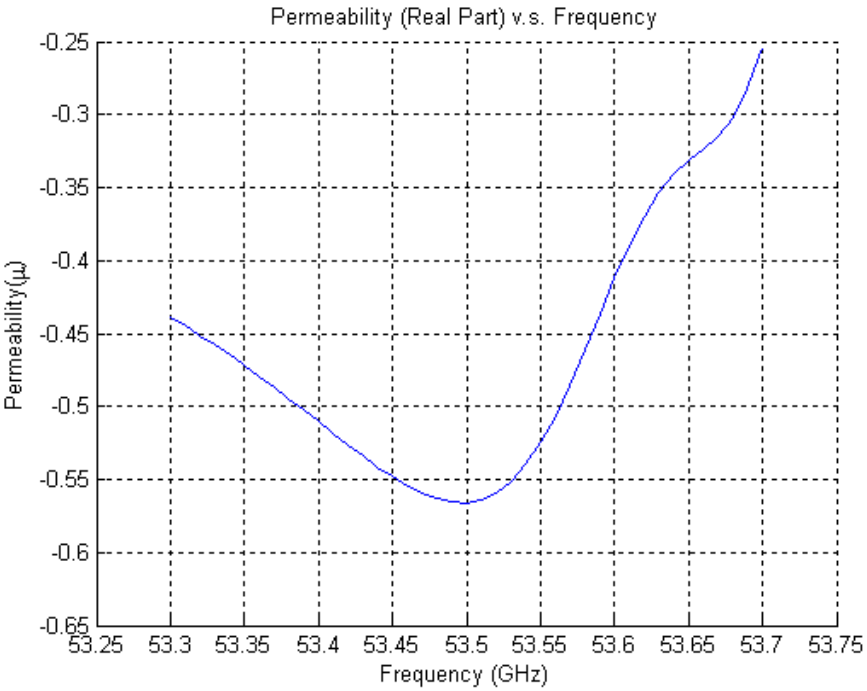

Figurer 4.12 Real part of effective permeability of cross-arranged CLL-P slab.

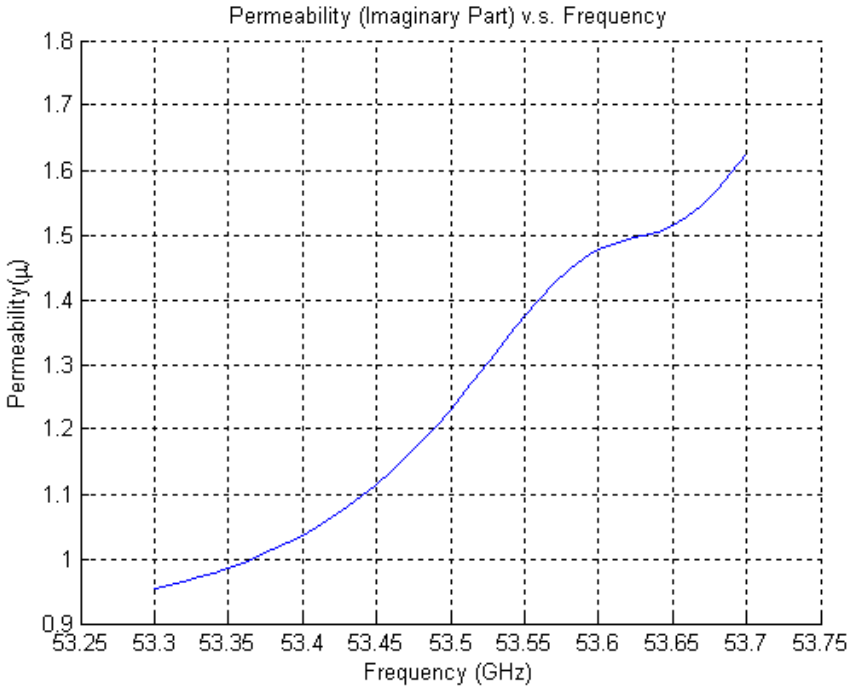

Figure 4.13 Imaginary part of permeability of cross-arranged CLL-P slab.

Per Plasma frequency theory proposed by J. B. Pendry [2], the artificially synthesized metal structure can bring the Plasma frequency of metal down to millions of times, and the permittivity and permeability will show negative values around Plasma frequency. All these suggest us that the resonance frequency at 53.5 GHz is a Plasma frequency of CLL-P slab. Knowing the refractive index in free space is 1, the refractive index of other medium can be calculated through

$$n = \pm\sqrt{\varepsilon_r \mu_r} \tag{4-12}$$

where ε_r and μ_r are relative permittivity and permeability of the medium. The sign of the square root in (4-12) depends on the signs of ε_r and μ_r. With the negative value that relative permittivity and permeability has in Figure 4.10 and 4.12, the refractive index will be calculated using (4-12) with negative sign. Since the both ε_r and μ_r are complex numbers, the resulting effective refractive index also should be a complex number. Figure 4.14(a) and 4.14(b) show real and imaginary part of the refractive index calculated.

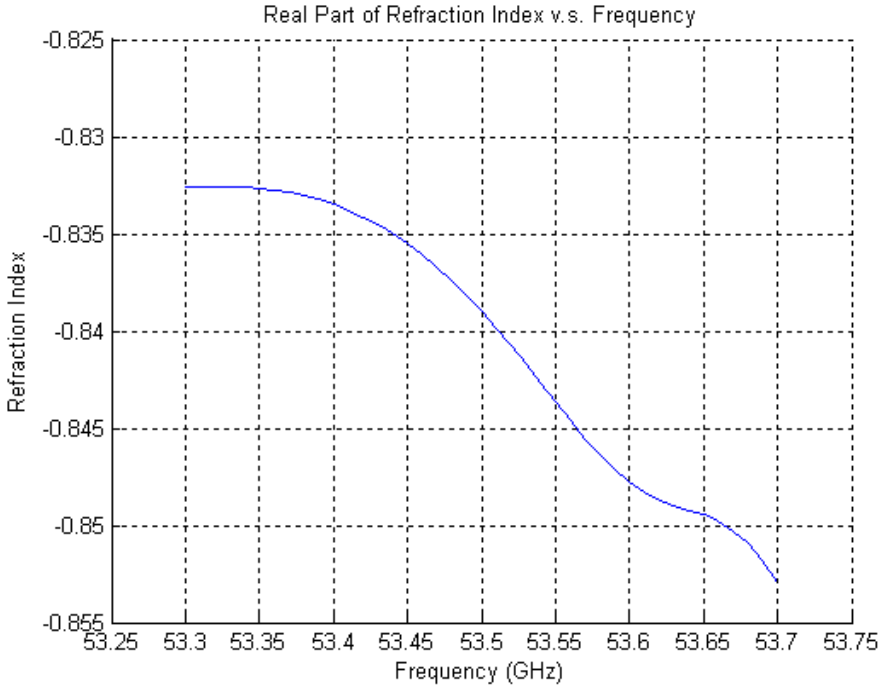

(a)

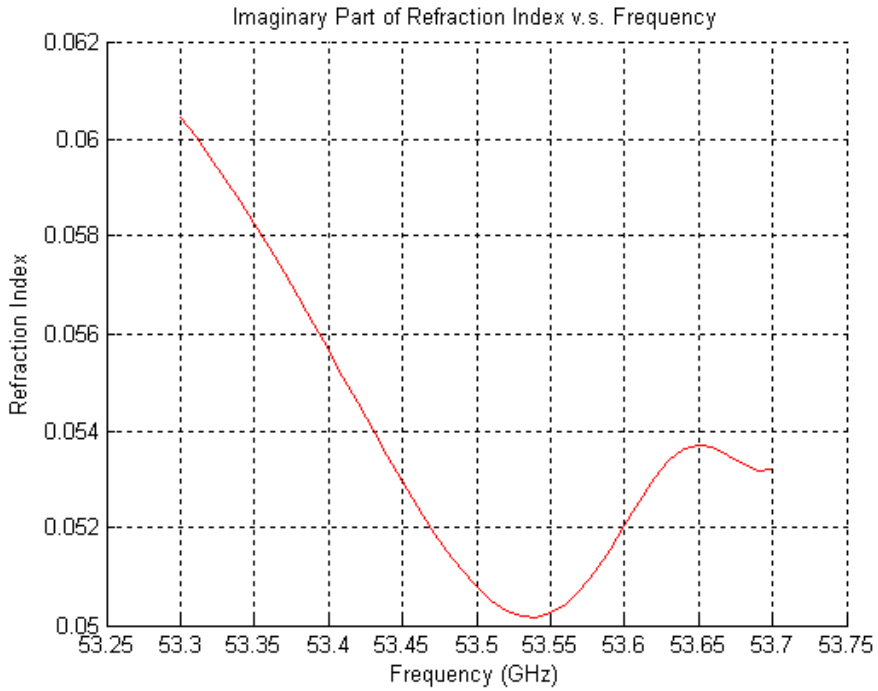

(b)

Figure 4.14 Refractive index calculated from effective permittivity and permeability for cross-arranged CLL-P slab.

In Figure 4.14(a), we can see that the refractive index shows -0.85 at resonance frequency and negative value in quite broad range. The incident wave will be highly attenuated once the frequency is drifted way from resonance point. So only the refractive index close to resonance frequency will be worthy of a closer look. Figure 4.15 shows the E_z field intensity when receive probes are located at 1500 mil away from the source at different incident angles.

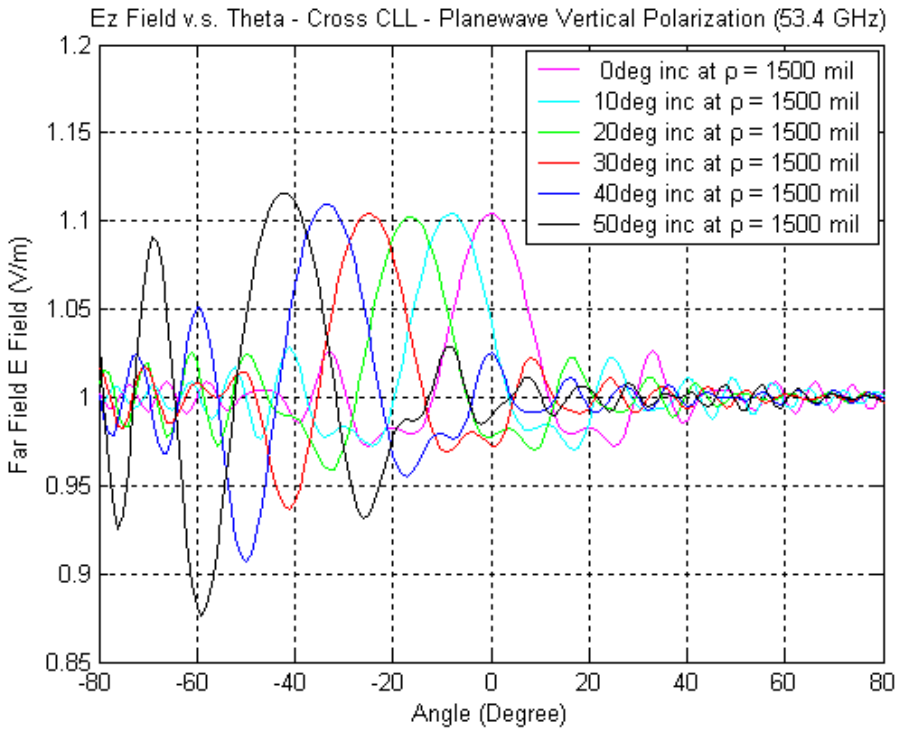

Figure 4.15 Far field intensity when receive probes are located at ρ = 1500 mil for different incident angles.

The received peak field intensities at different incident angles except zero clearly show that incident waves are bent when they pass through CLL-P slab. Using the geometry methodology discussed in Section 4.2, the calculated refractive indexes at different angles are illustrated in Figure 4.16.

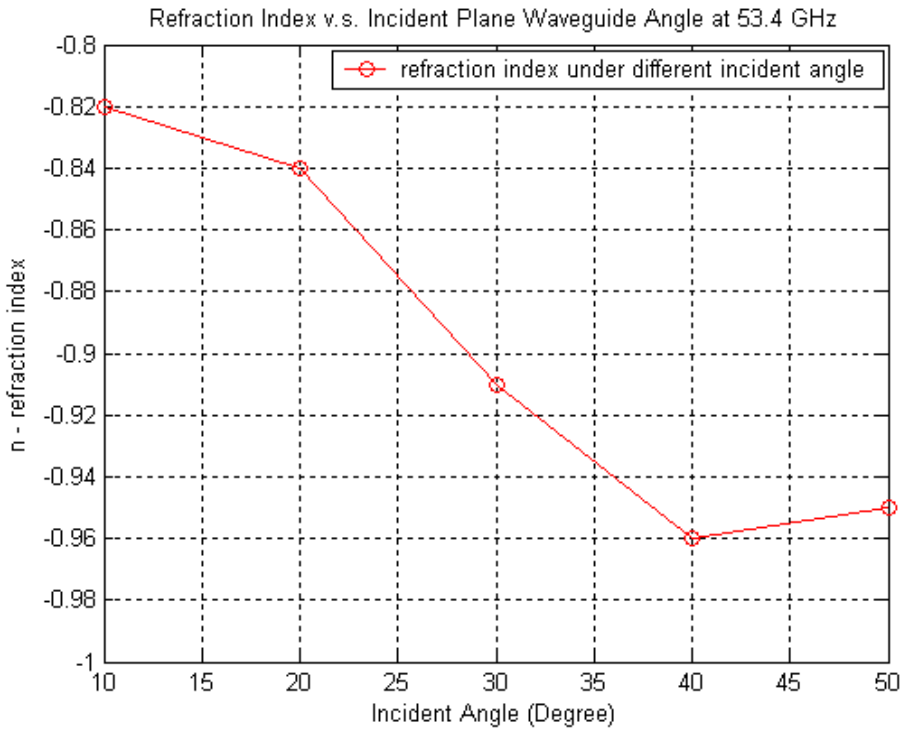

Figure 4.16 Calculated refractive index using geometrical approaches for cross-arranged CLL-P slab at different incident angles (53.4 GHz).

The calculated refractive index at 10 and 20 incident angles are around -0.82 and -0.84; these values match the ones we obtained through effective permittivity and permeability. When incident angles are greater than 30 degree, there is relatively bigger difference on the refractive index values with the ones obtained on smaller incident angles. The difference is caused by the diffraction or reflection effect when incident wave direction is more close to the edge of CLL-P slab. This can be better explained by Figure 4.15, where the peak field strength at 50 incident angle is higher than the field strengths at smaller incident angles.

When incident wave enters from one medium to another medium, there will be reflections on the interface if two media do not match well, which will cause mismatch losses. Mismatch loss is an important issue in the study of the metamaterial. In [5], When J. B. Pendry proposed to make perfect lenses by using metamaterial, the prerequisite requirement of the metamaterial used is that it needs to have a perfect impedance match

with the surrounding medium. For example, let us assume that waves diverge from a point source which is located in free space. The free space has a relative permittivity ε_r = 1 and permeability μ_r = 1, which means that the relative wave impedance of the free space is η = 1, and the absolute impedance is Z_0 = 377*η = 377 Ω. In order to eliminate mismatch loss occurred on the interface, the wave impedance of the metamaterial Z_1 needs to be equal to Z_0. We know that wave impedance of the medium can be obtained through

$$Z_1 = \eta_1 \times Z_0 = \sqrt{\frac{\mu_r}{\varepsilon_r}} \times Z_0 \tag{4-12}$$

provided that ε_r and μ_r are known variables. To have a perfect match, we need to have Z_1 = Z_0, which means the relative impedance of the metamaterial $\eta_1 = \sqrt{\frac{\mu_r}{\varepsilon_r}}$ equal to 1. So any metamaterial slab with close to equal negative permittivity and permeability will meet the zero mismatch losses requirement. Based on results from Figure 4.10 to 4.13, the relative wave impedance of the cross-arranged CLL-P slab can be calculated and shown in Figure 4.17. In this figure, we can see that the normalized impedance value changes drastically from 0.4 to 075 on frequency range 53.3 – 53.7 GHz, and it achieves peak value around resonance point (at 53.5 GHz), again this indicates that CLL-P slab only works in a relatively narrow band. The normalized impedance at 53.4 GHz is about 0.7, which tells us that there is a small mismatch loss. Total mismatch losses happened on first and 2nd CLL-P slab interface can be calculated through following:

$$Losses = 2 \times \frac{1 - 0.7}{1 + 0.7} = 0.35 \Rightarrow Losses \approx -4.56\, dB \tag{4-13}$$

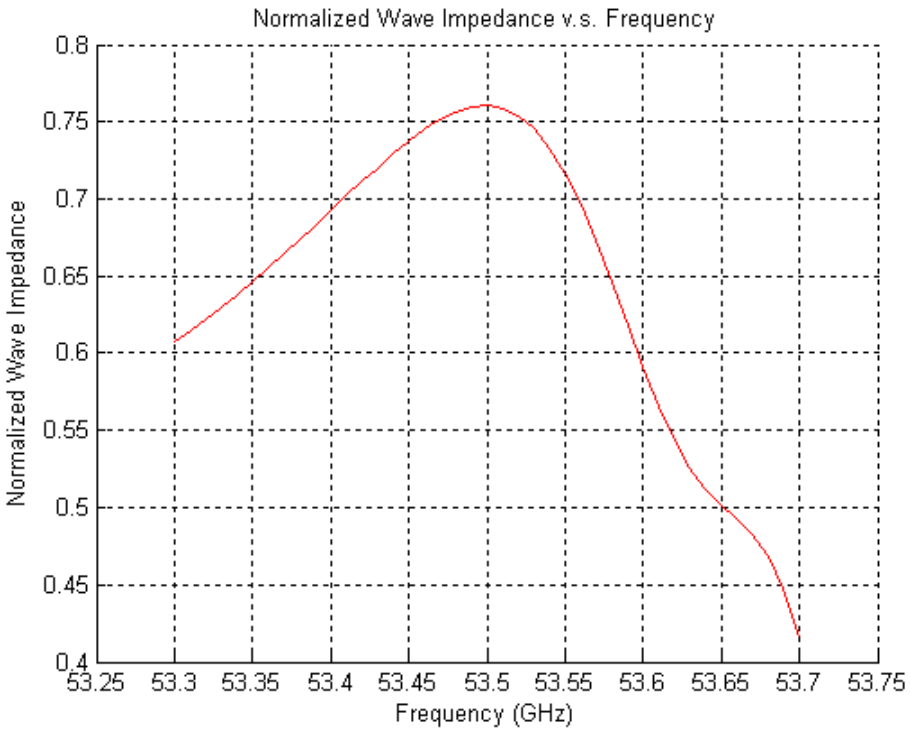

Figure 4.17 Normalized wave impedance versus frequency for cross-arranged CLL-P slab.

4.4 Comparison of Different Arranged CLL-P Slabs

In CLL-P slab unit cell composed by dipole and CLL loop, usually the dipole contributes to negative permittivity, and the CLL loop contributes to negative permeability of the metamaterial. So the placement of dipole and loop relative to incident wave direction could affect the characteristics of the metamaterial slab. In this section, we will compare three different types of CLL-P slabs which are composed by dipoles and CLL loops with different arrangement: cross-arranged-CLL-P slab, parallel-arranged-CLL-P slab and normal or vertical-arranged-CLL-P slab. The cross-arranged-CLL-P slab has been mentioned section 4.3, and we will not cover its synthesis any more. The parallel and vertical-arranged-CLL-P slab are named according to the relationship between the incident magnetic field polarization direction and CLL loop plane. Figure 4.18 (a) and (b) show the sketches of these two types of CLL-P slab.

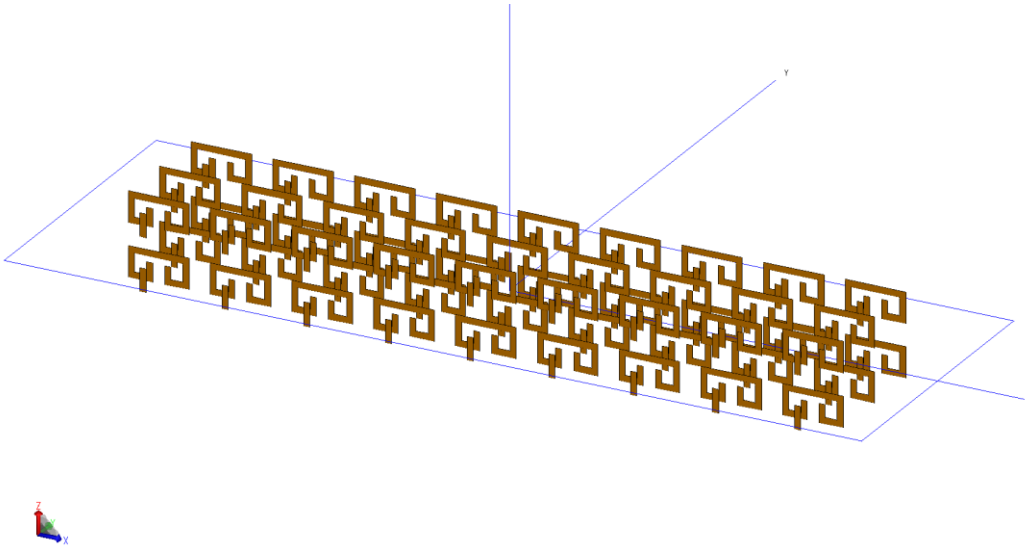

(a)

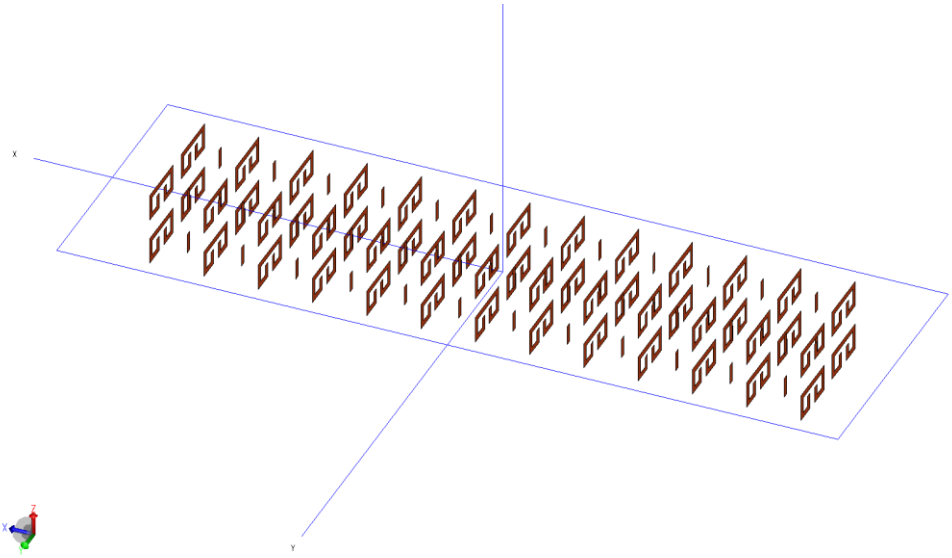

(b)

Figure 4.18 (a) Sketch of parallel-arranged CLL-P slab (b) Vertical-arranged CLL-P slab.

In a parallel-arranged CLL-P slab, the printed dipole and CLL loop layers are located in *x*-*z* plane, and interleaved with each other, and the distance between layers is 20 mils. Within same CLL loop layer, the distance between adjacent CLL loops are 14 mils, in both vertical *x* and *z* directions. The thickness of dielectric where the printed dipoles and CLL loops are attached is 10 mils. When incident wave with vertical polarization

propagates along *y* axis and enter the slab normally, both electric and magnetic field direction will be in a plane parallel to CLL loops. That is how parallel-arranged CLL-P slab is named. Similarly in a vertical-arranged CLL-P slab, the printed dipole and loop layer are located in the plane parallel to *y*-*z* plane and interleaved with each other. When incident wave with vertical polarization enters the slab normally, the plane where electric and magnetic fields polarize is normal to CLL loop plane. The dimensions of individual printed dipoles and loops are the same as the ones in cross and parallel-arranged CLL-P slabs. Within same CLL loop layer, the spacing of loops is 14 mils in both *y* and *z* directions.

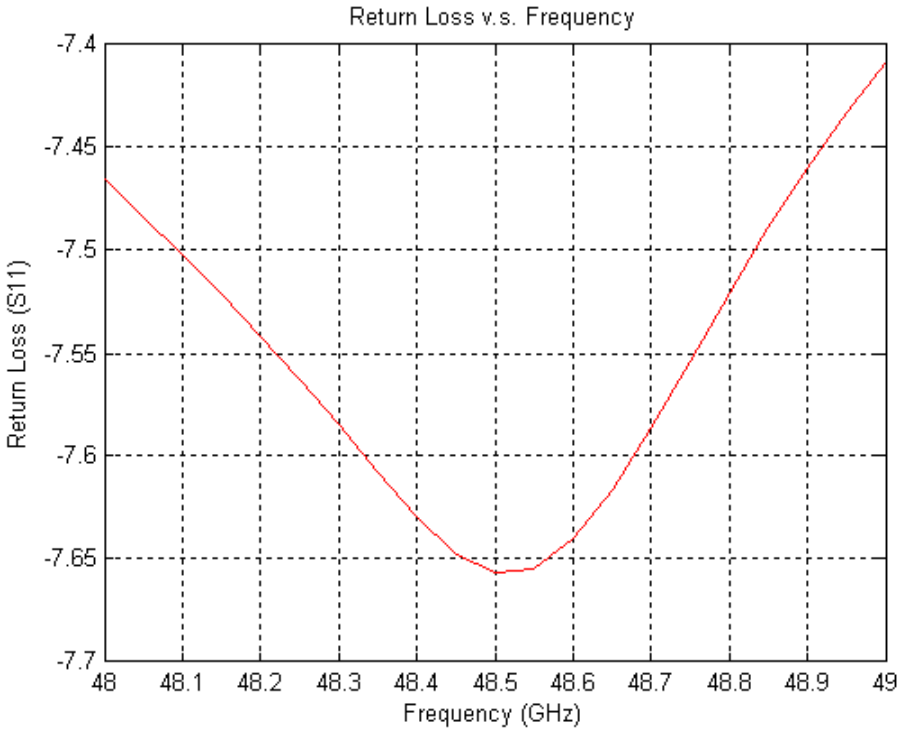

(a)

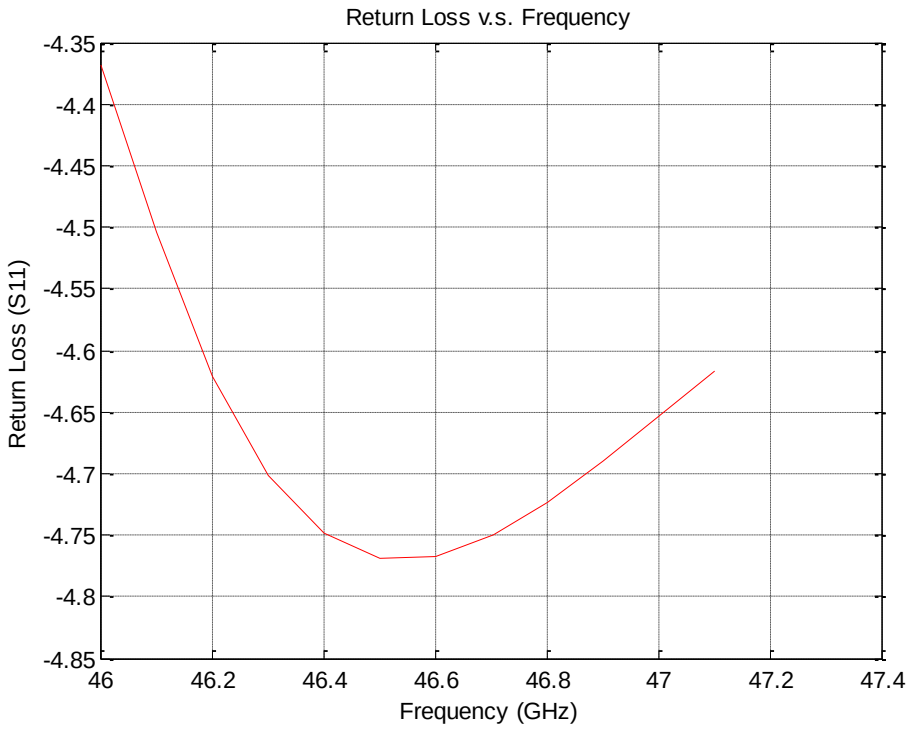

(b)

Figure 4.19 (a) Return loss of parallel-arranged CLL-P slab. (b) Return loss of vertical-arranged CLL-P slab.

Due to change of the arrangement, the corresponding resonance frequency will also be shifted for those two slabs. Figure 4.19 shows the return loss for parallel and normal or vertical-arranged CLL-P slab. From figure we can see that there is 2 GHz shift for resonance frequency. Compared with resonance frequency for cross-arranged CLL-P slab, they are quite close. However, normal or vertical-arranged CLL-P slab has the higher return losses among three different slabs. Due to the asymmetric nature of parallel and vertical-arranged CLL-P slab in x and y directions, the relationship between refraction indexes and different incident wave angles is of interest. Figure 20 shows the received electrical field intensity at ρ = 1000 mil, where we can observe that the field intensity changes drastically with variation of incident angle.

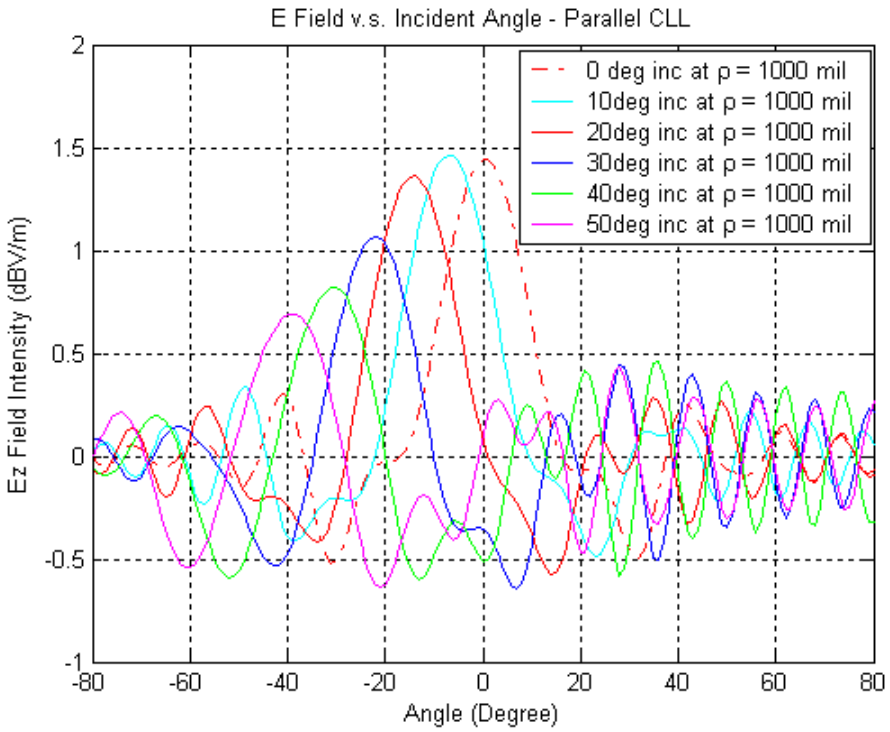
E Field v.s. Incident Angle - Parallel CLL
0 deg inc at ρ = 1000 mil
10deg inc at ρ = 1000 mil
20deg inc at ρ = 1000 mil
30deg inc at ρ = 1000 mil
40deg inc at ρ = 1000 mil
50deg inc at ρ = 1000 mil
Ez Field Intensity (dBV/m)
Angle (Degree)
2
1.5
1
0.5
0
-0.5
-1
-80
-60
-40
-20
0
20
40
60
80

(a)

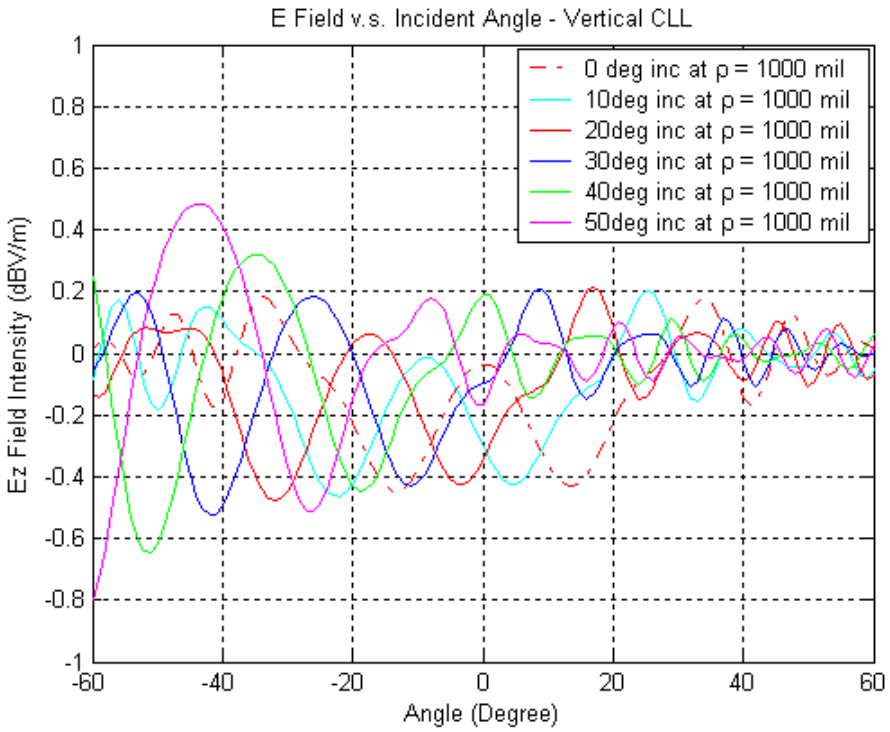
E Field v.s. Incident Angle - Vertical CLL
0 deg inc at ρ = 1000 mil
10deg inc at ρ = 1000 mil
20deg inc at ρ = 1000 mil
30deg inc at ρ = 1000 mil
40deg inc at ρ = 1000 mil
50deg inc at ρ = 1000 mil
Ez Field Intensity (dBV/m)
Angle (Degree)
1
0.8
0.6
0.4
0.2
0
-0.2
-0.4
-0.6
-0.8
-1
-60
-40
-20
0
20
40
60

(b)

Figure 4.20. Far field intensity when receive probes are located at ρ = 1000 mil for different incident angles (a) Parallel-arranged CLL-P slab (b) Vertical-arranged CLL-P slab.

From received peak E_z field intensity at different incident angles for parallel-arranged CLL-P slab, we can observe that field intensities drop sharply with the increase of incident angles, which is about 1 dB difference between 0 degree and 50 degree incident angle. This suggests that the parallel-arranged CLL-P slab has anisotropic nature. This can be further confirmed by refraction index, which is shown in Figure 4.21, calculated based on geometric approach. The calculated refractive index ranges from -0.7 to -1.03 at different angles, but it decreases with the increase of angles. This can be explained by effective permittivity and permeability theory. As we know when the planar wave enters slab normally, the electric field resulted from printed dipole will cause symmetric push-push currents on the CLL loop behind the dipole. Further the magnetic fields caused by the currents interact with the electric fields resulted from dipole and determine the effective permittivity and permeability of the slab for normal incident angle. When incident angle is away from normal, push-push currents will become asymmetric due to oblique incident angle. This kind of asymmetry will become more severe when the incident angle increases. Asymmetrical currents will weaken the coupling between printed dipole and CLL loop, which further affects the effective permittivity and permeability. From the definition, refractive index is determined by square root of permittivity and permeability. Thus the final refractive indexes will not be constant due to inconsistent coupling between printed dipole and CLL loop.

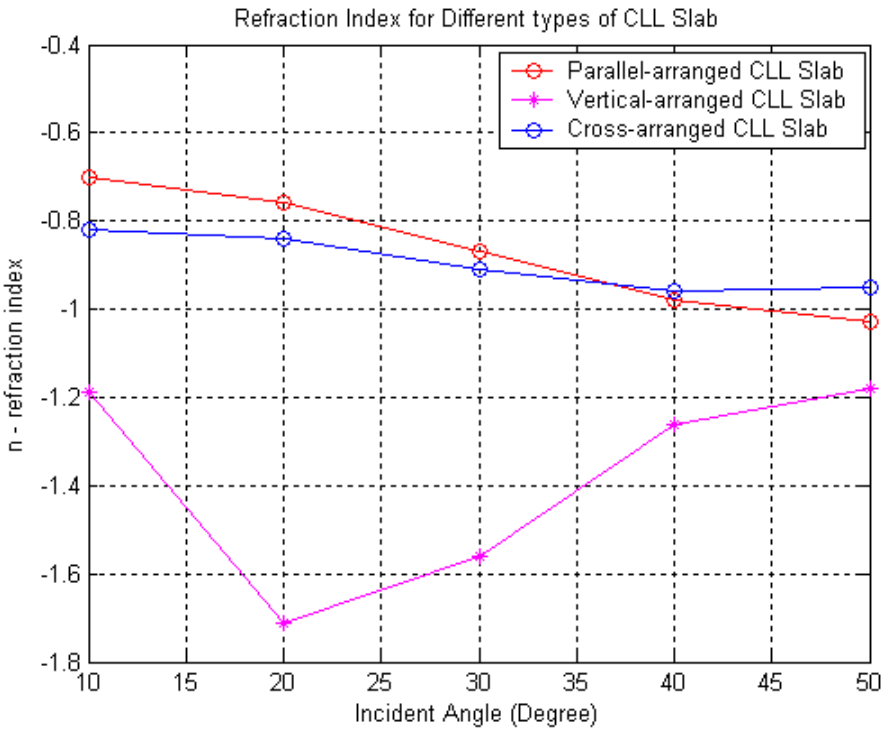

Figure 4.21 Comparison of the refractive index for different types of CLL-P slabs.

Same theory can be applied for the vertical-arranged CLL-P slab. When incident wave enters slab normally, there is symmetric push-push current incurred on CLL loop. And when incident angle is away from normal, the current will become asymmetrical, and cause inconsistent coupling between dipole and CLL loop. We can see inconsistent refractive indexes for the vertical-arranged CLL-P slab as shown in Figure 4.21. In order to make comparison, we also add refractive indexes of the cross-arranged CLL-P slab. Compared with other two types of CLL-P slabs, cross-arranged CLL-P slab has a relatively constant refractive index at different incident angles. This can be explained by the symmetrical CLL loop structure in the cross-arranged CLL-P slab, and coupling between CLL loop and dipole less likely to be affected by variations of incident wave angles. As mentioned before in period structure composed by dipole and loop, the thin-wire-like dipole contributes to negativity of permittivity and loop contributes to negativity of the permeability.

The effective permittivity and permeability of those three types of CLL-P slabs are calculated. Figure 4.22 shows the real part relative permittivity and permeability for the parallel-arranged CLL-P slab obtained from S parameters when the incident wave hits the slab with normal angle. The permittivity ranges from -1.78 to -1.66 around resonance frequency, while the permeability forms a dip at resonance frequency. As a comparison, the permittivity and permeability of vertical-arranged CLL-P slab are shown in Figure 4.23, similarly the effective permeability achieves minimum value close to resonance frequency. Taking a closer look, we can find that the effective permittivity of vertical-arranged CLL-P slab is much smaller than parallel-arranged CLL-P slab. At the same time permeability of vertical-arranged CLL-P slab is slightly greater than parallel-arranged CLL-P slab.

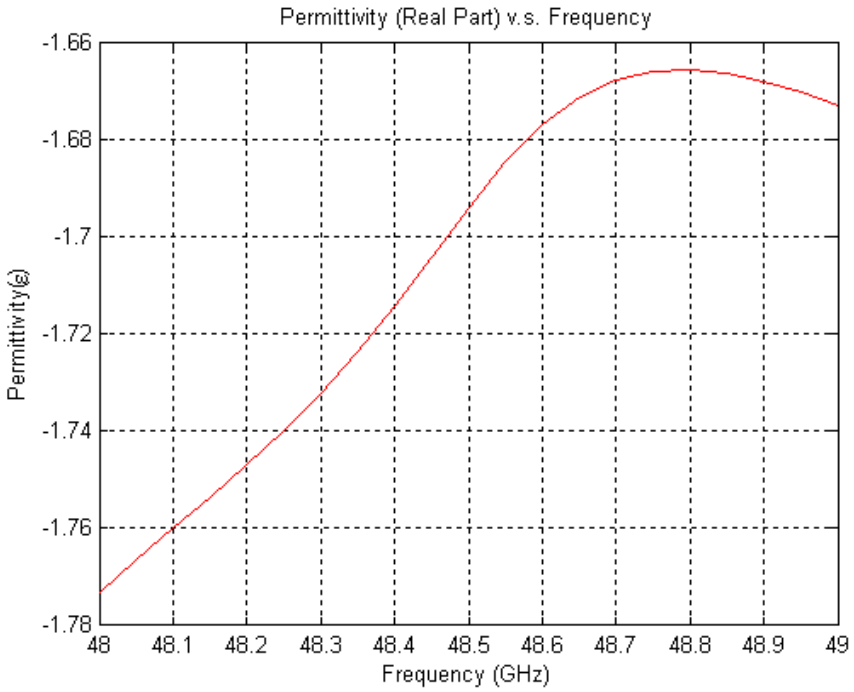

(a)

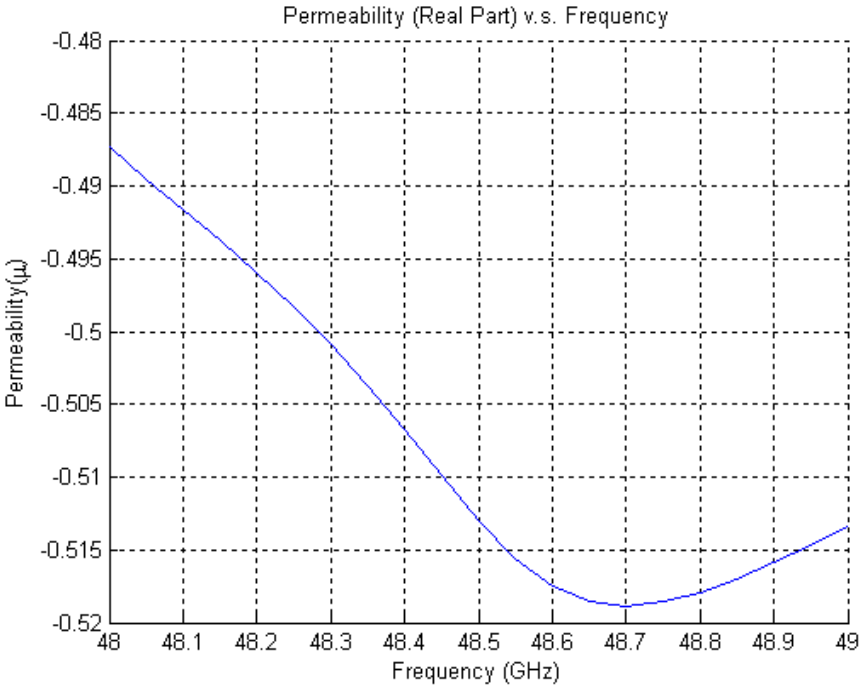

(b)

Figure 4.22 Permittivity and permeability of parallel-arranged CLL-P slab.

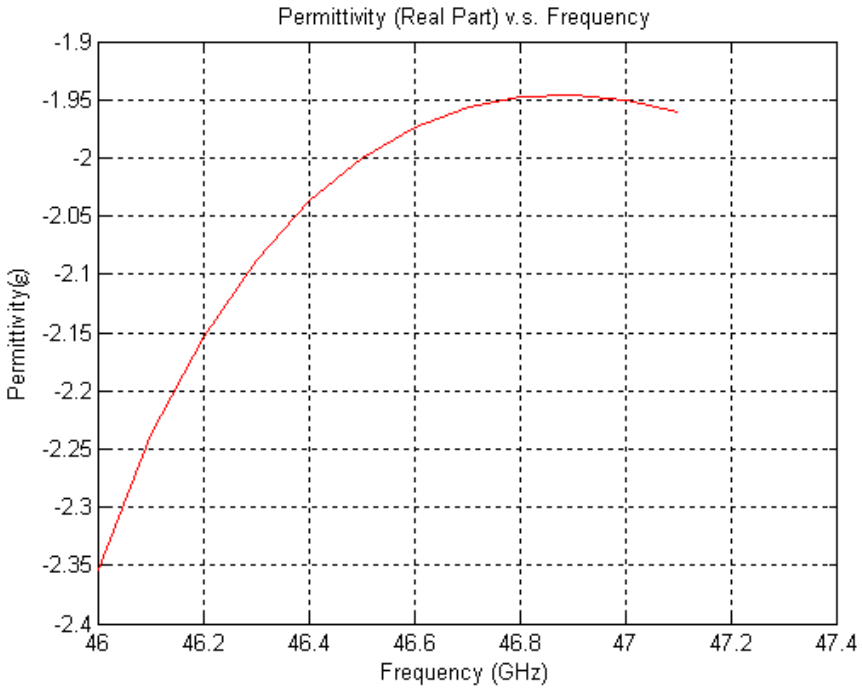

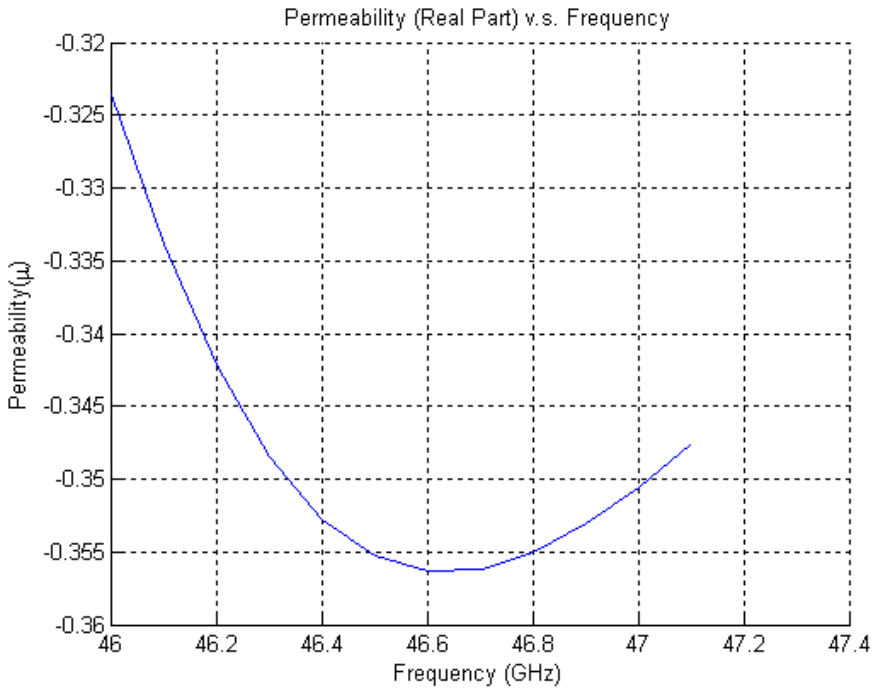

Figure 4.23. Permittivity and permeability of vertical-arranged CLL-P slab.

The results shown in last two figures can be explained as follows. When incident angle is normal, in parallel slab the magnetic field polarization direction is parallel with the CLL loop plane; it will be different in the vertical CLL-P slab. In the vertical-arranged CLL-P slab, the direction of magnetic field polarization is perpendicular to CLL loop plane, this will bring maximum coupling between CLL loop and incident magnetic field due to same direction between incident magnetic field and the magnetic field resulted from current on CLL loop. As a result of stronger coupling with magnetic field the vertical-arranged CLL-P slab will achieve greater effective permeability. This helps to explained why vertical-arranged CLL-P slab has greater effective permeability than parallel-arranged CLL-P slab.

Applying above theory, we also can explain why the maximum E_z field intensity will decrease with the increase of incident angle for parallel-arranged CLL-P slab. At the same time the maximum E_z field intensity in vertical-arranged CLL-P slab will increase with the increase of incident angle. We know that the coupling between incident

magnetic field and CLL loops will become greater with the increase of incident angle for parallel-arranged CLL-P slab. As a direct result, with the increase of incident angle, the effective permeability increases, and further the wave impedance in parallel-arranged CLL-P slab increases due to the fact that the wave impedance is determined by square root of ratio between effective permeability and permittivity. Finally the results shown in 4.20(a), indicate that the peak field intensity drops sharply as incident angle increases.

For vertical-arranged CLL-P slab, the situation is reversed. At normal incident angle, the magnetic field polarization direction is perpendicular to the CLL loop plane, and resultant effective permeability has maximum value at this time. With the incident angle shift away from normal, coupling between magnetic field and CLL loop is getting weaker. As a consequence, the effective permeability will getting smaller, thus the wave impedance will decreases with the increase of incident angle. Eventually, we get the result shown in Figure 4.20b, which is the peak E_z field intensity increases with the incident angle increase.

4.5 Simulation Result at Ku-Band

Ku-band is ranges from 12-18 GHz. Most satellite communication and radar systems operate at Ku band. So the metamaterial has broader application in this frequency band. In this section, we will look at the performance of cross-arranged CLL-P slab in Ku-Band. In section 4.4, we already discussed the CLL-P slabs based metamaterial around 50 GHz, so the best way to build cross-arranged CLL-P slab at Ku band is to scale the dimension of the counterpart up four times. The dimension of individual CLL loop of periodic structure shown in Figure 4.7 will become 160 x 80 mil in terms of length and height, which is also shown in Figure 4.24..

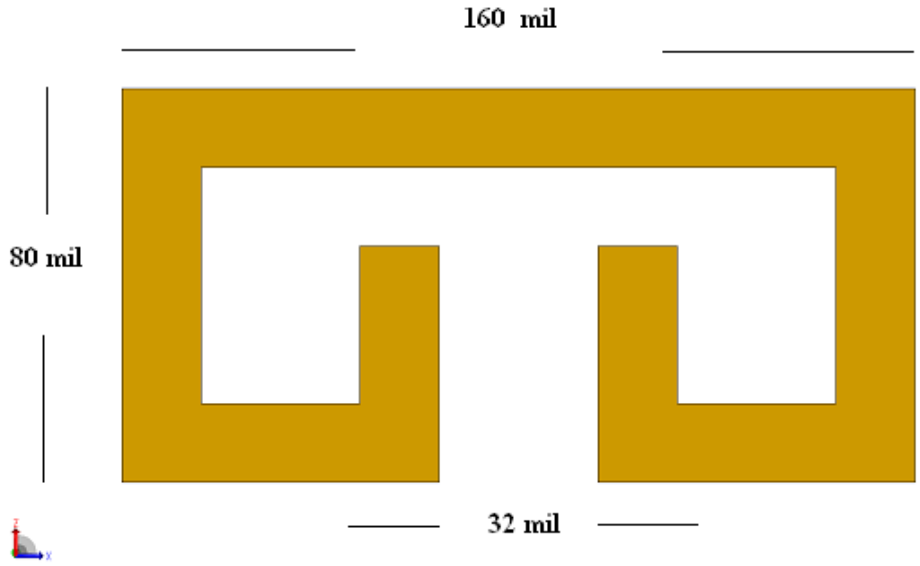

Figure 4.24. Dimension of CLL loop in Ku Band.

The width of printed line is 16 mils, and the spacing between adjacent loops is 56 mils along both horizontal and vertical directions. The height of the probe in front CLL loop has a height of 60 mils and a width of 16 mils. With this dimension, the cross-arranged CLL-P slab will achieve resonance at frequency of 13.486 GHz, and the corresponding insertion losses is illustrated in Figure 4.25.

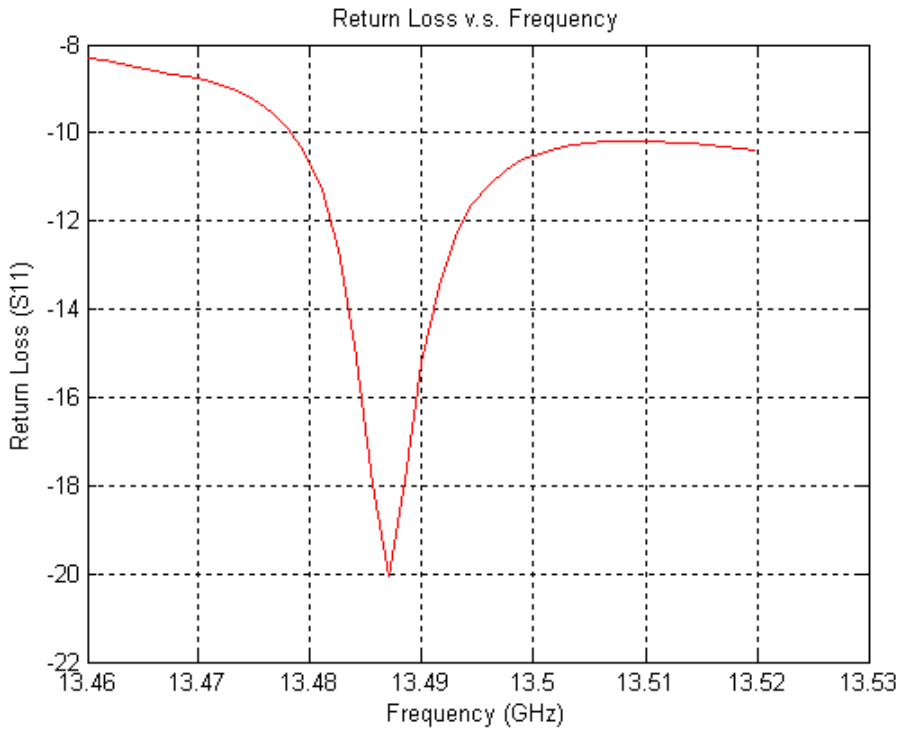

Figure 4.25. Insertion losses for cross-arranged CLL-P slab at Ku band.

From Figure 4.25, we can see that the insertion loss forms a sharp dip at resonance frequency, which suggests that the slab will work in a narrow band. Beyond resonance frequency, the system will degrade rapidly. Using scattering matrix, the effective permittivity and permeability can be calculated and shown in Figure 4.26 and Figure 4.27. Both real parts of permittivity and permeability are functions of frequencies. They have negative values around resonance frequency, and the real part of permeability has a dip at resonance frequency. The imaginary part of permittivity has negative sign, and the corresponding part of permeability has positive sign, but both of them are close to zero; which suggests that CLL-P slab has small loss.

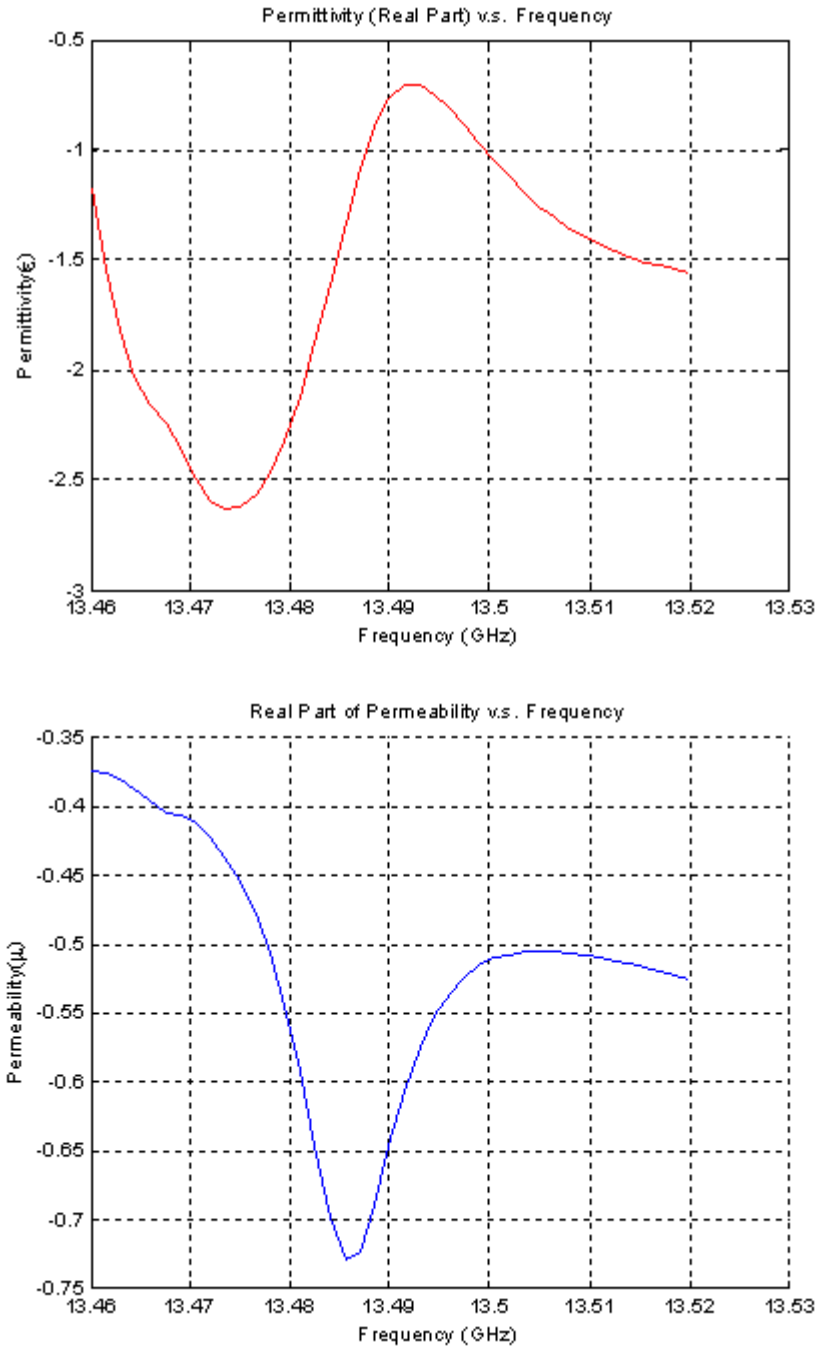

Figure 4.26 (a) Real part of permittivity (b) real part of permeability for cross-arranged CLL-P slab.

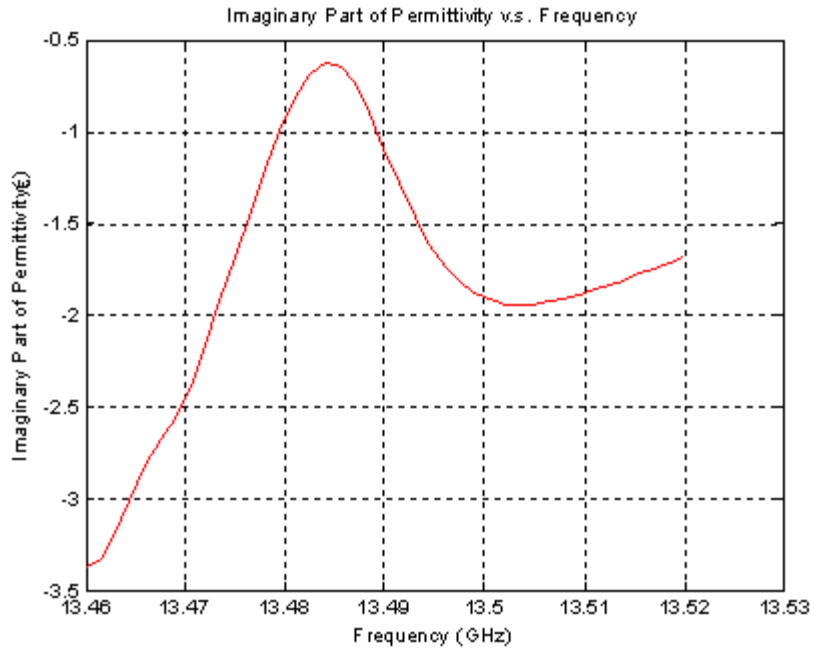

(a)

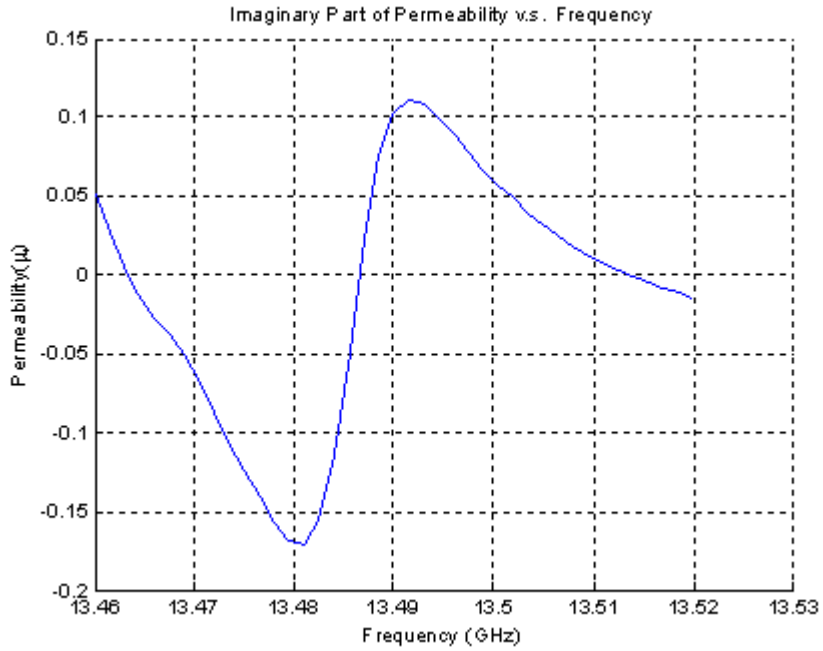

(b)

Figure 4.27. (a) Imaginary part of permittivity (b) Imaginary part of permeability for cross-arranged CLL-P slab

With the effective permittivity and permeability, we can calculate effective refractive index by using $n = -\sqrt{\varepsilon_r \mu_r}$. The reason the negative sign was selected is due to the negativity of real part of permittivity and permeability. The real part of effective refractive index is shown in Figure 4.28.

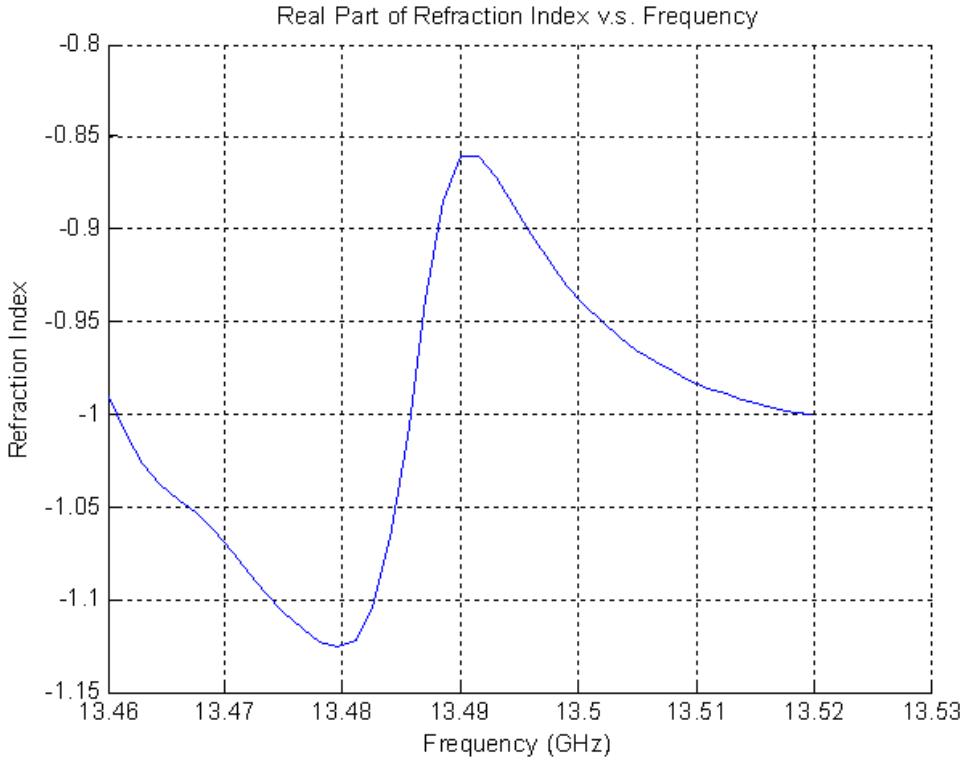

Figure 4.28. Real part of effective refractive index calculated from ε_r and μ_r for cross-arranged CLL-P slab.

At resonance frequency, the real part of effective refractive index is about -0.95. As a comparison, Figure 4.29 shows the calculated refractive index under different incident angles using geometric approach. From both figures, we see that the refractive indexes under different incident angles are ranging from 0.91 to 0.98, which are quite close to the value obtained from effective permittivity and permeability.

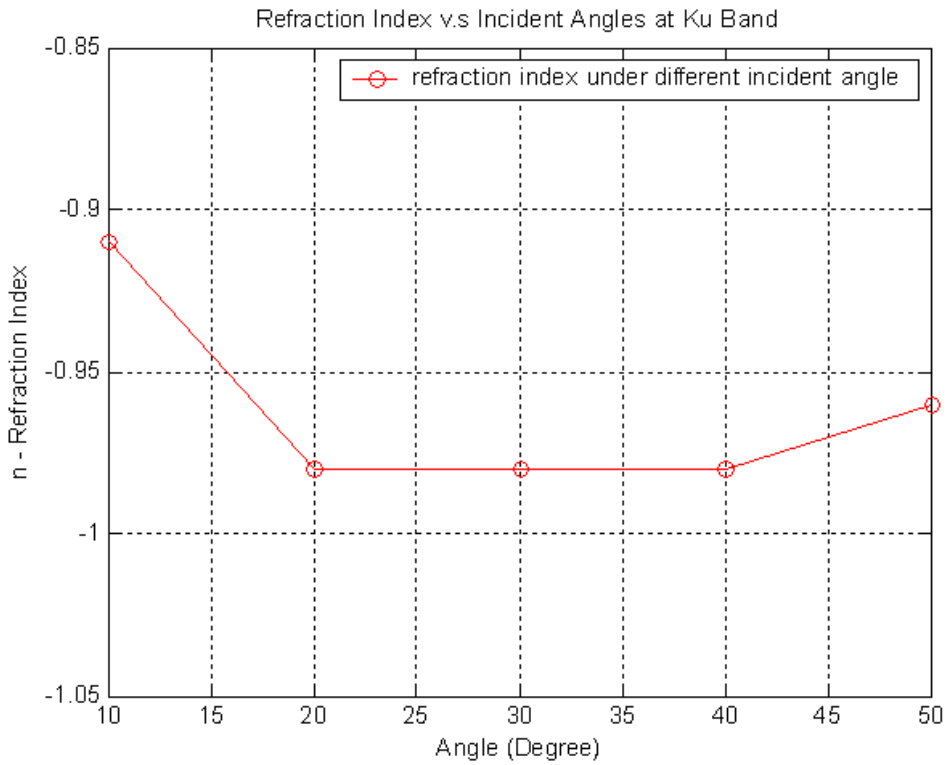

Figure 4.29. Refractive index under different plane wave incident angle for cross-arranged CLL-P slab at 13.486 GHz.

Also we can see that refractive indexes are almost constant with different incident angles, which also suggests that cross-arranged CLL-P slab shows a characteristic of isotropy at different incident angles. The far field E_z intensity (ρ = 1000 mil) at different incident angles, which is shown in Figure 4.30, further confirm this. In Figure 4.30, the peak E_z intensities are at same level from 0-30 degree incident angles, and getting slight increase when incident angles are getting close to the edge of slab. The increase at incident angle greater than 40 degree could be attributed to edge diffraction effect.

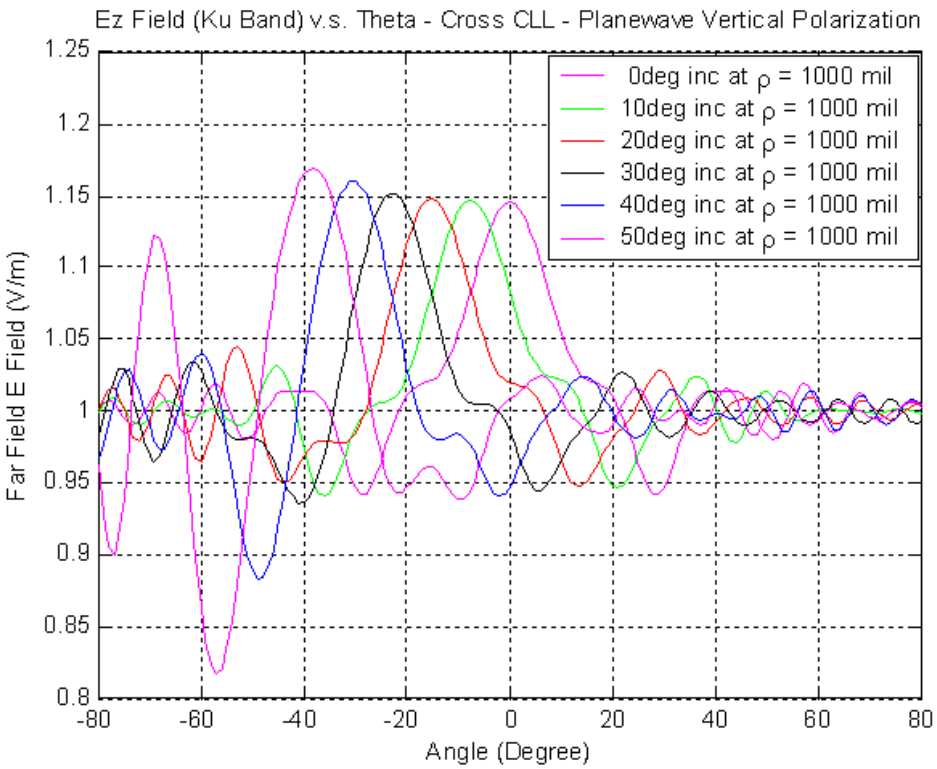

Figure 4.30. Far field intensity when receive probes are located at ρ = 1000 mil at different incident angles for cross-arranged CLL-P slab.

The reason that peak E_z field can be kept constant lies in that the way CLL loops are arranged in cross-arranged CLL-P slab. When incident wave enters the slab normally, there is the strongest coupling between incident magnetic wave and the loop in *y*-*z* plane since the magnetic wave polarization direction is perpendicular to *y*-*z* plane. When incident wave is shifted away from normal angle, the couplings between incident magnetic waves and CLL loops located in *y*-*z* plane will become weaker, but the couplings between incident magnetic wave and CLL loops located in *x*-*z* plane will become stronger. As a combination of those two effects, the total couplings between incident magnetic field and slab will be kept constant. Thus the effective permeability and wave impedance appeared for cross-arrange CLL-P slab will be independent of incident angles. Figure 4.31 and 4.32 show calculated wave impedances and mismatch loss respectively.

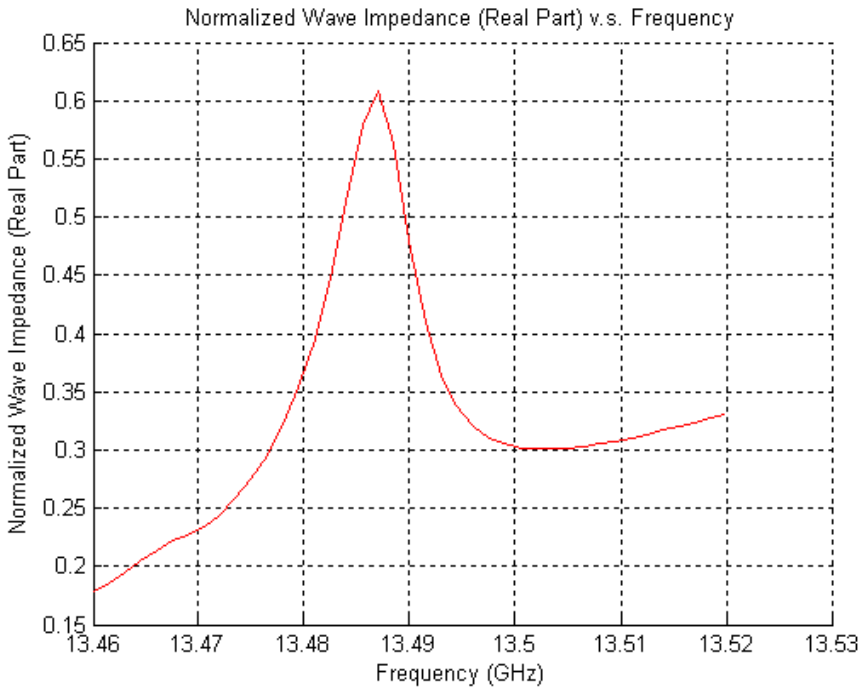

Figure 4.31. Wave impedance for cross-arranged CLL-P slab at Ku band.

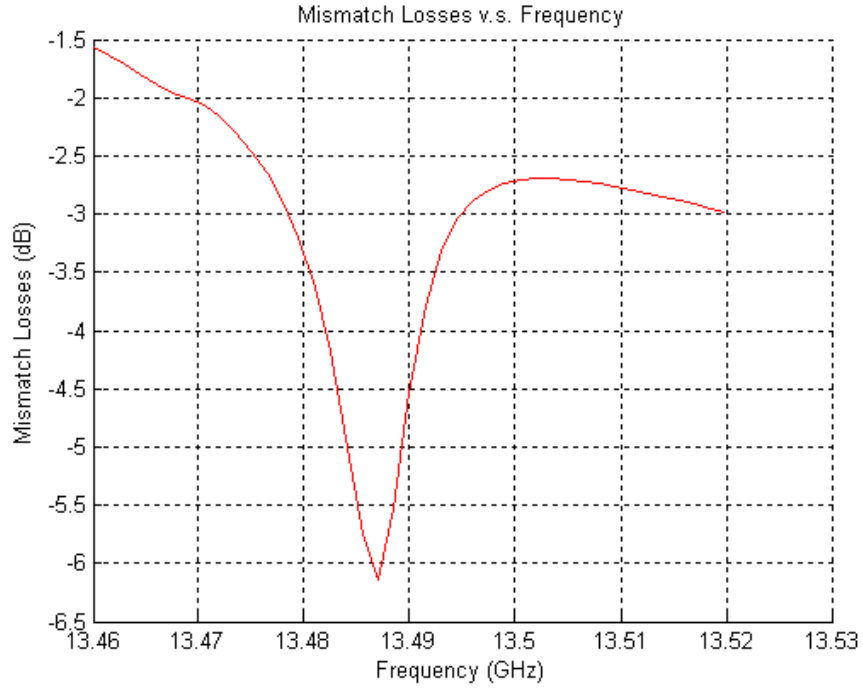

Figure 4.32. Mismatch losses for cross-arranged CLL-P slab at Ku band.

Chapter 5 Conclusions

Negative refraction is a disputed topic for metamaterial, and is the cause of many doubts expressed by several researchers. The objective of this thesis work was to study the claim of existence of the negative refraction and the mechanism behind it through full-wave simulations, which lays the foundation for future of metamaterial study.

Through the study of parallel-arranged CLL-P slabs using different feeding methods, both refractive focusing and negative refraction effects were observed clearly around resonance or Plasma frequency of CLL-P slab in software based simulation. This tells us that the periodic CLL-P slab is one type of the metamaterial with negative refraction. The CLL-P simulation results in this thesis agree with prior simulation and measurements of refractive focusing of the same structure.

To further quantify the negative refractive index and the effective permittivity and permeability, a geometric approach was developed in the thesis to calculate the refractive index. At same time, a numerical method was to obtain the effective permittivity and permeability through scattering matrix was implemented. Both techniques were further used to investigate the performance of different types of CLL-P slabs. Through the simulation results of three different types of metamaterial: parallel-arranged, vertical-arranged, and cross-arranged CLL-P slabs, the following conclusions can be drawn:

1) Negative refraction effects are simulated in all three types of slabs.

2) The effective permittivity and permeability (real part) of them show negativity around resonance frequencies.

3) The refractive indexes obtained at different incident angles are almost constant for cross-arranged CLL-P slab, which suggests the cross-arranged CLL-P slab's characteristic of isotropy.

4) The refractive index is calculated through two different approaches in the full-wave simulations: using geometric relationship and using simulated effective permittivity and permeability. The results obtained from above two methods match well.

5) The refractive indexes for parallel and vertical-arranged CLL-P slabs at different angles vary drastically; this indicates that both these types of CLL-P slabs are anisotropic medium.

6) The attenuation of the electric field strength under different incident angles further proves the isotropy of cross-arranged CLL-P slab.

7) The coupling between CLL loop and incident magnetic field reaches the maximum when their directions are perpendicular, and achieves the minimum when both directions are parallel. This explains the attenuation behavior for parallel and vertical-arranged slabs.

Beside the achievements obtained in this thesis, the author feels the following areas need to be further investigated.

1) The work carried related to this thesis is focus on 2D structure. In order to validate the 3D isotropy property, simulation with combined vertical and horizontal incident angle is needed.

2) The experimental verification of the refractive focusing of the CLL-P slab [20] can be followed by experimental verification of the isotropic negative refractive index at different angles of incidence.

3) Contribution in this study may lead to perform optimization of lens design using metamaterials.

References

[1] V. G. Veselago, "The electrodynamics of substance with simultaneously negative values of ε and μ," *Sov. Phys. Usp*, vol. 10, no. 4, pp. 509-514, January-February 1968

[2] J. B. Pendry, A. J. Holden, D. J. Robbins, and W. J. Stewart, "Magnetism from Conductors and Enhanced Nonlinear Phenomena" IEEE Trans. Microwave Theory Tech. **47**, 2075 (1999).

[3] Smith D. R., Padilla W., Vier D. C., Nemat-Nasser S. C., Schultz S. (2000). A Composite medium with simultaneously negative permeability and permittivity, Phys. Rev. Lett., **84**, 4184

[4] Shelby R.A., Smith D.R., Shultz S., (2001) Experimental verification of a negative index of refraction, Science, 292, 77

[5] J. B. Pendry, "Negative Refraction Makes a Perfect Lens", Physical Review Letters, Vol. 85, number 18, 30 October 2000

[6] C. G. Parazzoli, R. B. Grefor, K. Li, B. E. C. Koltenbah, and M. Tanielian, "Experimental verification and simulation of negative index of refraction using Snell's law, Phys. Rev. Lett., vol. 90, 2003

[7] R. B. Greegor, C. G. Parazzoli, K. Li, B. E. C. Koltenbah, and M. Tanielian, "Experimental determination and numerical simulation of the properties of negative index of refraction materials," *Opt. Exp.*, vol. 11, pp. 688–695, 2003.

[8] R. Ziolkowski, "Design, fabrication and testing of double negative metamaterials," *IEEE Trans. Antennas Propagat.*, vol. 51, no. 7, pp. 1516–1529, Jul. 2003.

[9] E. Ozbay, K. Aydin, E. Cubukcu, and M. Bayindir, "Transmission and reflection properties of composite double negative metamaterials in free space," *IEEE Trans. Antennas Propagat.*, vol. 51, no. 10, pp. 2592–2595, Oct. 2003.

[10] J. Huangfu, L. Ran, H. Chen, X. Zhang, K. Chen, T. Grzegorczyk, and J. A. Kong, "Experimental confirmation of negative refractive index of a metamaterial composed of -like metallic patterns," *Appl. Phys. Lett.*, vol. 84, pp. 1537–1539, 2004.

[11] J. S. Derov, B. W. Turchinetz, E. E. Crisman, A. J. Drehman, S. R. Best, and R. M. Wing, "Free Space Measurements of Negative Refraction With Varying Angles of Incidence", IEEE MICROWAVE AND WIRELESS COMPONENTS LETTERS, VOL. 15, NO. 9, SEPTEMBER 2005

[12] P. M. Valanju, R. M. Walser, and A. P. Valanju, "Wave Refraction in Negative-Index Media: Always Positive and Very Inhomogeneous", Physical Review Letters, Vol. 88, No. 18, 6 May 2002.

[13] M. Sanz, A. C. Papageorgopoulos, W. F. Egelhoff, Jr., M. Nieto-Vesperinas, and N. Garcia, "Transmission measurements in wedge-shaped absorbing samples: an experiment for observing negative refraction," *Phys. Rev. E*, vol. 67, pp. 067 601-1–067 601-4, 2003.

[14] Ben A. Munk, "Metamaterials: Critique and Alternatives", John Wiley & Sons, Inc. 2009

[15] A.I. Zaghloul, Y. Lee and S. Weiss, "Measurements of Refraction Focusing Using Negative-Refractive-Index Metamaterials ," USNC/URSI National Radio Science Meeting, San Diego, California, July 2008

[16] Winston E. Kock, "Metal-lens antenna", in Proceeding, IRE and Waves and Electrons, pp. 828-836, November 1946.

[17] J. B. Pendry, "Extremely Low Frequency Plasmons in Metallic Mesostructures", Vol. 76, No. 25, Physical Review Letters, 17 June, 1996.

[18] George V. Eleftheriades, Omar Siddiqui, and Ashwin K. Iyer, "Transmission Line Models for Negative Refractive Index Media and Associated Implementations Without Excess Resonators", IEEE MICROWAVE AND WIRELESS COMPONENTS LETTERS, VOL. 13, NO. 2, FEBRUARY 2003

[19] A.I. Zaghloul and Y. Lee, "Simulation of Refraction Focusing Using Negative-Refractive-Index Metamaterials ," IEEE International Symposium on Antennas and Propagation, San Diego, California, July 2008.